National Research FLAGSHIPS Climate Adaptation

CSIRO

Impact of Climate Variability and Climate Change on Rainfall Extremes in Western Sydney and Surrounding Areas: Component 4 - Dynamical Downscaling

Deborah Abbs and Tony Rafter
29 September 2009

Report to the Sydney Metro Catchment Management Authority and Partners

www.csiro.au

Enquiries should be addressed to:
Deborah Abbs
CSIRO Marine & Atmospheric Research
PMB No 1, Aspendale, Victoria, 3195
E-mail Deborah.Abbs@csiro.au

Distribution list
Chief of Division

Flagship Director

Project Manager

Client

Authors

Other CSIRO Staff

National Library

CMAR Libraries

Important Notice

Use of this Report

The use of this Report is subject to the terms on which it was prepared by CSIRO. In particular, the Report may only be used for the following purposes.

- this Report may be copied for distribution within the Client's organisation;
- the information in this Report may be used by the entity for which it was prepared ("the Client"), or by the Client's contractors and agents, for the Client's internal business operations (but not licensing to third parties);
- extracts of the Report distributed for these purposes must clearly note that the extract is part of a larger Report prepared by CSIRO for the Client.

The Report must not be used as a means of endorsement without the prior written consent of CSIRO.

The name, trade mark or logo of CSIRO must not be used without the prior written consent of CSIRO.

Table of Contents

List of Figures

List of Tables

EXECUTIVE SUMMARY

In 2004, the Upper Parramatta River Catchment Trust expressed interest in undertaking a research project on extreme rainfall events and it is the results from that study that are presented herein.

Floods are responsible for annual damages averaging $314 million, which is about 30% of all Australian weather-related damages (BTE, 2001). Information about extreme rainfall intensity and frequency for event-durations ranging from hours to multiple days is commonly needed for use in flood impact, design and mitigation applications. Flood impact models also rely upon information about how rapidly the average rainfall intensity increases with decreasing area, i.e. depth-area curves. These relationships are likely to be altered by climate change. Quantifying these changes requires very fine spatial resolution (4 km) and temporal resolution (hourly) using both dynamical modelling and statistical methods. It is computationally intensive to quantify these changes Australia-wide; thus, studies such as this are usually restricted to a relatively large area centred on the region (or catchment) of interest.

Since the early 1970s scientists and policymakers have been aware of the possibility of human activities impacting on the composition of the global atmosphere. By the mid 1980s atmospheric observations had confirmed that the atmosphere was changing and over the following two decades there has been a major international research effort to establish the nature of the changes and the causes. Since the late 1980s the scientific findings on atmospheric change and the potential for human based changes in the Earth's climate have been reviewed and summarised by the Intergovernmental Panel on Climate Change (IPCC).

Climate changes projections are based upon the outputs from global and regional climate models that account for possible changes in the emissions of key greenhouse gases and aerosols. Studies based on different climate models and emissions scenarios show that by 2100, differences in emissions scenarios and different climate model sensitivities contribute similar amounts to the uncertainty in global average surface temperature change. Projections of future regional climate are subject to three key uncertainties. The first of these is related to uncertainties in greenhouse gas emissions and the second is related to the climate sensitivity of climate models. Climate sensitivity is a measure of the strength and rapidity of the surface temperature response to greenhouse gas forcing. The third uncertainty is related to differing spatial patterns of change (i.e. response of regional climate) between climate models. The development of climate change projections on a regional scale relies upon analysing as many Global Climate Models (GCMs) and Regional Climate Models (RCMs) as is feasible to ensure that uncertainty due to the climate sensitivity of different models is captured. It is necessary to use model output available with a daily temporal resolution to identify severe weather events, such as extreme rainfall and wind events. However, daily model variables are not available for many of the GCM simulations to which there is general access. Thus, our analysis is limited to the results from CSIRO climate models. When considering results from a single (or small number of) model simulation(s), there is concern as to the reliability and generality of the results and this concern needs to be considered when using the results described herein.

Of the six illustrative scenarios chosen by the IPCC, the A2 scenario has been used for most global climate modelling undertaken by CSIRO since the late 1990s and is the scenario considered in this report. At that time, this scenario (one of self reliance, continuously increasing population, regionally oriented economic growth and slow technological change) was considered to be a "worst case" condition and thus considered to provide the upper bound for climate change

projections and the impacts of climate change. The IPCC recognised that the capacity of the oceans and the terrestrial biosphere to absorb increasing emissions would decrease over time but recent observations (e.g Rahmstorf *et al.*, 2007; Canadell *et al.*, 2007) suggest that absorptive capacity has been falling more rapidly than estimated by the main models. If these trends continue, a greater proportion of emitted carbon dioxide will remain in the atmosphere in the coming years and this will exacerbate the warming trend consequences of these unexpectedly high levels of emissions in the early years of the twenty-first century will be felt in future decades. Thus, it appears that the choice of the A2 scenario can no longer be considered a "worst case" scenario and now may be considered as "realistic" or even "optimistic".

This study uses an "integrated hierarchy of models" as recommended in the IPCC Third Assessment report (IPCC, 2001). In this approach, coarse resolution global and regional climate models provide the initial and boundary conditions for progressively finer resolution models. In general, these high-resolution simulations have been able to represent the spatial distribution of extreme rainfall realistically and the magnitude of the extremes is close to observed, although there is an apparent over-estimation of extremes in various mountainous regions.

Climate changes simulations based on climates representative of 2030 and 2070, show that there is considerable spatial variation in the regions of extreme rainfall increase and the magnitude of that increase. To overcome difficulties inherent in the analysis of spatially varying outputs, ensemble averages and "consensus" maps were calculated.

Widespread increases in extreme rainfall intensity are not projected to occur until the second half of the 21st Century and will predominantly be experienced by shorter duration events. By 2070 the 2-hour and 24-hour rainfall events are projected to experience widespread increases in intensity for most regions. The 2-hours events are projected to experience a larger increase in intensity than the 24-hour and 72-hour events. By comparing the results obtained by averaging over the top 10 and top 50 events it is apparent that the less frequent events are projected to experience greater percentage increases in intensity than the more frequent events. In some locations, for example west of Katoomba, the recurrence interval curves for the current climate and 2070 are likely to cross, especially for rainfall durations of 24-hours and longer. For these durations the low frequency events are projected to become more intense in the future and the higher frequency events less intense. Thus, when extreme rainfall events occur in the future they are likely to be characterised by more intense bursts of rainfall than currently occurs but, in many locations, with a total accumulation smaller than occurs in the current climate. A comparison of the projections for 2030 indicates that the impact of global warming on extreme rainfall may be non-linear, with widespread decreases in extreme rainfall intensity in the early 21st Century which gradually change with time to become increases in extreme rainfall intensity.

Outputs from the Extreme Value Analysis (EVA) have been used to create (1) return period curves, (2) intensity-frequency-duration curves for selected locations in the study region, and temporal curves for the entire region. Examination of the return period and intensity-frequency-duration curves, combined with the spatial patterns of change results, highlights the difficulty of defining location-specific values for projected changes in extreme rainfall intensity due to climate change. Recommendations to accounting for climate change in hydrological applications are described and brief examples given. The temporal curves also suggest that in the future the main rainfall burst in longer duration (i.e. 72-hour) events may occur earlier than at present.

The results form this study highlight the importance of considering the results from more than one model when developing projections of climate change. The CCAM output used to initialise

RAMS in this study originates from simulations that have been undertaken between 2003 and 2007 using different versions and configuration of the model and different grid spacings. Ideally, any future downscaling work should use a standard configuration and version of the model so that this form of model uncertainty can be ruled out.

1. INTRODUCTION

The CSIRO Climatic Extremes research group (CER) is investigating rainfall intensity-frequency-duration (IFD) and depth-area curves for western Sydney and surrounding areas for present day and projected future conditions in collaboration with the Upper Parramatta River Catchment Trust (now the Sydney Catchment Management Authority) and its partners. The other objectives of the project are:

- Obtain a "broad brush" understanding of the likely changes in average and extreme rainfall under enhanced greenhouse conditions (core).
- Quantify the likely future changes to the rainfall frequency characteristics of the study area due to global warming (core).
- Assess the impact of decadal-scale climate fluctuations on rainfall frequency characteristics (subsidiary).

The work plan consisted of four components couched within a three-year timeframe. The objectives of Components 1 to 3 are to provide information on rainfall IFD and depth-area curves for durations *less* than 6 hr for present day and projected future conditions, respectively. This information is critical for flood design applications. The results from these components of the project will be presented in a separate report.

This report presents the results from Component 4 of the project, specifically the high resolution dynamical downscaling of extreme rainfall events for the current climate and the climates of 2030 and 2070. This component has been undertaken as a joint project with the Department of Climate Change (formerly the AGO). The tasks are:

1. Identification of candidate cases,
2. High-resolution simulation of extreme rainfall events at a grid spacing of approximately 5km,
3. Analysis of downscaled events and preparation of IFD and depth-area curves for durations of less than 1 hour to 72 hours.

Within this report results for three 40-year time slices are presented. The "1980" or current climate refers to the climate for the atmosphere with greenhouse gas concentrations corresponding to the 1961-2000 period, while the "2030" climate has projected concentrations corresponding to the 2011-2050 period for the A2 scenario. Similarly the "2070" represents the 40 year timeslice 2051-2090.

The report is set out as follows: Section 2 presents background information on climate change, it describes the uncertainties inherent in the science and provide some background on scenarios and the choice of scenario used in this report. Section 3 describes the data used in the dynamical downscaling components of the project. It introduces the Global and Regional Climate Models (GCMs and RCMs) and describes the observational data and climate model simulations utilised in this study.

In Section 4 we describe the synoptic typing procedure used to evaluate the skill of the regional climate models in representing the synoptic situations associated with observed present-day extreme precipitation events affecting the study region. Results and discussion from the synoptic typing are presented here and the impact of climate change on these weather systems addressed.

The results from the dynamical downscaling are presented jn Section 5. These results are presented in terms of maps showing the geographical distribution of the changes and graphs illustrating changes to Average Recurrence Interval (ARI) and Intensity-Frequency-Duration curves for selected locations. A discussion of the results is provided and recommendations as to how best to use the results is provided.

2. CLIMATE CHANGE

2.1 Impacts of climate change

Since the early 1970s scientists and policymakers have been aware of the possibility of human activities impacting on the composition of the global atmosphere. By the mid 1980s atmospheric observations had confirmed that the atmosphere was changing and over the following two decades there has been a major international research effort to establish the nature of the changes and the causes. Since the late 1980s the scientific findings on atmospheric change and the potential for human based changes in the Earth's climate have been reviewed and summarised by the Intergovernmental Panel on Climate Change (IPCC). The most recent report, the Fourth Assessment Report on the Physical Science Basis of climate change (IPCC 2007) had the following amongst its key conclusions:

- 'Global atmospheric concentrations of carbon dioxide, methane and nitrous oxide have increased markedly as a result of human activities since 1750 and now far exceed pre-industrial values determined from ice cores spanning many thousands of years '
- 'Warming of the climate system is unequivocal,'
- 'Most of the observed increase in globally averaged temperatures since the mid-20th century is very likely due to the observed increase in anthropogenic greenhouse gas concentrations. …Discernible human influences now extend to other aspects of climate, including ocean warming, continental average temperatures, temperature extremes and wind patterns '
- 'Continued greenhouse gas emissions at or above current rates would cause further warming and induce many changes in the global climate system during the 21st century that would very likely be larger than those observed during the 20th century. '

2.2 Uncertainties and climate change

Climate changes projections are based upon the outputs from global and regional climate models that account for possible changes in the emissions of key greenhouse gases and aerosols. The emissions are those due to human activities, such as energy generation, transport, agriculture, land clearing, industrial processes and waste. To provide a basis for estimating future climate change, the IPCC began the development of a new set of greenhouse gas emissions scenarios in 1996 (IPCC, 2000) that attempt to account for future population growth, technological change and social and political behaviour. The *Special Report on Emissions Scenarios* (SRES) produced a set of 40 scenarios based around 4 different "storylines" that describe the relationships between the forces driving the greenhouse gas emissions and their evolution (see Figure 1a). Carbon cycle models are used to convert these emissions into atmospheric concentrations (Figure 1b), allowing for various processes involving the land, ocean and atmosphere. Increasing concentrations of greenhouse gases affect the radiative balance of the Earth. This balance determines the Earth's average temperature. These SRES greenhouse gas concentrations are converted to a radiative forcing of the climate system.

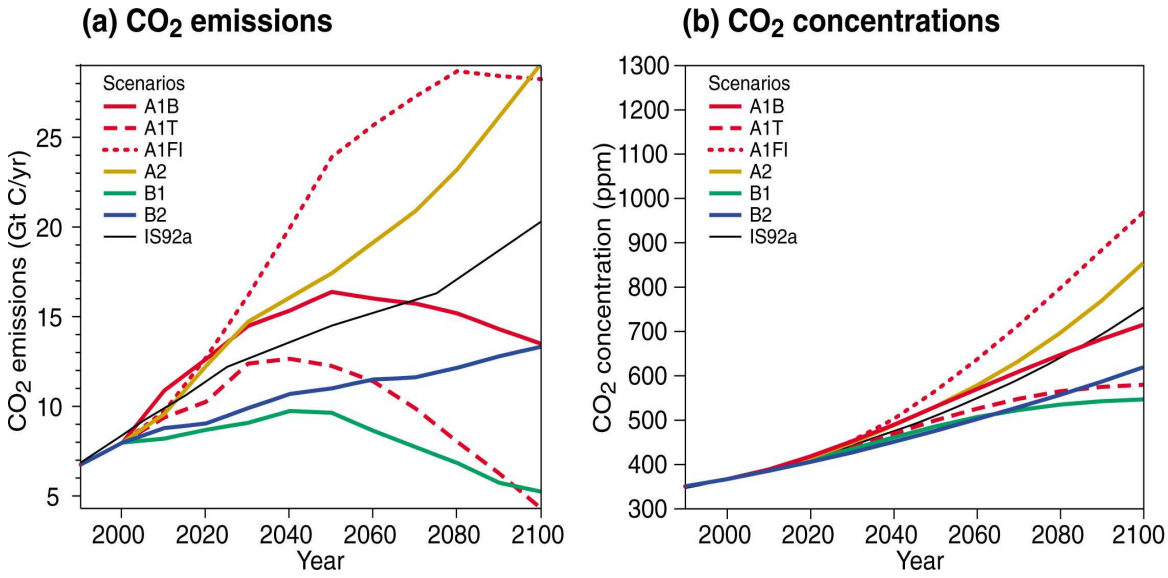

Figure 1: (a) Anthropogenic emissions and (b) atmospheric concentrations of carbon dioxide (CO_2) for six SRES scenarios and the IS92a scenario from the IPCC Second Assessment Report in 1996 (IPCC 2001).

Climate model equations are based on well-established laws of physics, such as conservation of mass, energy and momentum and have been tested against observations. This provides a major source of confidence in the use of models for climate projection. The other basis for confidence comes from the ability of models to represent current and past climates, as well as observed climate changes. The most important limitation of models is that a number of important physical processes occur at scales too small to be explicitly resolved by the model, and therefore these have to be represented in approximate form as they interact with the larger scales. Differences in the representation of such processes are the principal cause of differences in the magnitude and patterns of climate change found in different models. Climate model responses are most uncertain in how they represent feedback effects, particularly those dealing with changes to cloud regimes and ocean-atmosphere interactions. Studies based on different climate models and emissions scenarios show that by 2100, differences in emissions scenarios and different climate model sensitivities contribute similar amounts to the uncertainty in global average surface temperature change.

Projections of future regional climate are subject to three key uncertainties. The first of these is related to uncertainties in greenhouse gas emissions and the second is related to the climate sensitivity of climate models. Climate sensitivity is a measure of the strength and rapidity of the surface temperature response to greenhouse gas forcing. The third uncertainty is related to differing spatial patterns of change (i.e. response of regional climate) between climate models.

The development of climate change projections on a regional scale relies upon analysing as many Global Climate Models (GCMs) and Regional Climate Models (RCMs) as is feasible to ensure that uncertainty due to the climate sensitivity of different models is captured. It is necessary to use model output available with a daily temporal resolution to identify severe weather events, such as extreme rainfall and wind events. However, daily model variables are not available for many of the GCM simulations to which there is general access. Thus, our analysis is limited to the results from CSIRO climate models. When considering results from a single (or small number of) model simulation(s), there is concern as to the reliability and generality of the results and this concern needs to be considered when using the results described herein.

It is well known that there for any given application there is no one GCM that is superior to its counterparts in every aspect of interest. Nevertheless, previous studies suggest that a handful of models can be identified according to several (though incomplete) criteria. Suppiah *et al.* (2007) used measures of RMS error and pattern correlations to evaluate 23 climate model simulations performed for the IPCC 4th Assessment Report to produce climate change projections of Australian rainfall and temperature. They found that the CSIRO Mark 3 GCM (the parent model used in 2 of the 3 RCM simulations used herein) had a ranking of equal 11th out of the 23 models. A second study (Perkins *et al.*, 2007) used probability density functions of daily simulations of precipitation, minimum temperature, and maximum temperature for 12 regions of Australia to evaluate and rank coupled climate models used in the 4th Assessment Report of the IPCC. They found that over all three variables considered the CSIRO Mark 3 GCM ranked second in skill. Thus, in terms of Australian climate, the CSIRO Mark 3 GCM could be described as a "mid- to upper-level performer".

Rainfall changes are not directly forced by rising greenhouse gases but a warmer atmosphere can hold more water vapour, and hence produce heavier rainfall. Rainfall over some parts of Australia may change little, but elsewhere either decreases or increases may occur due to small differences in the circulation and other processes, discussed above. Projected rainfall changes for Australia are documented in CSIRO and Bureau of Meteorology, 2007. Near term projections (2030) are based on the mid-range A1B scenario as model to model differences are larger than the differences between the various emissions scenarios. *"Over the next few decades, the variation in emissions of greenhouse gases and aerosols represented by the SRES scenarios makes only a small contribution to uncertainty in global warming (and by extension regional warming and other changes in climate). This is because near-term changes in climate are strongly affected by inertia in the climate system due to past greenhouse gas emissions, whereas climate changes later in the century are more dependent on the particular pattern of greenhouse gas emissions that occur through the century."* Projected changes for 2030, can be summarised as a decrease in annual average rainfall for most of the continent, especially along the southern fringe. The 'top end' is likely to experience little change in annual average rainfall. For projected changes centred on 2050 and 2070, variations are due to differences between both models and emission scenarios. Projected changes for 2050 and 2070 for each of the emission scenarios are presents in Appendix A of that report.

Extreme values statistics have been applied to the outputs from a suite of international climate change simulations to create projections of changes in extreme rainfall intensity. The model simulations used are relatively coarse-resolution global climate models that were completed and made available for analysis as part of the IPCC's Fourth Assessment Report published in 2007. One of the simulations used in the extreme value analysis (CSIRO Mk3.0) has been further downscaled and the results are presented in this report. Figure 2 shows projected changes, relative to 1980, in the 20-year ARI for 2046-2065 for 9 of the models for the A2 scenario. These results illustrate the uncertainty in climate change studies described above, in particular differing spatial patterns of change (i.e. response of regional climate) between climate models.

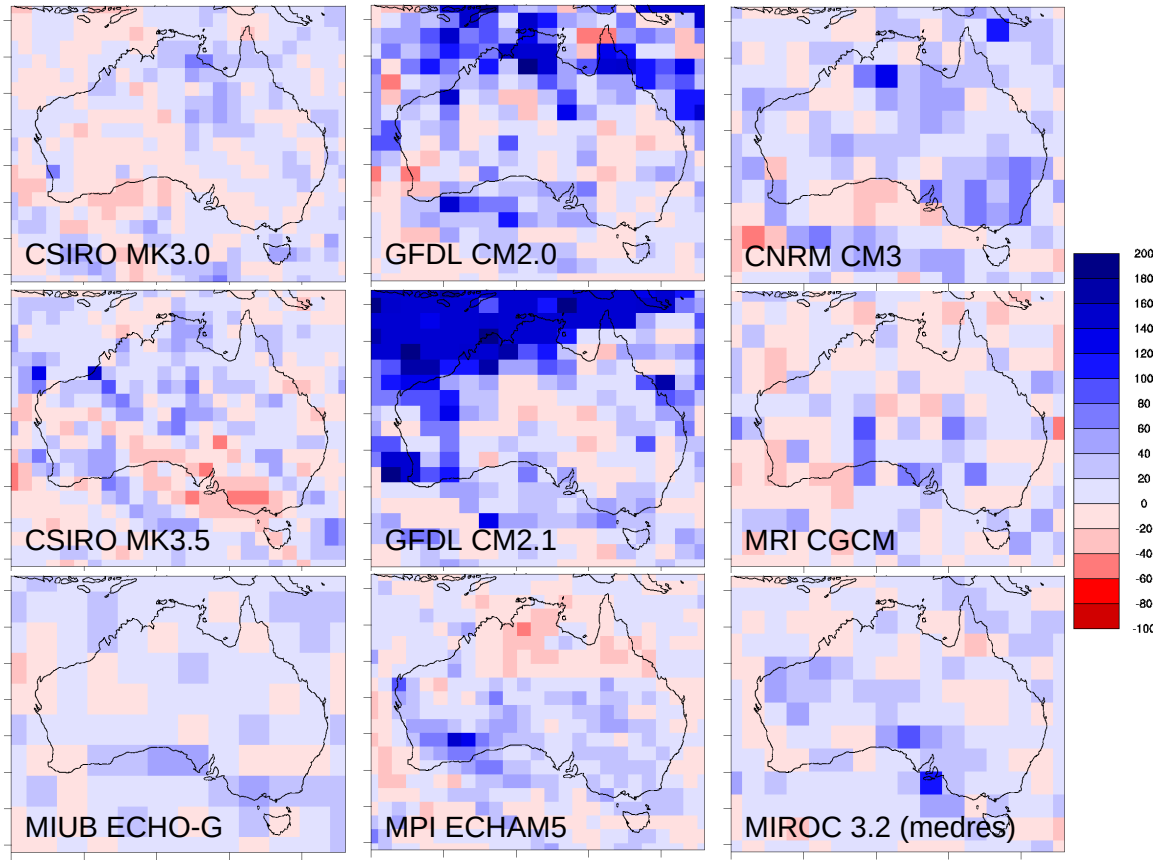

Figure 2: Projected change for 2046-2065 of the 20-year ARI 24-hour rainfall based on outputs from 9 international climate change GCMs forced with the A2 scenario.

The coarse spatial resolution of climate models remains a limitation on their ability to simulate the details of regional climate change, especially changes in extreme events. Statistical and dynamical downscaling techniques are used to translate the projections obtained from coarse-resolution climate models to the catchment and rain-gauge scale required by hydrologists and planners. Global and regional climate models show a broad qualitative agreement with the downscaled results. However, downscaling is able to identify important localised regions of projected increases in rainfall intensity not captured by the coarser models because the high resolution models are better able to represent local topographic effects (orography and land-sea contrasts) and better able to represent the convection that is a characteristic of extreme rainfall events.

2.3 Choice of scenario

The reader is referred to the report "Climate Change in Australia" (CSIRO and Bureau of Meteorology, 2007) for a description of the four storylines that form the basis of the scenarios used within climate change science. Of the six illustrative scenarios chosen by the IPCC, the A2 scenario has been used for most global climate modelling undertaken by CSIRO since the late 1990s and is the scenario considered in this report. At that time, this scenario (one of self reliance, continuously increasing population, regionally oriented economic growth and slow technological change) was considered to be a "worst case" condition and thus considered to provide the upper bound for climate change projections and the impacts of climate change.

Rahmstorf *et al* (2007) present recent observed climate trends for carbon dioxide concentration, global mean air temperature, and global sea level, and compare these trends to previous model

projections as summarized in IPCC (2001). Their results suggest that the climate system may be responding more quickly than climate models indicate. Their key results are:

- Since 1990 global mean surface temperature increase has been measured at 0.33ºC which is in the upper end of the range predicted by the IPCC in the Third Assessment Report in 2001.

- Since 1990 the observed sea level has been rising faster than the rise projected by models, as shown both by a reconstruction using primarily tide gauge data and, since 1993, by satellite altimeter data. Sea level rise since 1993 has shown a linear trend of 3.3 ± 0.4 mm/year. In 2001, the IPCC projected a best estimate rise of less than 2mm/year.

They state "*Overall, these observational data underscore the concerns about global climate change. Previous projections, as summarized by IPCC, have not exaggerated but may in some respects even have underestimated the change, in particular for sea level.*"

The changes that have been observed to date are a result of historic emissions due to the lag in the climate system resulting from the slow response of the oceans to absorb emissions. The IPCC Fourth Assessment Report recognised that the capacity of the oceans and the terrestrial biosphere to absorb increasing emissions would decrease over time. Observations suggest that absorptive capacity has been falling more rapidly than estimated by the main models. If these trends continue, a greater proportion of emitted carbon dioxide will remain in the atmosphere in the coming years and this will exacerbate the warming trend (Canadell *et al*., 2007).

Global emissions of carbon dioxide have accelerated sharply since about 2000 due to increases in fossil fuel burning and industrial processes, with this growth dominated by economic growth in major developing countries such as China and India. Initial analysis carried out for the Garnaut Review (Garnaut 2008) suggests the likelihood, under business as usual, of continued growth of emissions in excess of the highest IPCC scenarios. Assuming more realistic growth and energy intensity for China and India alone produces higher projected global emissions from fuel combustion than even the most pessimistic of the IPCC scenarios out to 2030 (Sheehan and Sun, 2007). The consequences of these unexpectedly high levels of emissions in the early years of the twenty-first century will be felt in future decades.

Thus, it appears that the choice of the A2 scenario can no longer be considered a "worst case" scenario and now may be considered as "realistic" or even "optimistic".

3. DATA AND MODELS

3.1 Study area & rainfall data

The study area has a homogeneous climate roughly bounded by longitudes 149.5º to 153º E; and latitudes 31.5º to 36ºS. The focus is on the coastal drainage areas of this region only (i.e., the SW corner of the region defined above would be ignored completely). The river basins included in the study area are shown in Figure 3.

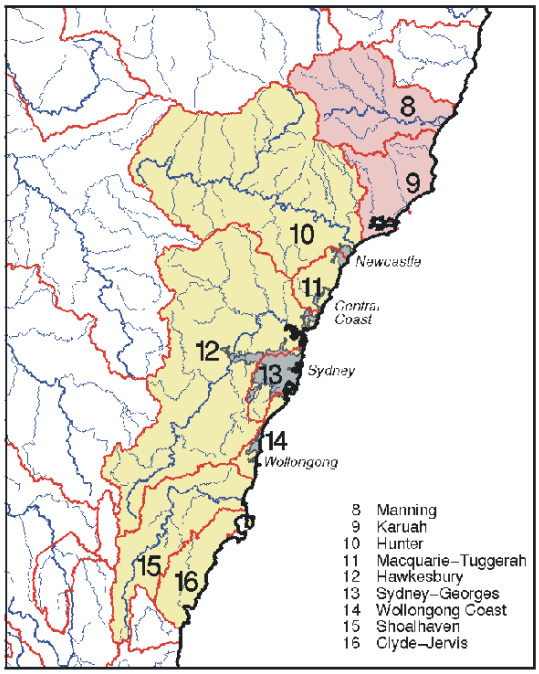

Figure 3: Location of Study Area

Rainfall data used in this component of the project comes from the Bureau of Meteorology's (BOM) rainfall network. This network includes over 6000 stations nation-wide, all of which record daily rainfall using standardised equipment and observing protocols. The observations are made at 0900 hours each day, with the 24-hour rainfall total being recorded against the day of observation. Mostly these gauges are operated by volunteers, often at workplaces like post offices, local government offices and farms. As a consequence, the quality of the data is quite variable, even for different time periods at a single station. Details of the stations used are tabulated in Appendix A.

Some of the data quality issues have been discussed by Lavery *et al.* (1992) and Viney and Bates (2004). The data quality is affected by a number of reasons including observer's inconsistencies and exposure changes (changes in the height or structure of the gauge; changes in the windfield associated with growing trees or the construction of nearby buildings).

Missing observations in the rainfall records arise from two main sources. The first appears to relate to communication and data management issues. The second source of missing data occurs when observers are absent from the station or otherwise unable to observe the gauge for a period of one or more days. When the observer returns to the gauge it contains rainwater that potentially

fell over a period of two or more days. In these circumstances the observer records the accumulation period as well as the rainfall amount, which is entered against the date of observation. Viney and Bates (2004) have discussed the issues related to these "untagged accumulations".

A second set of rainfall data have been used. These are gridded rainfall data obtained from the SILO dataset (Jeffrey *et al.*, 2001) produced and distributed by the Queensland Department of Natural Resources, Mines and Energy. These data are interpolations derived from the Bureau of Meteorology's rainfall network. The quality of the data varies across Australia, depending on the proximity of reporting stations. All plots based on observations use these data.

3.2 NCEP Reanalysis data

Mean sea level pressure (MSLP) data from the National Centers for Environmental Prediction (NCEP) reanalysis dataset have been used to characterise the synoptic scale weather systems that are conducive to extreme rainfall in the study region. The MSLP data are available in a gridded format at a horizontal resolution of 2.5°× 2.5° (approximately 250 km) every six hours from 1958 to the present. In this study the MSLP data have been analysed twice daily for the extreme rainfall events. Specific humidity, vertical velocity and winds at 850, 700 and 500 hPa have also been analysed for the extreme rainfall days. These fields help identify the mechanisms that produce extreme rainfall in the region.

3.3 The Global and Regional Climate Models

This study uses an "integrated hierarchy of models" as recommended in the IPCC Third Assessment report (IPCC, 2001). In this approach, coarse resolution global and regional climate models provide the initial and boundary conditions for progressively finer resolution models. The coarsest model "used" in this study is the CSIRO Global Climate Model. Outputs from 2 versions of the model were used - the Mark 2 and newer Mark 3 versions of the model. Two climate change simulations were available from the Mark 3 version of the model - the UK2 and M20 simulations. The CSIRO GCM has been used to simulate the climate from 1961 to 2100 under an SRES A2 greenhouse gas emissions scenario (IPCC, 2000). Mark 3 has a horizontal grid spacing of approximately at 1.85°× 1.85° and has 18 levels in the vertical. The older Mark 2 model has a grid spacing of approximately 3.5°× 3.5° and has 9 levels in the vertical

These three GCM simulations provided the initial conditions and boundary nudging for CSIRO's regional climate model known as the cubic conformal atmospheric model (CCAM). CCAM is a global model that utilises a stretched grid in which the Earth is mapped onto a cube. The mapping is such that higher resolution is focussed over the region of interest and lower resolution is on the opposite side of the Earth, remote from the region of interest. To overcome the potential errors that could result from the poor resolution in the remote areas, the model solution in the lowest resolution areas is nudged heavily towards the solution of the parent GCM. Two of the cubic conformal model simulations considered in this study had their highest resolution, of approximately 65 km, centred on Australia (see Figure 4). In this region the CCAM winds above 500 hPa are nudged towards those of the parent GCM. This approach ensures that the CCAM storm tracks do not diverge from those of the parent GCM (i.e. the gross features of the atmospheric circulation are maintained) whilst allowing the model to form smaller scale atmospheric features that are not evident in the parent GCM. Below 500 hPa the model solution is

allowed to evolve freely. The third simulation (CC-M20) had a finer grid of approximately 20 km centred over the lower Murray-Darling Basin.

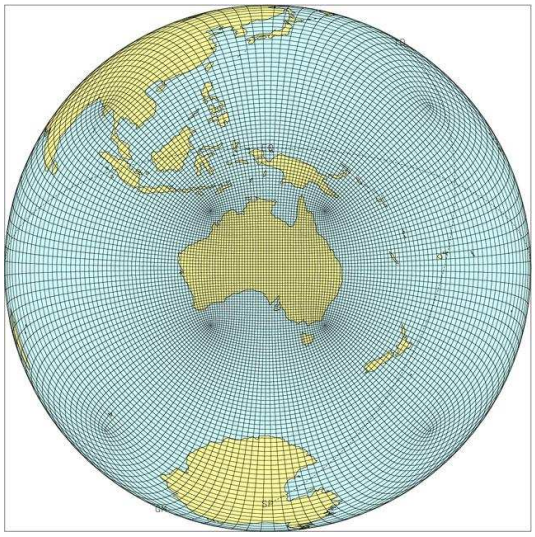

Figure 4: The stretched grid of the cubic conformal atmospheric model.

Outside the high resolution region, the CC-Mk2 model solutions were nudged towards those of the CSIRO Mark 2 simulation, the CC-UK2 model was nudged towards the simulation of CSIRO Mark 3-UK2 simulation and the CC-M20 model was nudged towards the simulation of the CSIRO Mark 3-M20 model. The improvements provided by these downscaling and nudging techniques are documented by Abbs and McInnes (2004) in a study of coincident extreme wind and rainfall events affecting southeast Queensland and northern New South Wales. They found that the CC-Mk2 and CC-UK2 models were better able to represent the climatology of the weather patterns that cause extreme winds and/or rainfall in this region than the Mark 3 GCM.

Further information related to the downscaling methodology is provided in Section 5.

4. CLIMATOLOGY OF EXTREME RAINFALL WEATHER EVENTS

4.1 Data, models and methodology

The data set used for the analysis of observed extreme rainfall days is the daily rainfall data set maintained by the Australian Bureau of Meteorology (BoM). The daily rainfall record based on these gauges is for the period 9:00 am on the preceding day to 9:00 am on the day of the record. On a site-by-site basis the daily rainfall record is variable both in length and quality. The stations considered in the analysis were all stations for which observations were available in the period between 1960 and 2000. The record was required to be at least 80% complete as identified by the "quality flag" for the station. 1960 was chosen as the start date for this analysis in an effort to balance the needs of using a long rainfall time series and covering the period for which NCEP reanalysis data is available.

Daily rainfall records for stations that meet these criteria were used to create station time series for 1-day, 2-day, 3-day, 4-day and 5-day totals. The days chosen for analysis were those on which the 1-day total exceeded 100 mm at one or more stations and on which at least 10% of study-region stations recorded at least 30 mm of rainfall. This method identifies the large-scale extreme rainfall events that result in riverine flooding, rather than the short duration, localised events associated with isolated thunderstorms and perhaps flash flooding. Frequently the days selected using this technique were consecutive days that were part of a multi-day rainfall event. The selected were manually edited so that only the day of highest rainfall from each rainfall event was used in the synoptic typing. For example, the selection criteria described above identified the period 5-7 August 1986 as an extreme rainfall event and 6 August 1986 was selected as being the period of maximum rainfall for this event. A similar technique was used to identify the extreme rainfall days from the climate models.

Thus the model data set has been used to provide a set of extreme rainfall days based on the modelled rainfall. Modelled rainfall is very sensitive to the horizontal resolution of the parent model, and thus with a coarse model grid spacing (eg. 60km × 60km in CCAM) the model is unable to capture the small-scale convective processes that produce extreme rainfall. In reality, many extreme rainfall events are embedded within larger synoptic-scale systems such as east coast lows, monsoon depressions and mid-latitude frontal systems. These events are often associated with the "ingredients" conducive to extreme rainfall – high levels of atmospheric moisture; strong ascent, high time-averaged precipitation efficiency and they are long-lived. Weather systems such as these are captured by the global and regional scale climate models, and thus any change in their frequency and intensity may impact on the characteristics of extreme rainfall in a region.

4.2 Synoptic typing

The pressure patterns associated with extreme rainfall are analysed to determine the synoptic-scale weather patterns that are conducive to the extreme weather conditions in the study region. The technique used is known as synoptic typing and follows the method of Yarnal (1993). This is a correlation-based, gridded map-typing technique in which days are grouped based on the Pearson product-moment correlations (r_{xy}) to establish the degree of similarity between map pairs. Similar fields are identified on the basis of similar spatial structures (i.e. highs and lows in similar positions) with little emphasis on the magnitude of the patterns.

To establish a synoptic climatology compatible with the output from the climate models, this technique was first applied to NCEP 12 UTC MSLP fields corresponding to the period approximately 12 hours before the recorded rainfall events. Thus, for the example used previously, the selection criteria identified 6 August 1986 as the date of maximum rainfall and thus the MSLP field for 12 UTC 5 August 1986 was selected for synoptic typing. The MSLP fields were extracted for the 81 points (9×9) corresponding to 145E to 165E and 45S to 25S: the region outlined by the dashed rectangle in Figure 5. The synoptic typing procedure is described fully in Appendix B.

The correlation-based synoptic typing technique has one significant advantage over other traditional synoptic climatological approaches such as Principal Components Analysis (Hewitson and Crane, 1992): the map patterns that are established by the typing procedure effectively define a “fingerprint” that can be directly used to "type" GCM output. A disadvantage of the approach is that by emphasizing the surface pressure fields it ignores the three-dimensional nature of atmospheric processes that are important in many applications including extreme rainfall.

4.2.1 Synoptic classification of modelled extreme rainfall events

After the typing procedure was completed for the observed extreme rainfall days using the NCEP reanalyses, the synoptic patterns were then used to identify similar patterns in each model and thus derive a climatology of modelled extreme rainfall types. The MSLP pattern for each day was first interpolated from the model grid to the 2.5°× 2.5° NCEP grid. The interpolated MSLP fields were then correlated with the MSLP grid for the “key days” identified in the synoptic typing of the observational dataset. The extreme rainfall days were classified into the synoptic type with the highest correlation above a threshold of 0.7. This analysis provides a measure of the number of extreme rainfall days in the model that can be classified according to the observed synoptic types and can also be used to identify the impact of climate change on the frequency of these events..

4.3 Synoptic climatology of observed events

The techniques described in Section 4.2 have been used to classify the weather events associated with extreme rainfall in the Central Coast of NSW study region. The resulting distribution is presented in Table 1.

Figure 5 shows the composite pressure patterns for each of the 5 types associated with extreme rainfall events affecting the Central Coast of NSW. The composite patterns have been obtained by averaging the MSLP patterns for the days that contribute to each synoptic type. These 5 synoptic types account for 77% of days considered. The remaining days were unclassified.

Extreme Rainfall Events (119 events)		
Type	**Number of events**	**Percentage of events**
1. Tasman High (NE flow)	37	31
2. East Coast Low	23	19
3. Tasman High (E flow)	14	12
4. East Coast Low	12	10
5. Bass Strait High (SE flow)	6	5
Unclassified	27	23

Table 1: The distribution of synoptic types for extreme rainfall events affecting the Central Coastal region of New South Wales

Type 1 is characterised by a high-pressure system in the Tasman Sea and a trough over inland Queensland. This pattern produces a large area of onshore north-easterly flow into the study region. The Type 1 case is characterised by a cut-off low above 700 hPa. This is accompanied by strong moisture advection, between 500 and 850 hPa, from the Coral Sea. Strong ascent is coincident with the high moisture values and these are centred over the study region. Types 2 and 4 are East Coast Lows; the main difference between the two patterns being the location of the surface ridge to the south. In these cases the cut off low extends from the surface to middle and upper levels of the atmosphere. The East Coast Lows are accompanied by strong moisture advection from the Coral Sea and a concentrated region of strong ascent centred over the study region.

The geographic distribution of rainfall for each synoptic type is shown in Figure 6. The Type 1, 2 and 4 distributions indicate that on average rainfall associated with these types is more widespread than for Types 3 and 5. Except for the Type 1 events, the highest rainfall maxima tend to occur in the Blue Mountains or along the Illawarra coastline south of Sydney. The Type 1 events also experience significant rainfall along the coastal strip between Newcastle and Sydney. The Hunter catchment tends to experience extreme rainfall under Type 1 or Type 2/4 conditions.

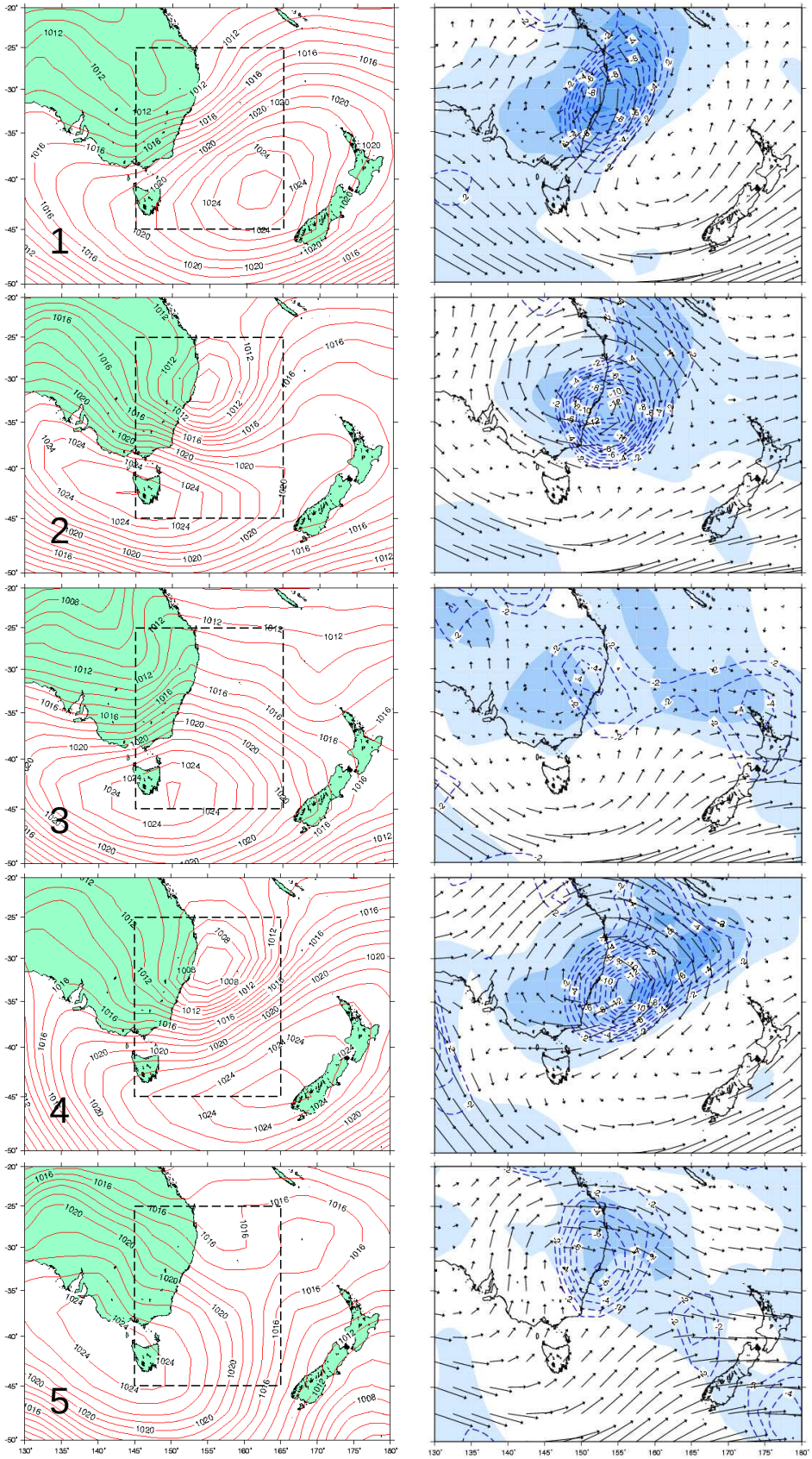

Figure 5: (left) Composite MSLP fields for the synoptic types associated with extreme rainfall along the Central Coast of NSW. (right) Composite upper level fields for each type. Shading denotes above average moisture content, the dashed lines enclose the region of strong ascent and the vectors indicate the direction and speed of the wind at 700hPa. Type 1 – 31%, Type 2 – 19%, Type 3 – 12%, Type 4 – 10% and Type 5 – 5%.

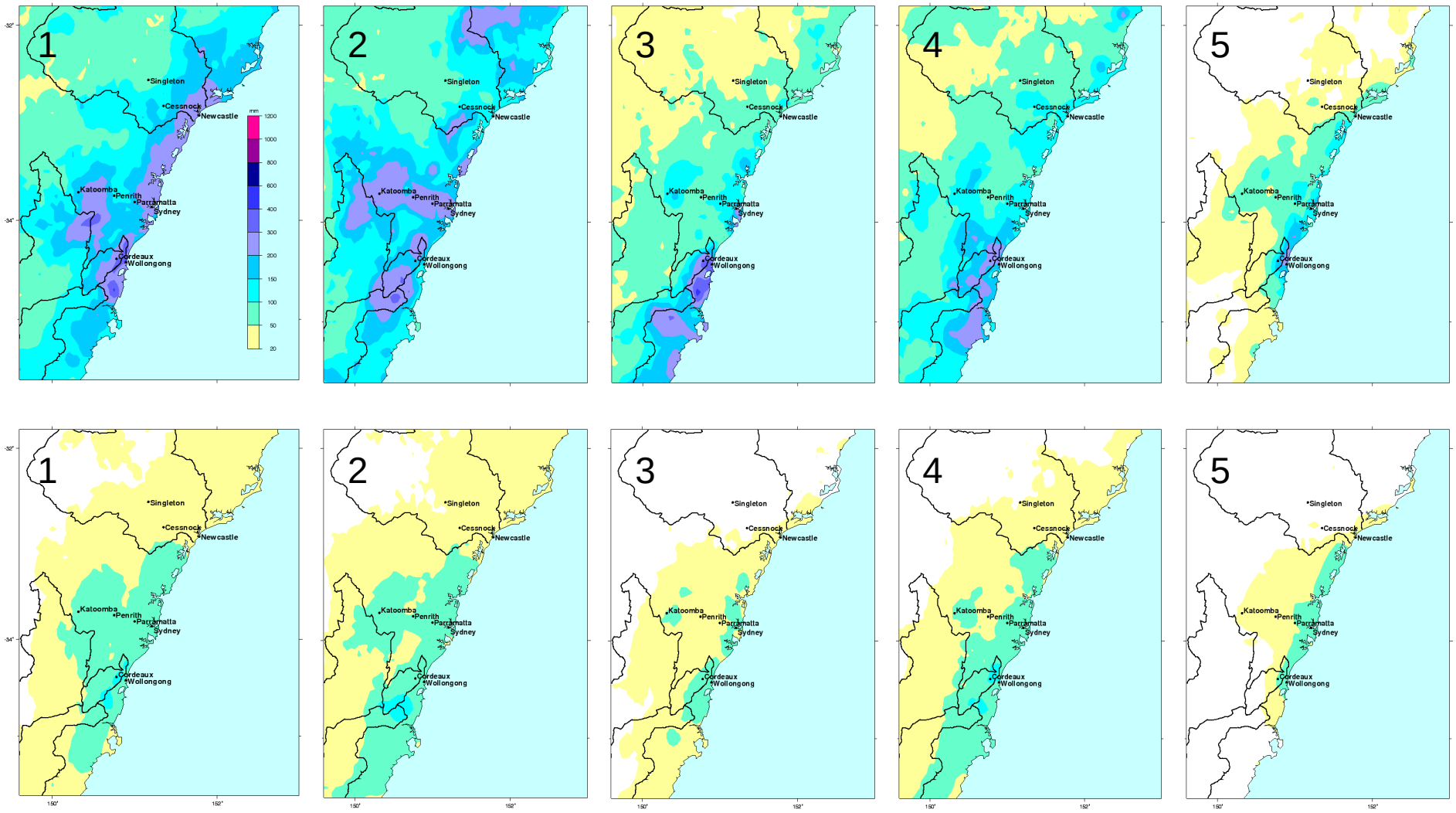

Figure 6: Geographic distribution of (top) maximum rainfall associated with each of the 5 synoptic types and (bottom) average rainfall associated with each type. The Hunter, Warragamba, Shoalhaven and Upper Nepean-Woronora catchments are indicated on each figure.

The MSLP pattern for each keyday has been used as a "finger print" to identify all days from 1960-2000 that correspond to these 5 types. The totals for the two East Coast Low Types (Types 2 and 4) have been combined in this analysis. The results from this analysis are presented in Table 2.

Days corresponding to Extreme Rainfall Types (1960-2000) 14976 days			
Type	**Number of days**	**Annual Mean (days)**	**Standard Deviation (days)**
1. Tasman High (NE flow)	686	17	5.7
2+4 East Coast Low	422	10	5.0
3. Tasman High (E flow)	976	24	7.7
5. Bass Strait High (SE flow)	730	18	6.0

Table 2: The occurrence of days with an MSLP pattern similar to those of extreme rainfall events.

MSLP patterns similar to those of extreme rainfall events occur on approximately 18% of days, with the Type 3 (Tasman High) case the most common; approximately 6% of days. East Coast Lows are the least frequent types occurring on approximately 3% of days.

The seasonal climatology of these events is shown in Figure 7 and shows that most events occur during the summer (DJF) and autumn (MAM) season for all types.

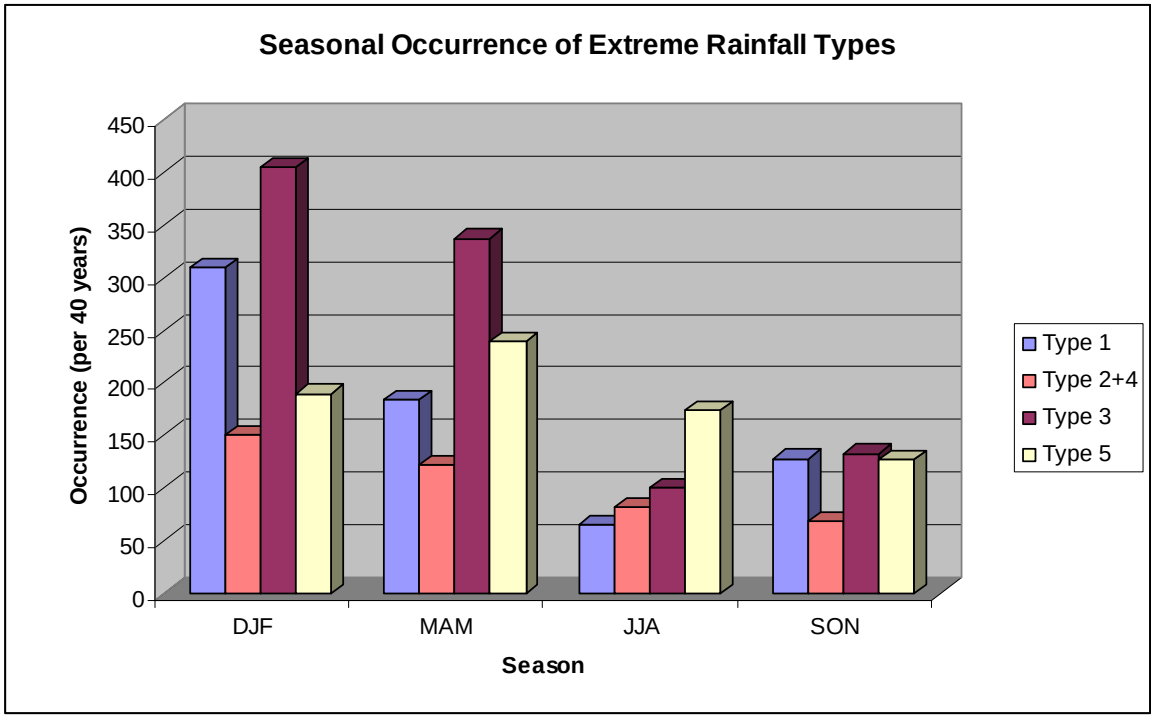

Figure 7: Seasonal occurrence of days with an MSLP pattern similar to those of extreme rainfall events. DJF=December-February, MAM=March-May, JJA=June-August, SON=September-November.

The time series from the synoptic typing analysis are presented in Figure 8. The time series for the total number of days corresponding to extreme rainfall types illustrates the significant inter-annual and inter-decadal variability of extreme rainfall; with the 1960s and 1970s characterised by more extreme rainfall events in most years when compared with the 1980s and 1990s.

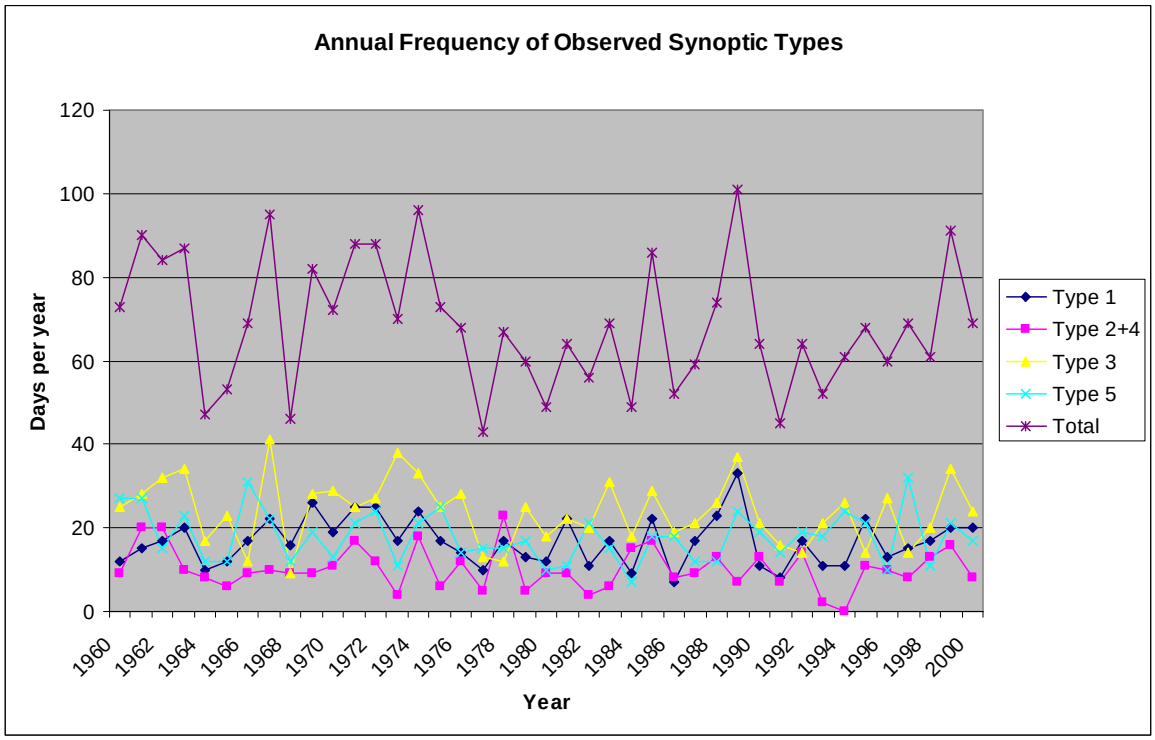

Figure 8: Time series of the annual frequency of synoptics types based on the NCEP reanalyses.

4.3.1 Synoptic climatology of modelled events

The synoptic types identified above have been used to "type" all days in the three climate simulations considered - CC-Mk2, CC-UK2, and CC-M20 - both to assess the ability of the models to capture these weather systems by comparing with the results in Table 2 and to identify possible impacts of climate change on the occurrence of these events. The results of this analysis are conducted for three time slices. The first time slice is referred to as the "current" or "1980" climate and refers to model outputs from the period when the concentrations of greenhouse gases used in the model are representative of the 40-year period, 1961-2000. Similarly, the "2030" and "2070" climates refer to the 40-years time slices 2011-2050 and 2051-2090 respectively.

The results of the climate model typing for the 1980 climate are shown in Table 3 and compared with the results from the NCEP reanalyses. These results indicate that the CC-UK2 and CC-M20 models are able to capture the occurrence of most weather types associated with extreme rainfall in the region, however, they under-estimate the frequency of East Coast Lows by approximately 50%. The CC-Mk2 model performs significantly worse than these models and under-estimated the occurrence of all types by at least 50%. Overall, the percentage of extreme rainfall types in CC-Mk2 is 40% of that found in the NCEP reanalyses. However, although the CC-Mk2 model under-estimates the occurrence of extreme rainfall types, the stratification by rainfall type (in percentage terms) is similar to that from the NCEP reanalyses.

Days corresponding to Extreme Rainfall Types 1980 time slice (40 years)				
Type	**NCEP (av/s.d./total/ %)**	**CC-UK2 (av/s.d./total/ %)**	**CC-M20 (ave/s.d./total/ %)**	**CC-Mk2 (ave/s.d./total/ %)**
1. Tasman High (NE flow)	17 / 5.7 / 686 / 25	24 / 7.7 / 974 / 28	18 / 5.6 / 706 / 30	8 / 3.8 / 302 / 27
2+4. East Coast Low	10 / 5.0 / 422 / 15	5 / 3.4 / 210 / 8	6 / 2.7 / 227 / 10	5 / 2.6 / 208 / 18
3. Tasman High (E flow)	24 / 7.7 / 976 / 35	24 / 6.7 / 978 / 38	23 / 6.4 / 939 / 40	6 / 4.0 / 302 / 28
5. Bass St High (SE flow)	18 / 6.0 / 730 / 25	10 / 3.5 / 410 / 16	11 / 4.4 / 447 / 20	8 / 3.6 / 309 / 27
Total	69 / 15.6 / 2814 / 100	63 / 14.3 / 2572 / 100	58 / 10.0 / 2319 / 100	28 / 8.4 / 1121 / 100

Table 3: The occurrence of days in the 3 climate models with an MSLP pattern similar to those of observed extreme rainfall events. av = annual average, s.d = standard deviation of yearly counts, total = total number of days per 40-year time slice, and % = percentage frequency of extreme rainfall type.

As illustrated in Figure 7, the seasonal distribution of extreme rainfall types shows a distinct maximum during the summer (DJF) and autumn (MAM) seasons. A similar analysis for the 3 models (Table 4) shows a similar distribution. The CC-UK2 and CC-M20 simulations over-estimate the occurrence of summer and autumn days while the CC-Mk2 model produces too many days in autumn and too few in summer.

Seasonal Distribution of Extreme Rainfall Days 1980 time slice (40 years)				
	DJF (%)	MAM (%)	JJA (%)	SON (%)
NCEP	37	31	15	16
CC-UK2	46	36	8	9
CC-M20	46	38	6	10
CC-Mk2	28	42	17	13

Table 4: Seasonal distribution of days in the 3 climate models with an MSLP pattern similar to those of observed extreme rainfall events.

4.3.2 Impact of climate change

The typing method has also been applied to future climate time slices and the results are presented in Table 5. The two better-performing models (CC-M20 and CC-UK2) both produce an 18% increase in the occurrence of East Coast Low days by 2070 and a possible increase in the occurrence of Type 3 systems. If this increase in East Coast Low occurrence is used to scale the current climate occurrence of these weather types, East Coast Lows will increase from an average of 10 days per year to 12 days per year in 2070. However, for the remaining types there is no agreement between these 2 models in possible changes in occurrence of MSLP patterns associated with extreme rainfall. Only the CC-UK2 model projects a decrease (3%) in the frequency of MSLP patterns similar to those that produce extreme rainfall events. The largest increase in frequency for these events is for the CC-M20 model which projects an increase of 13% by 2070 relative to the 1980 climate.

Number of days corresponding to Extreme Rainfall Types Future climate time slices (40 years)			
Type	**CC-UK2 (1980/2030/2070)**	**CC-M20 (1980/2030/2070)**	**CC-Mk2 (1980/2030/2070)**
1. Tasman High (NE flow)	974 / 878 / 883	706 / 747 / 815	302 / 339 / 364
2+4. East Coast Low	210 / 222 / 245	227 / 216 / 269	208 / 184 / 119
3. Tasman High (E flow)	978 / 999 / 999	939 / 1042 / 1101	302 / 336 / 378
5. Bass St High (SE flow)	410 / 424 / 371	447 / 423 / 446	309 / 383 / 315
Total	2572 / 2523 / 2498	2319 / 2428 / 2631	1121 / 1242 / 1176

Table 5: The total number of days per 40-year times slice in the 3 climate models with an MSLP pattern similar to those of observed extreme rainfall events. Results are presented for the 1980, 2030 and 2070 time slices.

5. DYNAMIC DOWNSCALING OF EXTREME RAINFALL

5.1 Dynamical downscaling methodology

The outputs from the three RCM simulations (CC-UK2, CC-M20 and CC-Mk2) have been used to identify extreme rainfall events affecting the study region and these events have been downscaled with a grid spacing of 4 km using The Regional Atmospheric Modelling System (RAMS). RAMS is a high-resolution, compressible, non-hydrostatic model. The physical processes represented by the model include an atmospheric boundary layer, soil and vegetation effects, long and short wave radiation, and the complex cloud processes that result in precipitation (ice, liquid and water vapour). It is a suitable tool for the simulation of extreme rainfall events and has previously been used to model the extreme rainfall events described in Abbs (1998) and McInnes *et al.* (2002). The configuration and validation of the model used here is presented in Abbs (2006). Seven extreme rainfall events that have affected the study region since the mid-1970s have been modelled and brief results are presented in Appendix C.

Three levels of interactive grid nesting were used; the outer grid had a resolution of 48km with the middle and finest resolution grids having a horizontal grid spacing of 16 km and 4 km respectively. At this grid spacing the shortest waves that can be resolved have a wavelength of 16 km; this is due to numerical constraints common to all atmospheric models (Pielke, 1984; Grasso, 2000). The terrain used on all model grids was interpolated from the Geosciences Australia 9 second digital elevation model. The vegetation was obtained from a USGS 30 second dataset. The impact of climate change on soil and vegetation has not been included in these simulations. The sea surface temperatures were interpolated from the RCM output. The high-resolution domain and terrain used for this study is shown in Figure 9.

For each set of RCM-based downscaling simulations, the most intense 1-day and 3-day rainfall events were identified for the study region grid points, for the “1980” or “current” climate and the “2030” and “2070” climates. The dates corresponding to these events were collated and individual events identified for downscaling. The corresponding atmospheric output fields were then extracted and these outputs interpolated horizontally and vertically to the outer model grid of RAMS. The climate model output also provided the temporal forcing on the lateral boundaries of the outer model grid. The temporal forcing is applied by nudging the model solution at each model time step to the atmospheric fields provided by the analyses. This nudging is stronger on the model boundaries than in the centre of the model domain. In this way the model solution keeps track of the large-scale atmospheric forcing while also developing its own fine-scale circulations that are a response to the orography, land-surface moisture and temperature and smaller scale atmospheric processes. Since the modelling approach used in this study was multi-day ‘event-based’, rather than a continuous, multi-decadal length simulation, the prescription of boundary conditions does not suffer from the issues that are problematic for limited-area regional climate models. Instead, the prescription of boundary conditions for the event-based approach follows that developed and used successfully for numerical weather prediction.

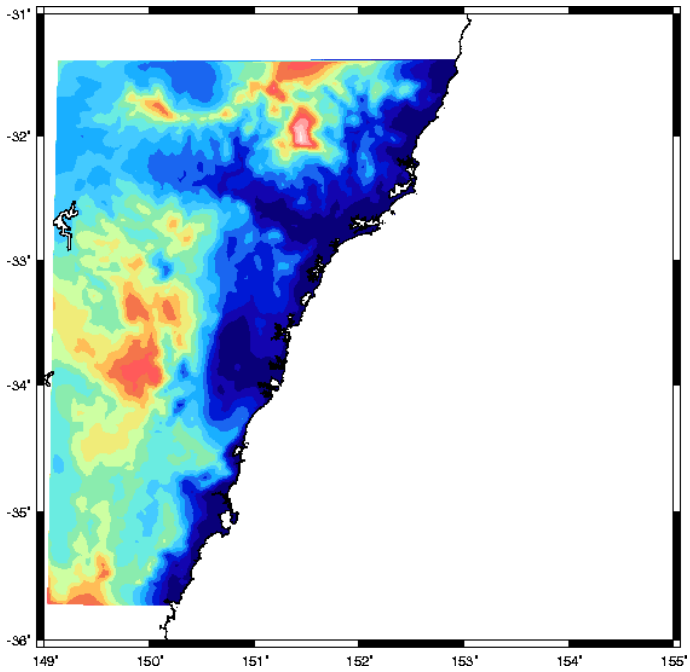

Figure 9: High-resolution (4 km grid spacing) domain and terrain used for the simulations described herein.

Each of the identified extreme rainfall events was simulated from day (–2) to day (+2) and model fields archived with a 30-minute increment. The shortest simulations cover a 96-hour period centred on the rainfall event but most simulations are of longer duration. The 30-minute rainfall output from the simulations has been used to define the 2, 12, 24, 48, 72 and 96-hour rainfall maxima for each event. The following analysis concentrates on the maximum rainfall falling within the 2, 24 and 72-hour periods. At least one hundred events were simulated for each of the current, 2030 and 2070 climates from each of the three RCMs. This number (100) was determined in a pilot study based on the Mark3 GCM. In that study extreme rainfall events corresponding to the 1980 climate were selected for the study region and downscaled in 25-member sub-sample blocks starting with the highest-ranked events. This method implicitly assumes that the highest rainfall events simulated by the GCM will also be the highest rainfall events when downscaled. When various statistics (such as return period curves) derived from the total number of events no longer changed significantly the sub-sampling ceased as it was assumed that the most intense rainfall events affecting the region had been sampled. This occurred after (approximately) the 70 most extreme GCM events had been downscaled. The sample size was increased to 100 and it was considered that the results from that sample size were robust and representative of the climate for current climate extreme rainfall events. It is assumed that an identical sample size is adequate for analysis of the 2030 and 2070 climates. For the remainder of this report, unless otherwise stated, the nomenclature, R-CC-Mk2, R-CC-UK2 and R-CC-M20 refers to results from RAMS nested in the respective RCM.

5.2 Comparison with observed extreme rainfall and the impact of climate change.

Gridded daily rainfall data from the SILO dataset have been extracted for the region for the 40-year period 1960-1999. For each grid point, the daily rainfall time series has been sorted and the heaviest rainfall events in the 40-year period identified. The most extreme 1-day and 3-day rainfall events for each grid point are plotted in Figure 10.

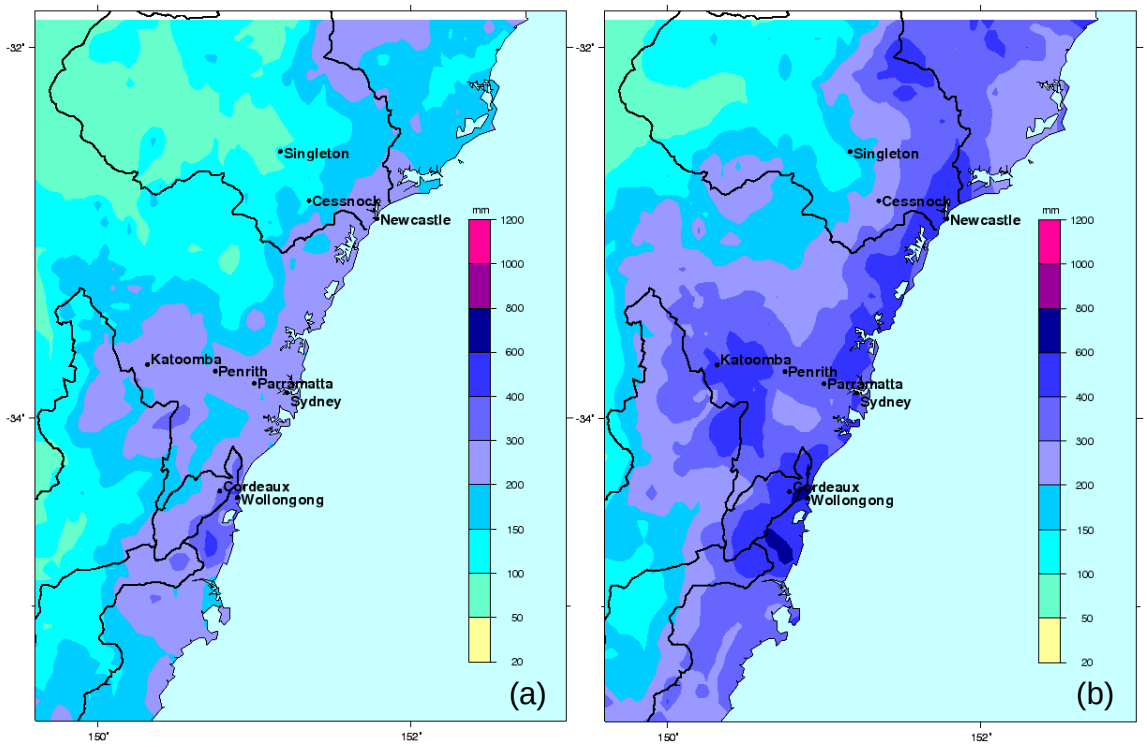

Figure 10: Most extreme (a) 1-day rainfall and (b) 3-day rainfall for each grid point in the SILO dataset for the period 1960-1999. The Hunter, Warragamba, Shoalhaven and Upper Nepean-Woronora catchments are indicated on each figure.

These figures show the preferred regions for extreme rainfall to be in the mountainous regions especially the Illawarra escarpment and the Blue Mountains, with 3-day total in excess of 600 mm recorded near Wollongong and Robertson. It should be noted that these data are based on 24 hr accumulations for the period ending at 9:00 a.m. on each day rather than 24 hour totals such as those that may be obtained from a continuously recording rain gauge. This means that if 200 mm of rainfall fell between 3:00 p.m. of day 1 and 9:00 a.m. of day 2 and 300 mm fell between 9:00 a.m. and mid-day of day2 then the observational dataset would record daily rainfall data of 200 and 300 mm for two consecutive days rather than a 24-hour value of 500 mm. Thus there is the potential to underestimate the observed rainfall maxima for some locations.

5.2.1 Spatial Patterns of Extreme Rainfall

The spatial patterns of modelled extreme rainfall for the 1980 climate are shown in Figure 11 for 2-hour rainfall events, in Figure 12 for 24-hour events and in Figure 13 for the 72-hour events for each of the 3 sets of downscaled simulations. There are major differences between the three simulations. This is to be expected as the population of extreme rainfall types varies from model to model as illustrated in Table 3, but some of the differences can also be attributed to changes to the dynamical and physical parameterisation schemes used in the CCAM system. The results from RAMS nested in CC-M20 are much wetter than from the two other models, with RAMS nested in CC-Mk2 being the driest of all models, especially for 2-hour and 24-hour rainfall accumulations. It appears that as CCAM evolves, it has become wetter as the CC-Mk2 simulations are older than those of CC-UK2 which in turn is older than the CC-M20 simulation. Compared with Figure 10 the R-CC-UK2 simulation underestimates both 1-day and 3-day extreme rainfall accumulations in the Sydney region. None of the models capture the high rainfall region adjacent to the coastline between Newcastle and Jervis Bay.

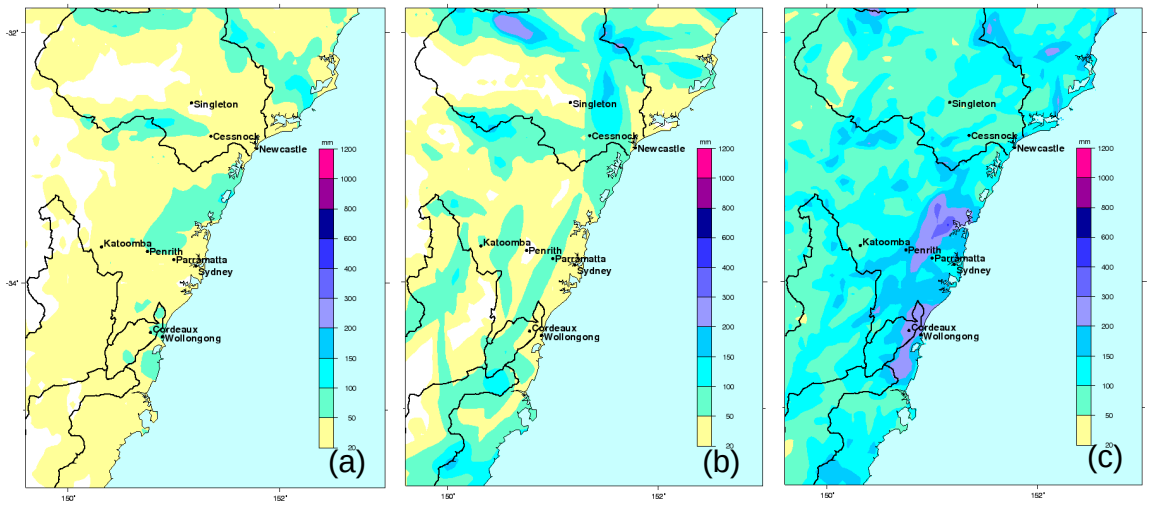

Figure 11: Simulated most extreme 2-hour rainfall for RAMS nested in (a) CC-Mk2, (b) CC-UK2 and (c) CC-M20.

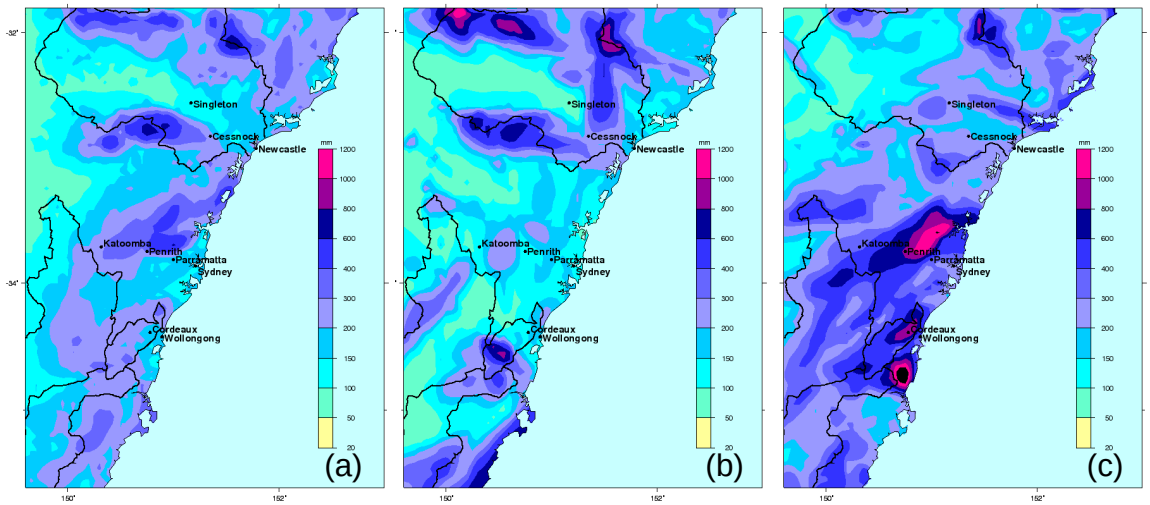

Figure 12: Simulated most extreme 24-hour rainfall for RAMS nested in (a) CC-Mk2, (b) CC-UK2 and (c) CC-M20.

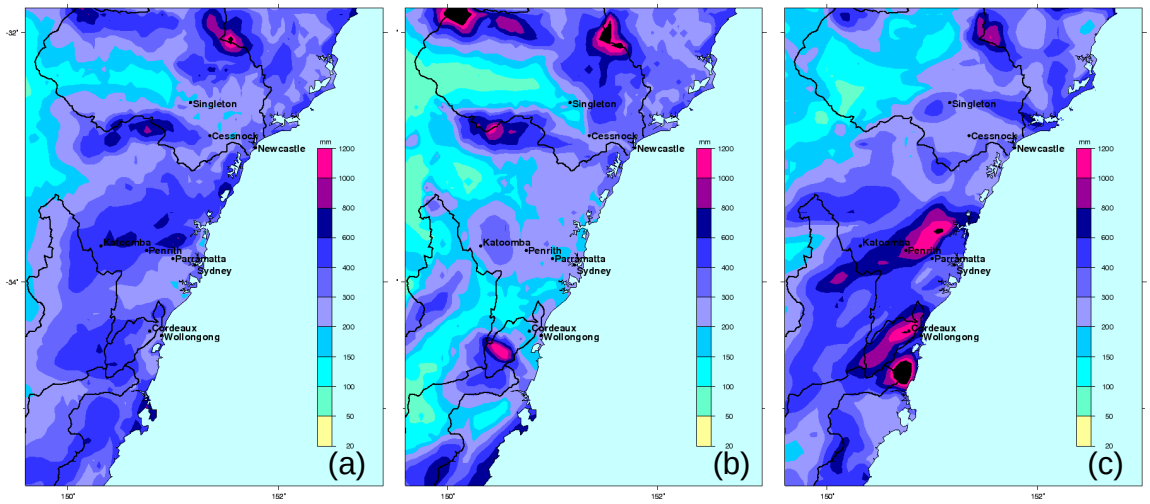

Figure 13: Simulated most extreme 72-hour rainfall for RAMS nested in (a) CC-Mk2, (b) CC-UK2 and (c) CC-M20.

5.2.2 Extreme Value Analysis

Event Selection and Regionalisation

Extreme value statistics have been applied to the modelled rainfall to create gridded values of rainfall accumulation for standard recurrence intervals. The RAMS model produces rainfall output for each grid point within the domain with a time step of 30 minutes. These outputs were used to form an event-based series for each grid point for standard durations of 2, 12, 24, 48, 72 and 96 hours. In order to produce a smoother distribution of results the model outputs were regionalised for each event prior to the application of the statistical package. This method involved an examination of the rainfall at each grid point within a 20 km radius and with less than 100 metres difference in elevation; if a higher rainfall value for the same event existed at one of these nearby points this higher value was incorporated into the series in place of the lower value. This method accounts for the low population size based on the model results which reduces the likelihood that extreme rainfall would be "recorded" at a particular point. This method assumes that if an event caused a large amount of rainfall nearby it could also have occurred at the grid point under consideration.

Choice of Statistical Model

The statistical analysis used a branch of Extreme Value Analysis (EVA) called the Generalised Pareto Distribution (GPD). The main advantages of the GPD over the other EVA method investigated for use, the Generalised Extreme Value (GEV) distribution, is the use of a peaks-over-threshold method of selection of extreme data as opposed to the block-maxima approach used for the GEV, and the ability to choose an appropriate fit.

The GEV is typically used for analysis of extreme values within a cycle, e.g. annual maximum daily rainfall values in a lengthy time series. However for this study daily time series of downscaled rainfall did not exist and the "data" consisted of a limited number of events (100) over a 40 year period. Experiments using the GEV gave a generally poor fit to the data, and correspondingly large errors in return level projections from the resulting fit. The GEV approach also produced positive shape parameters for almost every series. A positive shape parameter indicates an unbounded distribution – the series increases to infinity for long return periods – suggesting an infinite amount of rainfall is possible, and produces unreasonably large estimates at longer return periods (> ~50 years).

The GPD method, using the peaks-over-threshold approach, maximised the data available for analysis, thus reducing the errors in projected return levels of extreme rainfall. It also had the added advantage that the shape parameters of the fits modelled could be constrained to be negative (i.e. bounded distributions) leading to more physically realistic estimates of return levels than possible using the GEV approach.

Selection of Appropriate GPD Thresholds

The main deterrent to the use of the GPD method is the need to select an appropriate threshold for each individual series. Usually this is done manually using visual analysis of mean residual life plots, where a threshold at which stability of the mean excess is approximately constant is chosen. The model outputs produce over 11000 series – one at each grid point of the domain – making this approach prohibitive. To counter this, an algorithm was developed to calculate the appropriate threshold for the GPD analysis of each series. This was achieved by iterating the threshold through small increments of rainfall (1 mm) until the minimum number of data points was reached, applying the Anderson-Darling (A-D) goodness-of-fit test (Anderson and Darling, 1952) for each GPD threshold, and then using the threshold giving the best A-D test result to the GPD model for

the production of return levels for that series. In this way the selection of an appropriate threshold was automated and outputs for such a large number of series could be calculated without need for individual analysis.

The results from this analysis for the 100 year ARI rainfall are presented in Figure 14 for RAMS nested in each of the three simulations.

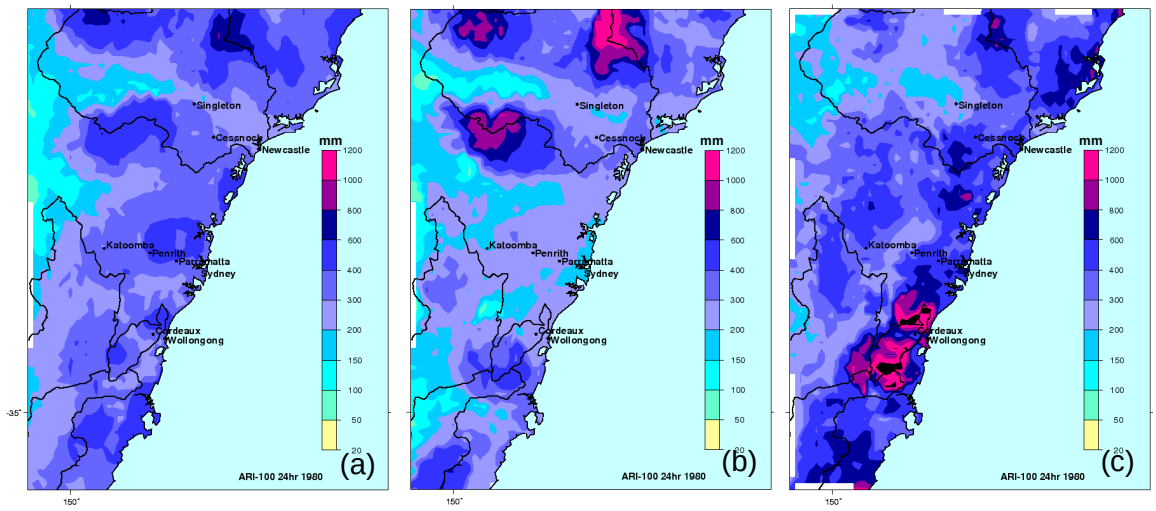

Figure 14 : Spatial distribution of the 1980 100 year ARI 24-hour rainfall depth derived using outputs from RAMS nested in (a) CC-Mk2, (b) CC-UK2 and CC-M20.

These results can be compared with those from Australian Rainfall and Runoff (1987) (see Figure 19a). They show unrealistically high levels in the mountainous regions north of Newcastle in CC-UK2 and along the Illawarra Escarpment in the CC-M20 simulation. The EVA has tended to enhance the high rainfall region adjacent to the coastline between Newcastle and Jervis Bay and the higher rainfall of the Blue Mountains.

5.3 Impact of Climate Change

The model rainfall outputs have been used to calculate the 5 year and 100 year ARI rainfall depths for 2-hour, 24-hour and 72-hour rainfall events for each simulation set for the current, 2030 and 2070 climates. Similar analyses are available for durations of 30-mintes, 1, 3, 6, 12, and 48 hours but are not presented here. In addition to these results, the 20 most extreme events from each of the 100 simulations for the 3 models have been used to quantify the consensus between the models as to the direction (i.e. an increase or decrease) of the projected change in extreme rainfall.

5.3.1 Spatial Patterns of Climate Change

In the following section spatial changes in rainfall depth due to climate change are presented. Results for 2030 are presented in Figure 15 (ARI-5) and Figure 16 (ARI-100) and 2070 results are in Figure 17 (ARI-5) and Figure 18. (ARI-100).

There is large variation in the patterns of change for the 3 sets of simulations. For the 2030 time slice, all models are projecting decreases in 100 year ARI rainfall intensity for the coastal region south of Jervis Bay. The CC-Mk2 and CC-M20 models are projecting regions of increase in the Warragamba catchment for short duration events in 2030. All three models project regions of decreases in rainfall extremes for the Hunter River catchment.

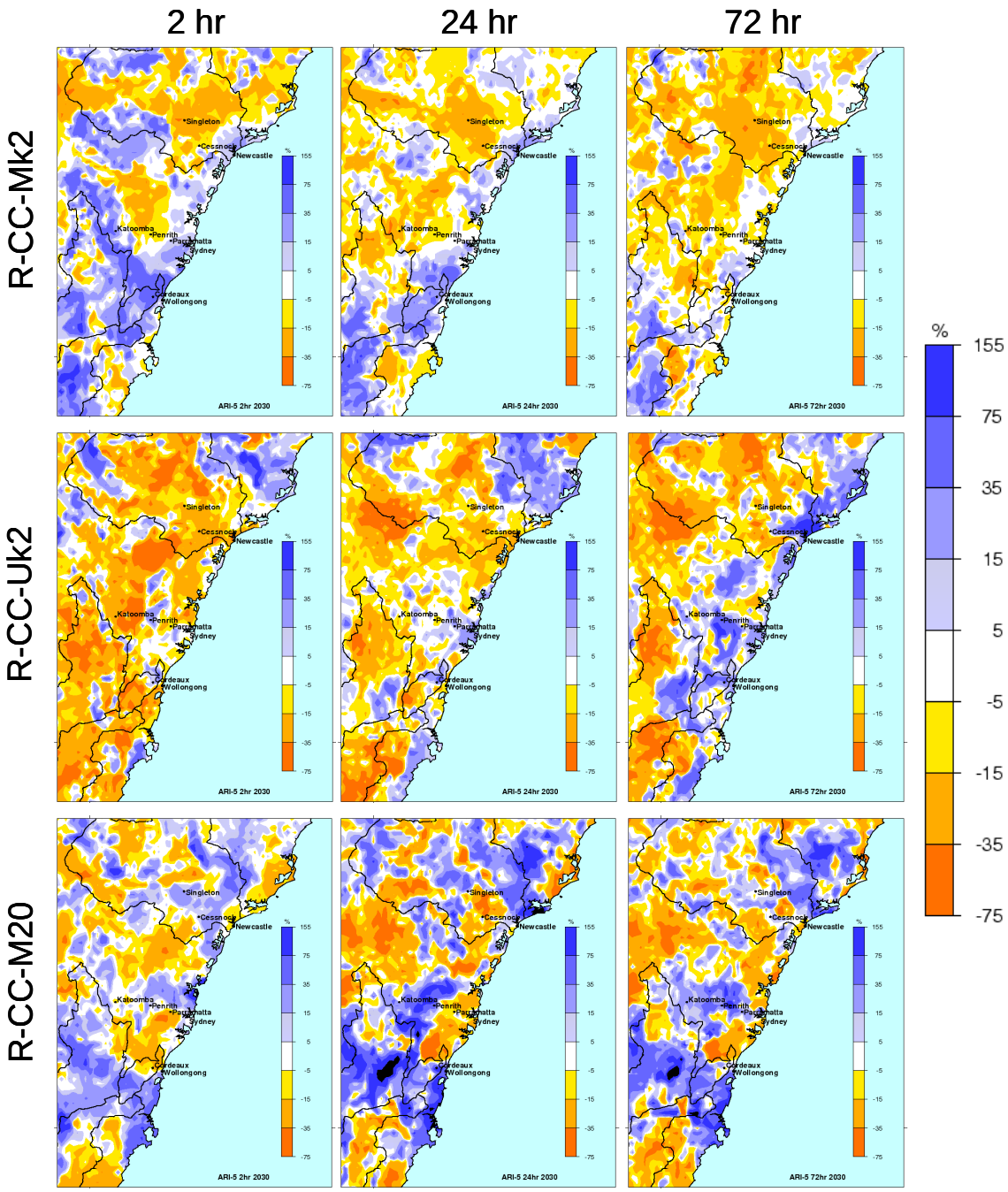

Figure 15: Percentage change in rainfall depth for 2030 for 5 year ARI rainfall events for durations of 2, 24 and 72 hours (vertical columns). Results for the three models are shown in rows.

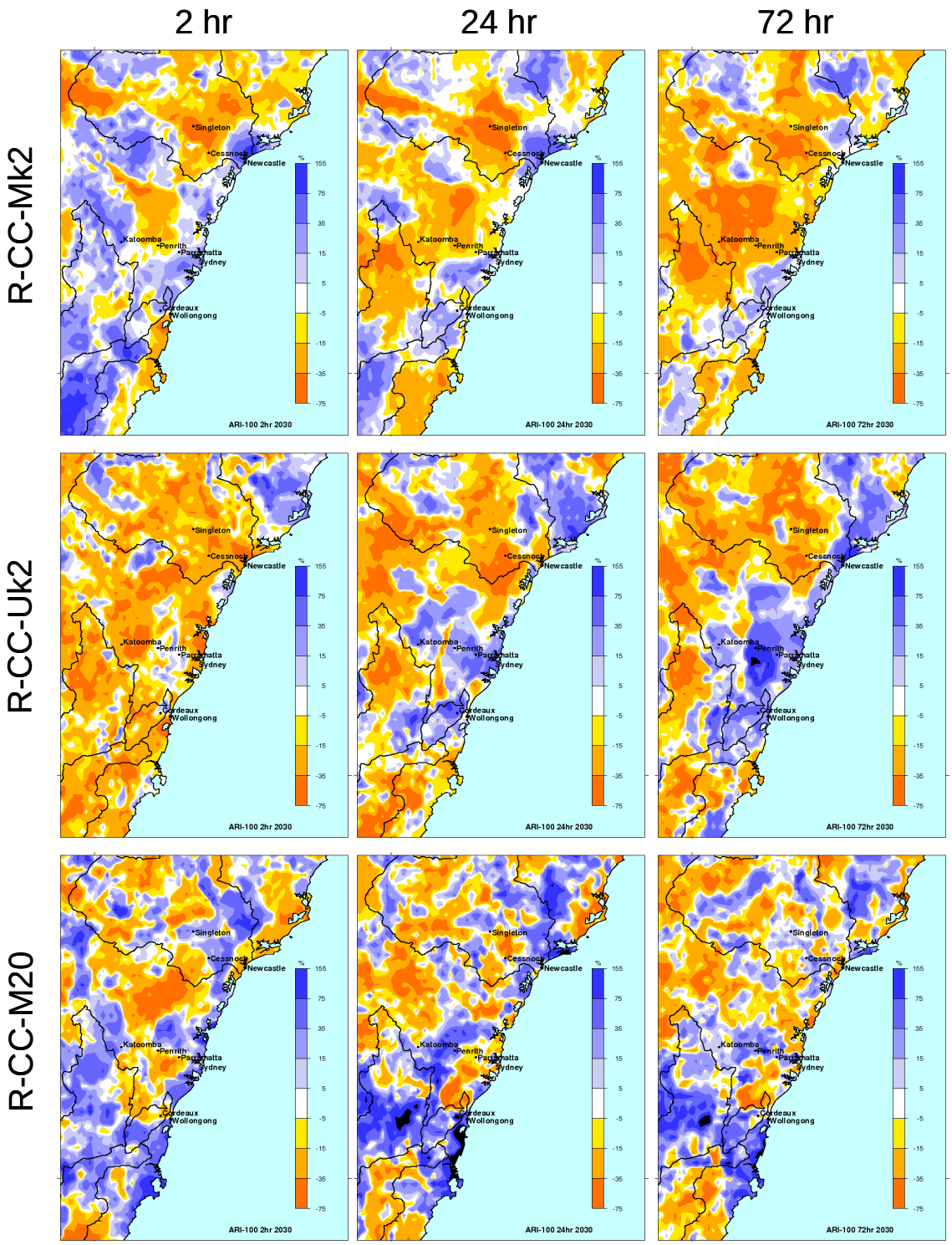

Figure 16: Percentage change in rainfall depth for 2030 for 100 year ARI rainfall events for durations of 2, 24 and 72 hours (vertical columns). Results for the three models are shown in rows.

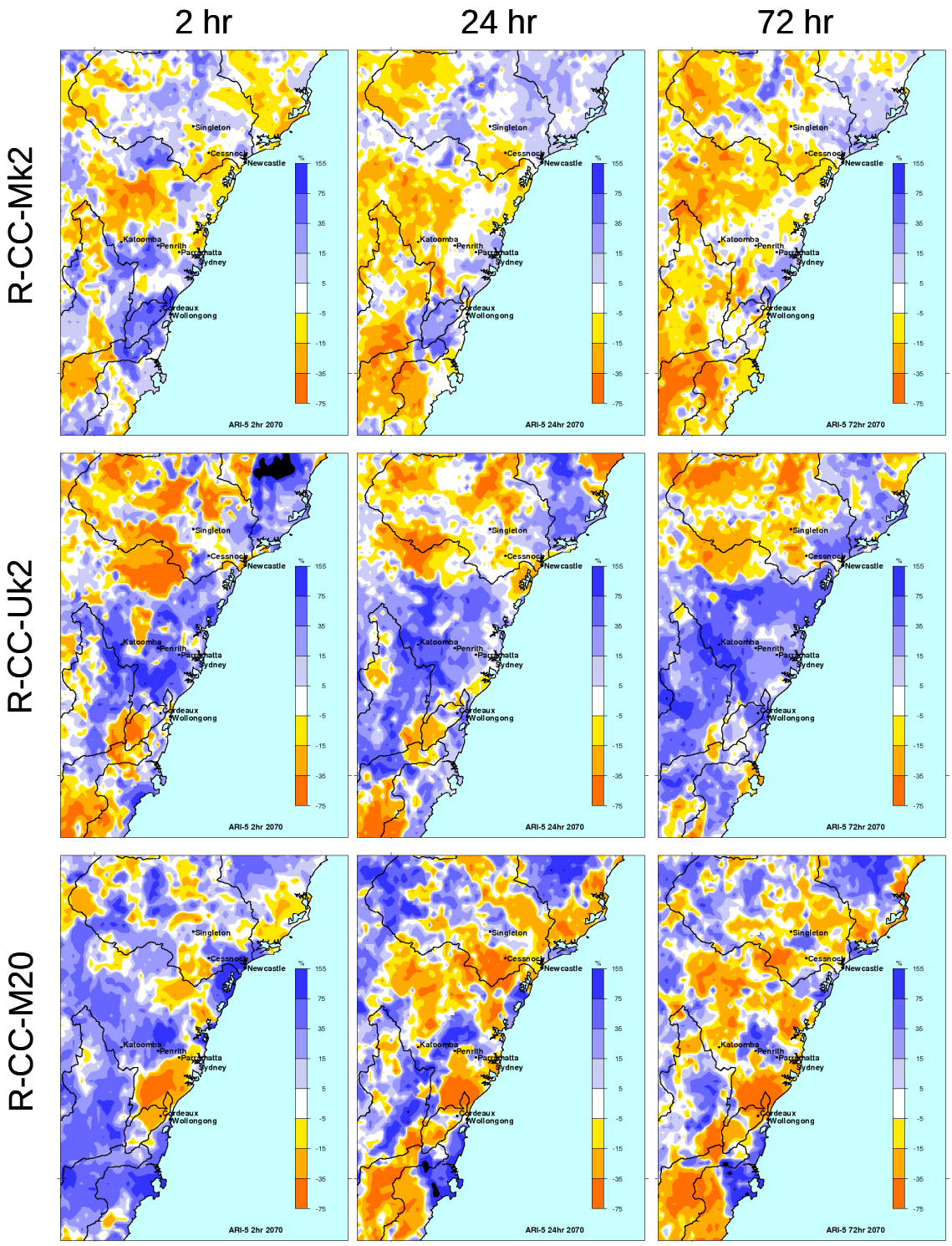

Figure 17: Percentage change in rainfall depth for 2070 for 5 year ARI rainfall events for durations of 2, 24 and 72 hours (vertical columns). Results for the three models are shown in rows.

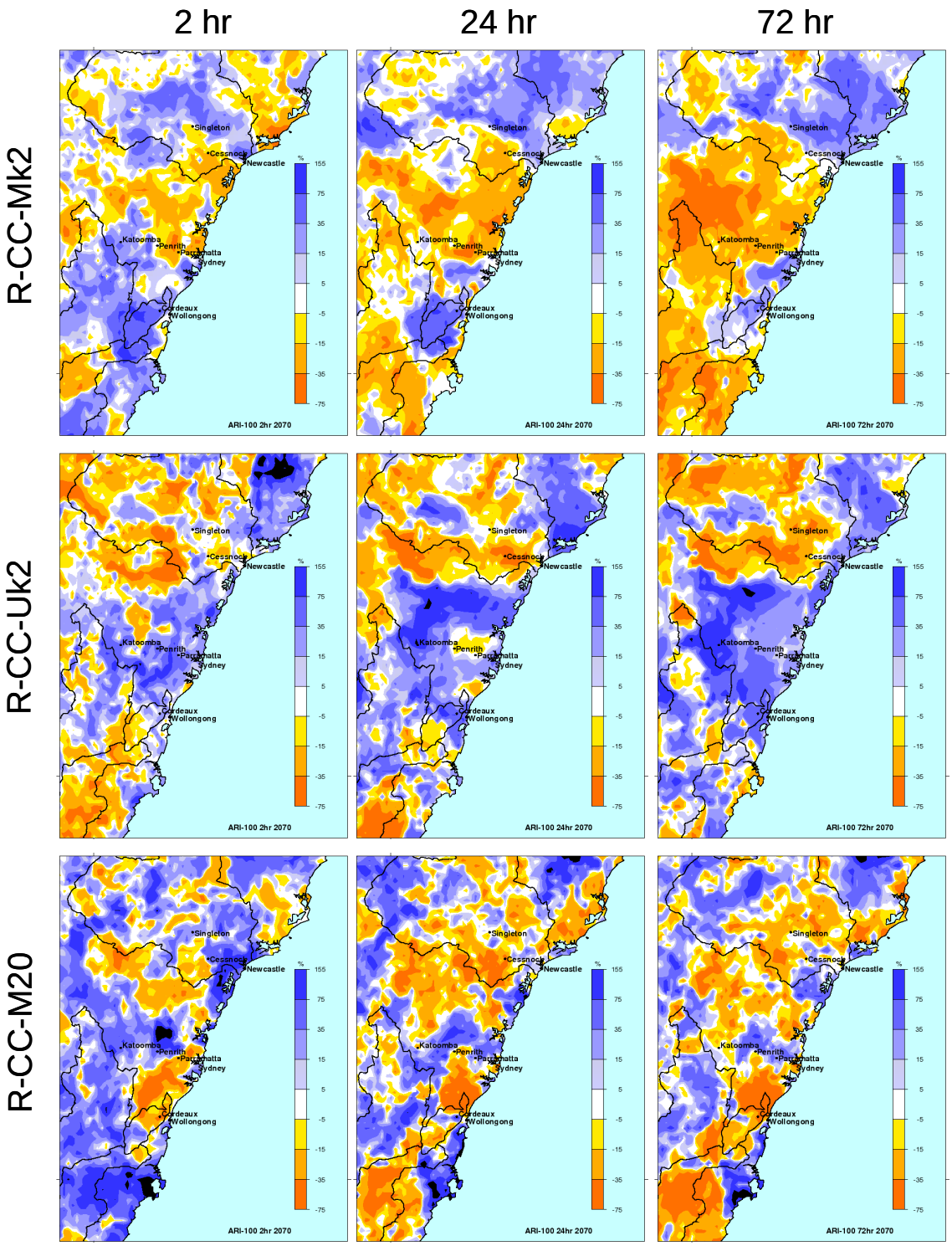

Figure 18: Percentage change in rainfall depth for 2070 for 100 year ARI rainfall events for durations of 2, 24 and 72 hours (vertical columns). Results for the three models are shown in rows.

By 2070 the pattern of change has changed between the models. The R-CC-Mk2 model projects large areas with a decrease in extreme rainfall intensity. In contrast, the R-CC-UK2 model is projecting a marked increase in rainfall extremes, especially for the region between the Hunter catchment and Jervis Bay.

The spatial variability between the models makes synthesis of the model outputs difficult and thus the results have been composited in an effort to identify consistent regions of projected increase or decrease in rainfall extremes. This step has been undertaken to aid in an analysis of the outputs rather than to provide quantitative estimates. It also has the advantage of removing any decadal or multi-decadal variability that exists within the results.

The ensemble-average of the 1980 24-hour 100 year ARI event is shown in Figure 19 and compared with the 24-hour 100 year ARI rainfall depths from Australian Rainfall and Runoff (ARR87) (I. E. Aust., 1987, 1997).

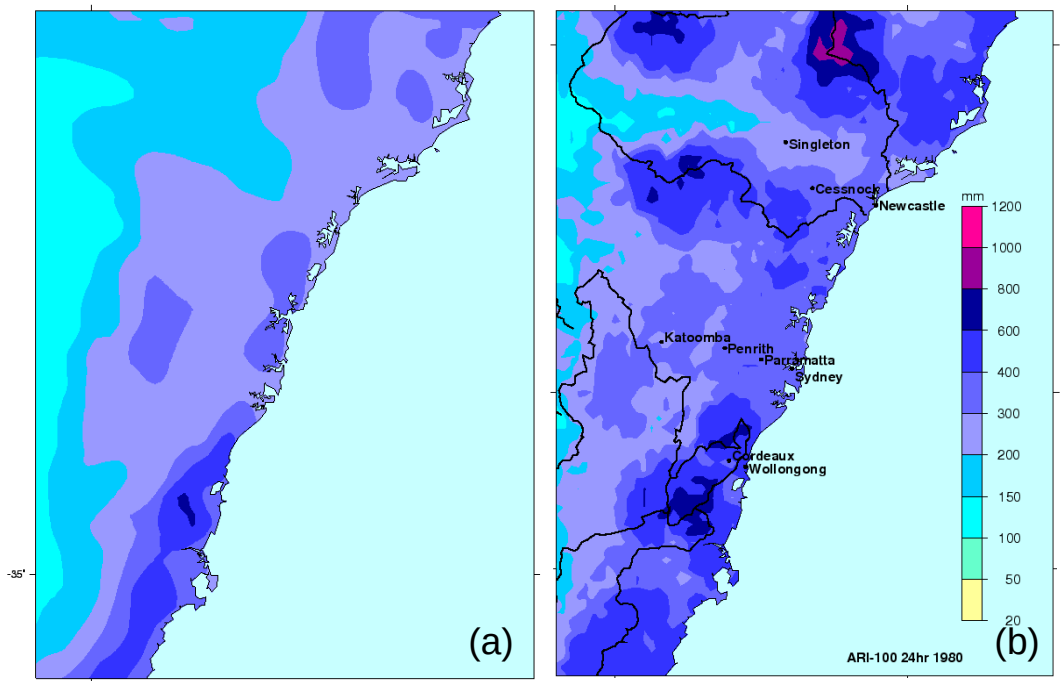

Figure 19: (a) 24-hour 100 year ARI rainfall depth from Australian Rainfall and Runoff (1987) and (b) ensemble average 1980 24-hour 100 year ARI rainfall depth based on the outputs from the 3 sets of RAMS simulations.

The ensemble-average 100 year ARI rainfall depths are still too high in the mountains north of Newcastle but they show the high rainfall region along the Illawarra Escarpment with its maximum at the north eastern end of the Shoalhaven catchment. The dual maxima occurring in the Sydney metropolitan region and over the Blue Mountains are also evident. Similar results (not shown) are obtained if only the R-CC-UK2 and R-CC-M20 simulations are used. In this case the main difference is in the magnitude of the 100 year ARIs for the high rainfall region along the Illawarra Escarpment, with larger values occurring in this region for the 2 model average. It should be noted that ARR87 was criticised for not including non-Bureau of Meteorology rainfall data in the mountainous regions; an examination of Figure 26 suggests that the coverage of locations with long-term records is not good in these areas.

The 5 year and 100 year ARI events for 2030 and 2070 have also been averaged and these results used to derive the composite changes shown in Figure 20 and Figure 21. Composite results based on 2 of the 3 models are provided in Appendix D for comparison. In each of these figures a "consensus" map is presented for rainfall durations of 2, 24 and 72 hours. These maps are derived by determining for each grid point how many of the 20 highest events for the future climate have a greater rainfall accumulation than the corresponding event in the current climate. These results are

combined for the 3 sets of model outputs to provide a measure out of 60 events. For the 2 model composites of Appendix D the "consensus" is based on a total of 40 events.

The spatial patterns of extreme rainfall change for both the 5 year and 100 year ARI events are similar for the 2030 time slice. They show a large region of projected decreases in extreme rainfall intensity for a large area to the north of the Sydney metropolitan area – this region is most extensive in area for the 72-hour events. The southern half of the Warragamba catchment and most of the Upper Nepean-Woronora catchment are projected to experience increased extreme rainfall intensity. Further south, in the Shoalhaven catchment and along the adjacent coastal strip, extreme rainfall intensities are projected to decrease for the longer duration events. These projected patterns of change are consistent with the patterns identified in the consensus maps.

By 2070 the projected patterns of extreme rainfall change have changed compared with those of 2030. The region of projected extreme rainfall increase has increased in area. The short duration rainfall events are projected to experience predominantly an increase in intensity for all regions except the Hunter River catchment. The ensemble-averaged results show a largish region with large projected decreases in extreme rainfall intensity for the 2-hour events between Sydney and Wollongong, however the inter-model consensus for this result is low and the results for the individual models show that 2 out of the 3 models are projecting an increase in extreme rainfall intensity for this region. In general, the 2-hours events have a larger increase in intensity than the 24-hour and 72-hour events. The 24-hour and 72-hour events are projected to experience large decreases in rainfall intensity along the southern perimeter of the Hunter River catchment and in the Shoalhaven catchment.

Following a Steering Committee request, the average percentage change in the intensity of the most extreme events from each set of simulations has been calculated. This analysis uses the 10, 20 or 50 most extreme events, at each model grid point, from each of the models for the current and future climates. The analysis is performed for rainfall durations of 2, 24 and 72 hours. For each model grid point, the rainfall accumulation from the 100 simulations has been sorted and ranked for the current climate experiment. A similar analysis has been conducted for the future climate extreme rainfall events and the results from this analysis compared with the results for the current climate. Composite results of the average fractional change ($\overline{F}$) in extreme rainfall for the future climate, compared with the current, are presented in Figure 22 for 24-hour events and in Appendix E for 2-hour and 72-hour events

Mathematically,

$$\overline{F} = \frac{\sum_{n=1}^{10} F_n}{10}$$

where

$$F_n = \frac{P_{current}(n)}{P_{future}(n)}$$

and $P_{current}(n)$ is the 2, 24 or 72-hour precipitation at the grid point for the n^{th} ranked current climate event. $P_{future}(n)$ is similarly defined.

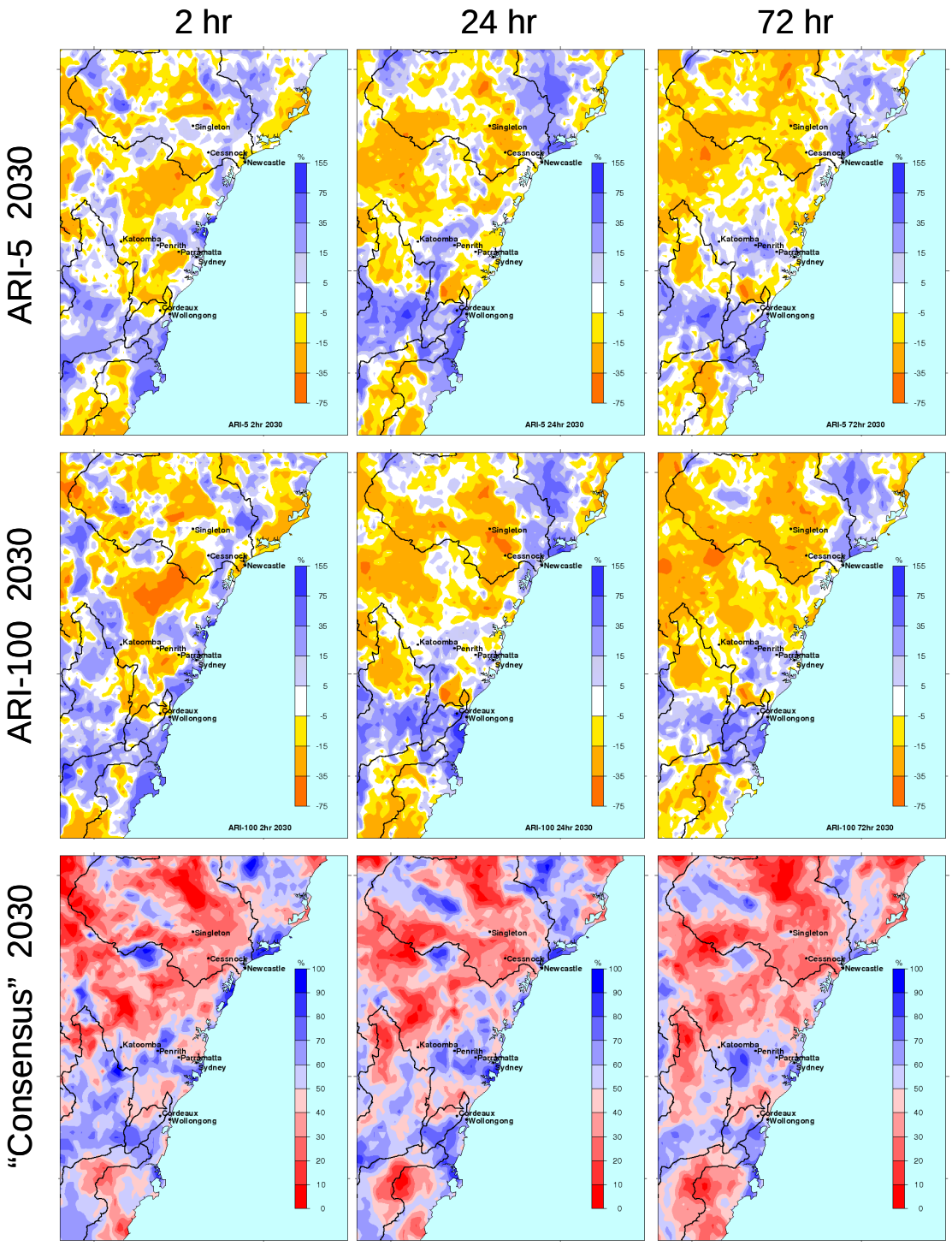

Figure 20: Ensemble average percentage change in rainfall depth for 2030 for (top) 5 year, and (middle) 100 year ARI rainfall events for durations of 2, 24 and 72 hours (vertical columns). The bottom row presents the inter- and intra-model consensus for 2030 – red shading indicates regions where the models project a decrease in extreme rainfall and blue regions where they project an increase in extreme rainfall. Darker shading indicates greater consensus between the models.

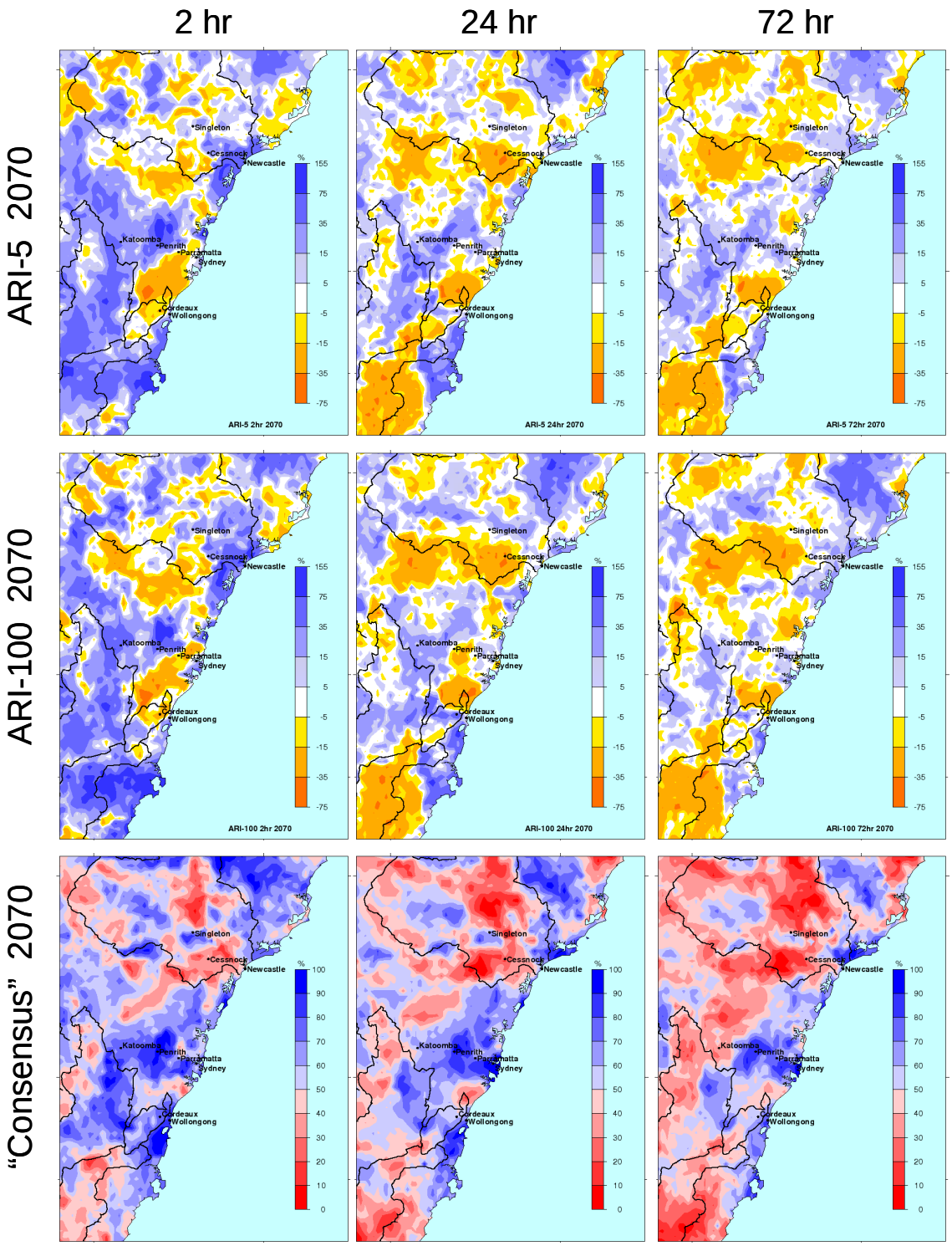

Figure 21: Ensemble average percentage change in rainfall depth for 2070 for (top) 5 year, and (middle) 100 year ARI rainfall events for durations of 2, 24 and 72 hours (vertical columns). The bottom row presents the inter- and intra-model consensus for 2070 – red shading indicates regions where the models project a decrease in extreme rainfall and blue regions where they project an increase in extreme rainfall. Darker shading indicates greater consensus between the models.

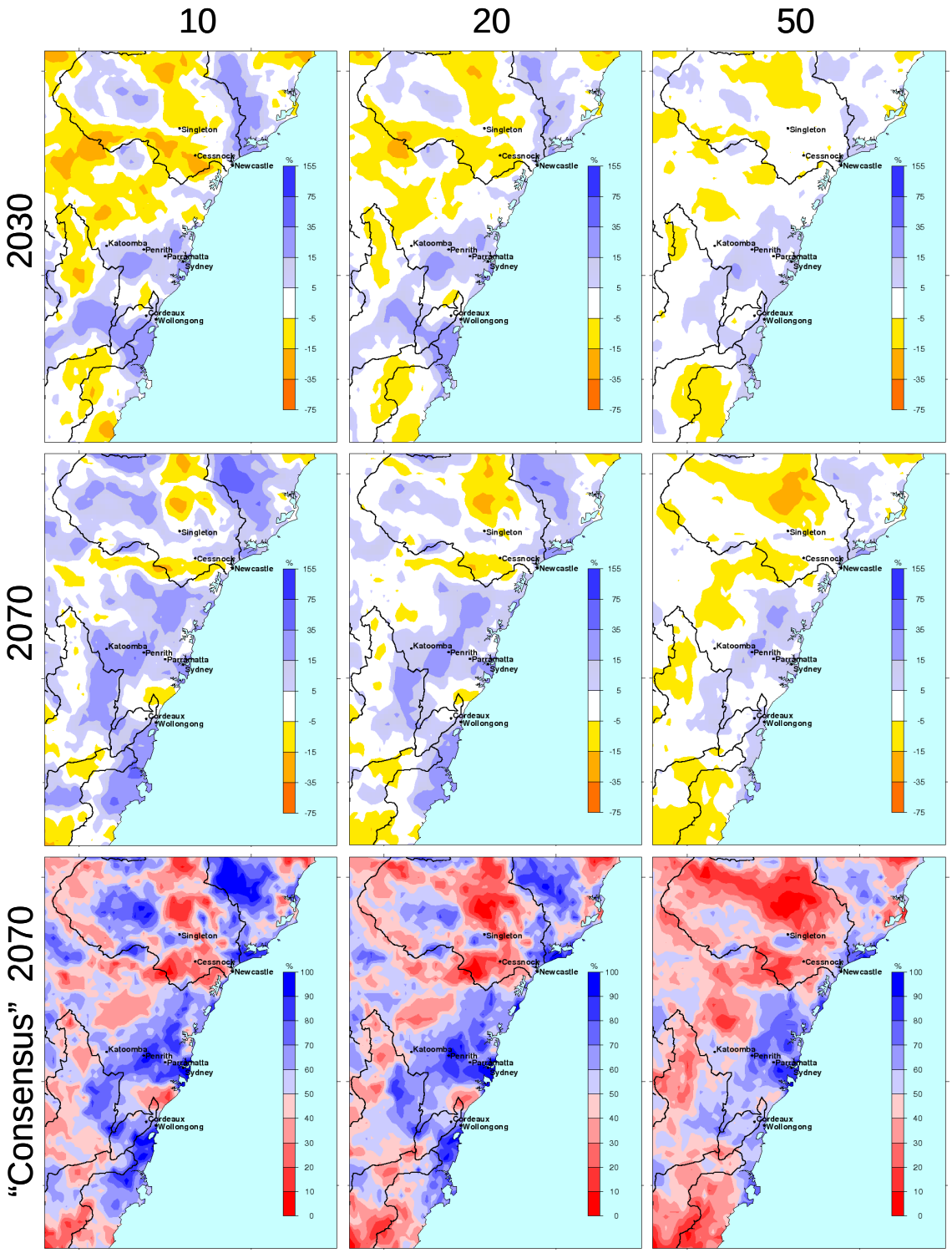

Figure 22: Ensemble average percentage change in rainfall depth for (top) 2030 and (middle) 2070 rainfall events for durations of 24 hours based on averaging the 10, 20 or 50 most extreme events (vertical columns) from each set of simulations. The bottom row presents the inter- and intra-model consensus for 2070.

This analysis method smooths out much of the spatial variability evident in Figure 20 and Figure 21 and helps highlight the findings from those figures. Widespread increases in extreme rainfall intensity are not projected to occur until the second half of the 21st Century and will predominantly be experienced by shorter duration events. By 2070 the 2-hour and 24-hour rainfall events are projected to experience widespread increases in intensity for most regions. The 2-hours events are

projected to experience a larger increase in intensity than the 24-hour and 72-hour events. By comparing the results obtained by averaging over the top 10 and top 50 events it is apparent that the less frequent events are projected to experience greater percentage increases in intensity than the more frequent events. In some locations, for example west of Katoomba, the recurrence interval curves for the current climate and 2070 are likely to cross, especially for rainfall durations of 24-hours and longer. For these durations the low frequency events are projected to become more intense in the future and the higher frequency events less intense. Thus, when extreme rainfall events occur in the future they are likely to be characterised by more intense bursts of rainfall than currently occurs but, in many locations, with a total accumulation smaller than occurs in the current climate. A comparison of the projections for 2030 indicates that the impact of global warming on extreme rainfall may be non-linear, with widespread decreases in extreme rainfall intensity in the early 21st Century which gradually change with time to become increases in extreme rainfall intensity. The reasons for this are unknown, and investigation of them beyond the scope of this project, but they are likely due to complex interactions involving the local terrain and thermodynamic state of the atmosphere.

5.3.2 Analysis of outputs for hydrological applications

The analysis of rainfall data is an important part of hydrological design procedures but the spatial variability of the results presented in Figure 20 and Figure 21 make it difficult to provide practitioners with definitive statements as to what to expect at a given location. Outputs from the Extreme Value Analysis (EVA) have been used to create (1) return period curves, (2) intensity-frequency-duration curves for selected locations in the study region, and temporal curves for the entire region but these should be used with caution. In Section 5.4 suggested methods for dealing with the uncertainty in climate simulations and the spatial variability in these simulations is provided. Following the analysis described above, an ensemble average of the return period curves has been calculated and sample results are presented in Figure 23. These curves also show the error associated with recurrence interval estimate. Examination of these figures, combined with the results presented in Figure 20 and Figure 21, highlights the difficulty of defining a single value for projected changes in extreme rainfall intensity due to climate change. IFD curves have also been calculated based on a limited selection of durations (2, 12, 24, 48, 72 and 96 hours) for return period of 2, 5 and 100 years – curves for only the 100 year ARI events are presented in Figure 24. As with the return period curves it is difficult to ascertain any meaningful trends associated with climate change for most sites.

Design flood estimation requires the formulation of a design rainfall event for input to a runoff routing model. A design rainfall event is specified by a rainfall duration and average rainfall intensity for a particular average recurrence interval (ARI) and a rainfall temporal pattern. A rainfall temporal pattern gives the proportion of total rainfall in different periods within a rainfall "burst". A rainfall burst is the period of heaviest rainfall of a given duration (e.g. 24 hours) that occurs within an extreme rainfall event. Temporal curves for the study region have been calculated using the method adopted by Australian Rainfall and Runoff (ARR87) (I. E. Aust., 1987, 1997) and described by Pilgrim *et al.* (1969) and Rahman *et al*. (2005). This method is known as the "Method of Average Variability" (MAV). The MAV was applied to 30-minute modelled rainfall rates to derive temporal curves of 30-minute resolution for durations of 24 hours and 72 hours. The 30-minute model rainfall archive is too coarse to identify any temporal variability within 2-hour events and so these were not considered. The rainfall bursts selected by identifying those bursts are those corresponding to the 50 highest bursts for each time slice from each of the three models. Thus these curves are also representative of the ensemble rather than individual models. The temporal patterns derived using this approach are presented in Figure 25.

The 24-hour pattern shows a double peak in rainfall intensity, similarly in the current climate 72-hour pattern. It is not known whether this pattern is a characteristic of extreme rainfall events in the study region or if it is a figment of the MAV. A possible reason for this pattern may be that the rainfall events used in the analysis are sampled from different synoptic types and that, for example, the Type 2 and 4 events (East Coast Lows) have a different temporal pattern to the blocking high patterns of the other 3 types. Combining these patterns may account for the dual peaks seen in the temporal curves and will be investigated at a later date. The temporal curves also suggest that in the future the main rainfall burst in longer duration events may occur earlier than at present.

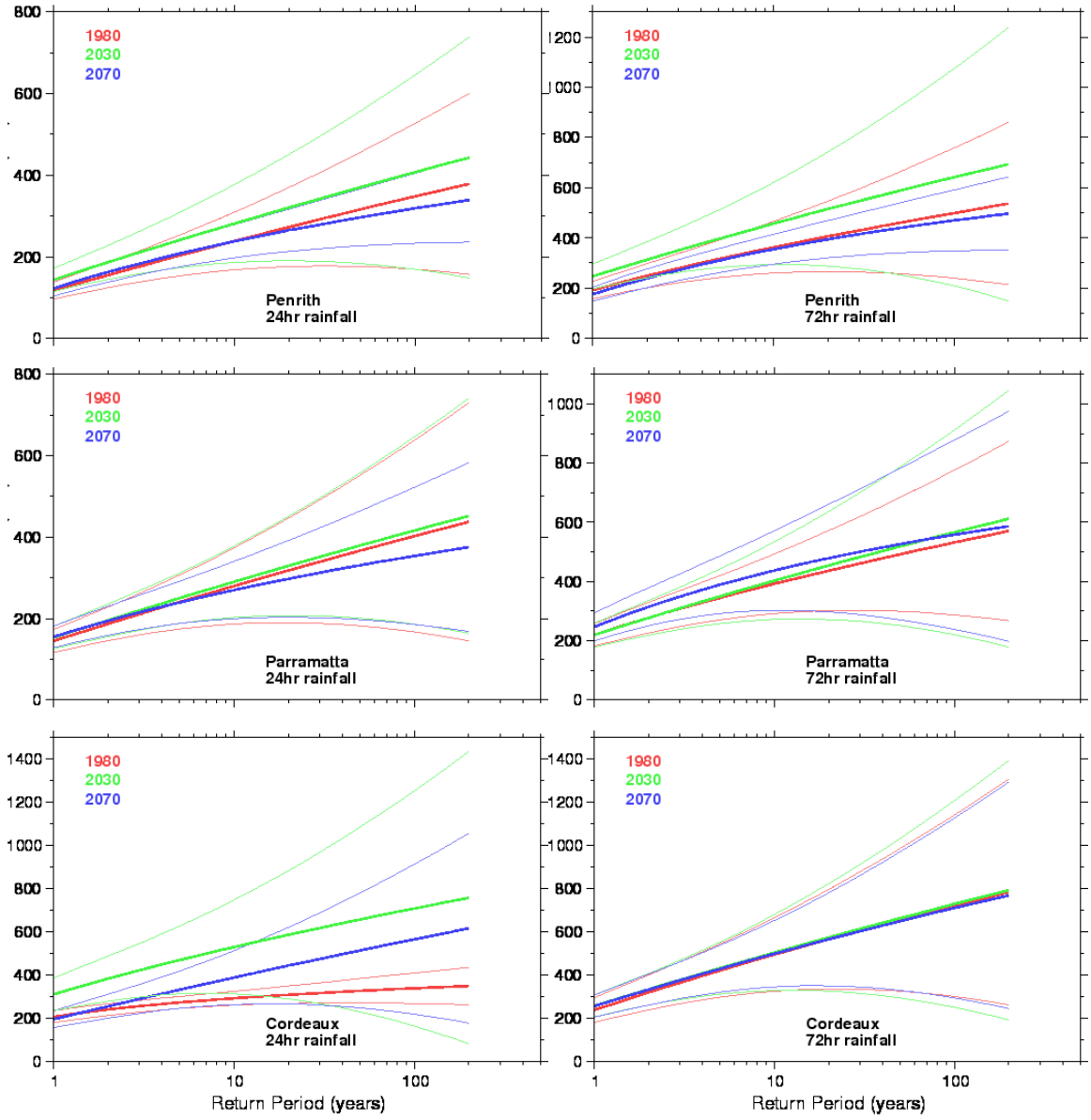

Figure 23: Sample return period curves for 24-hour and 72-hour rainfall accumulations for the locations indicated on the figures. The heavy lines show the ensemble-average curves and the lighter curves indicate the error in the estimation. Curves are shown for (top to bottom) Cessnock, Newcastle and Katoomba. Curves for Penrith, Parramatta, and Cordeaux are presented in Figure 23 (cont'd).

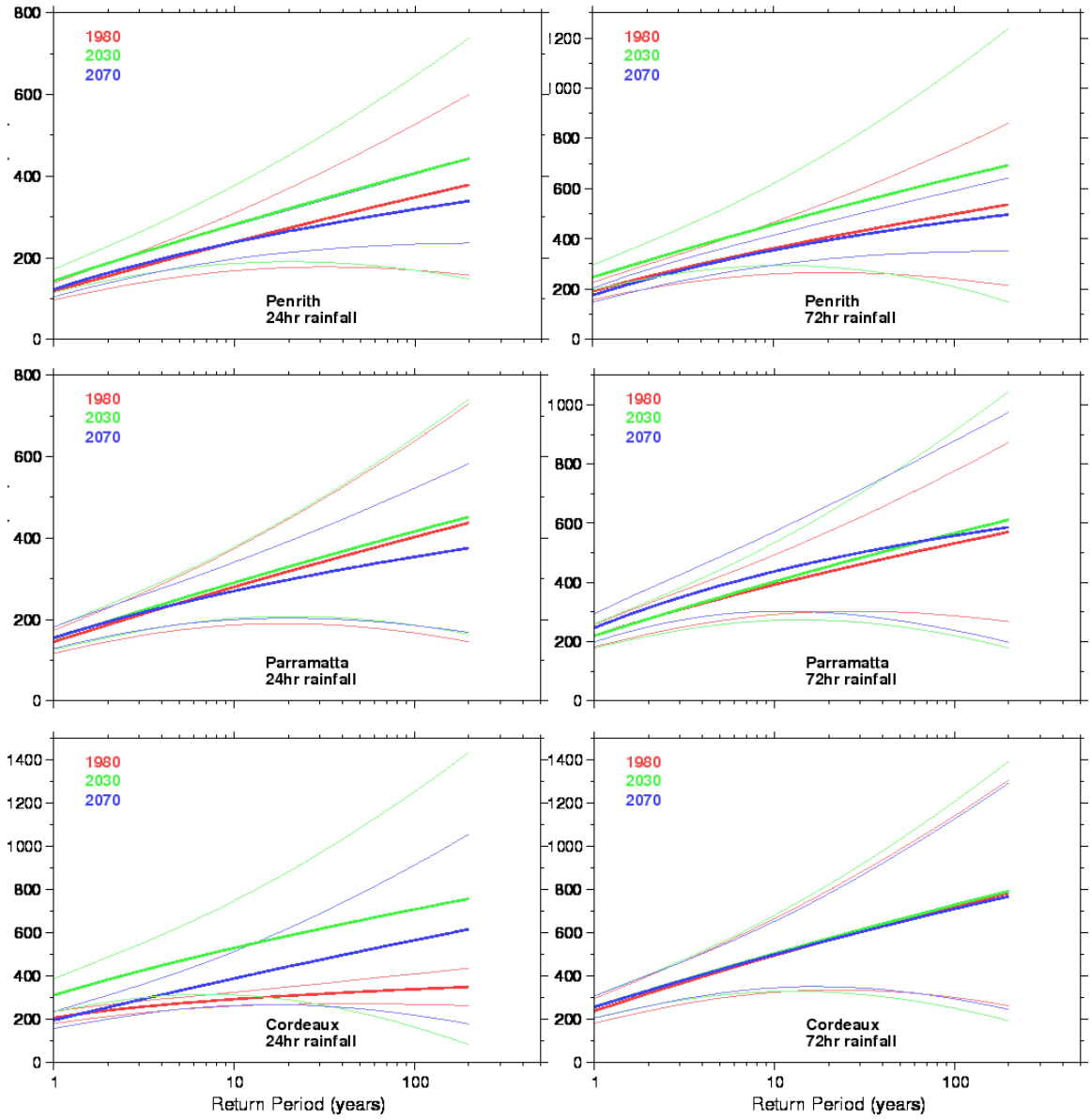

Figure 23 (cont'd).

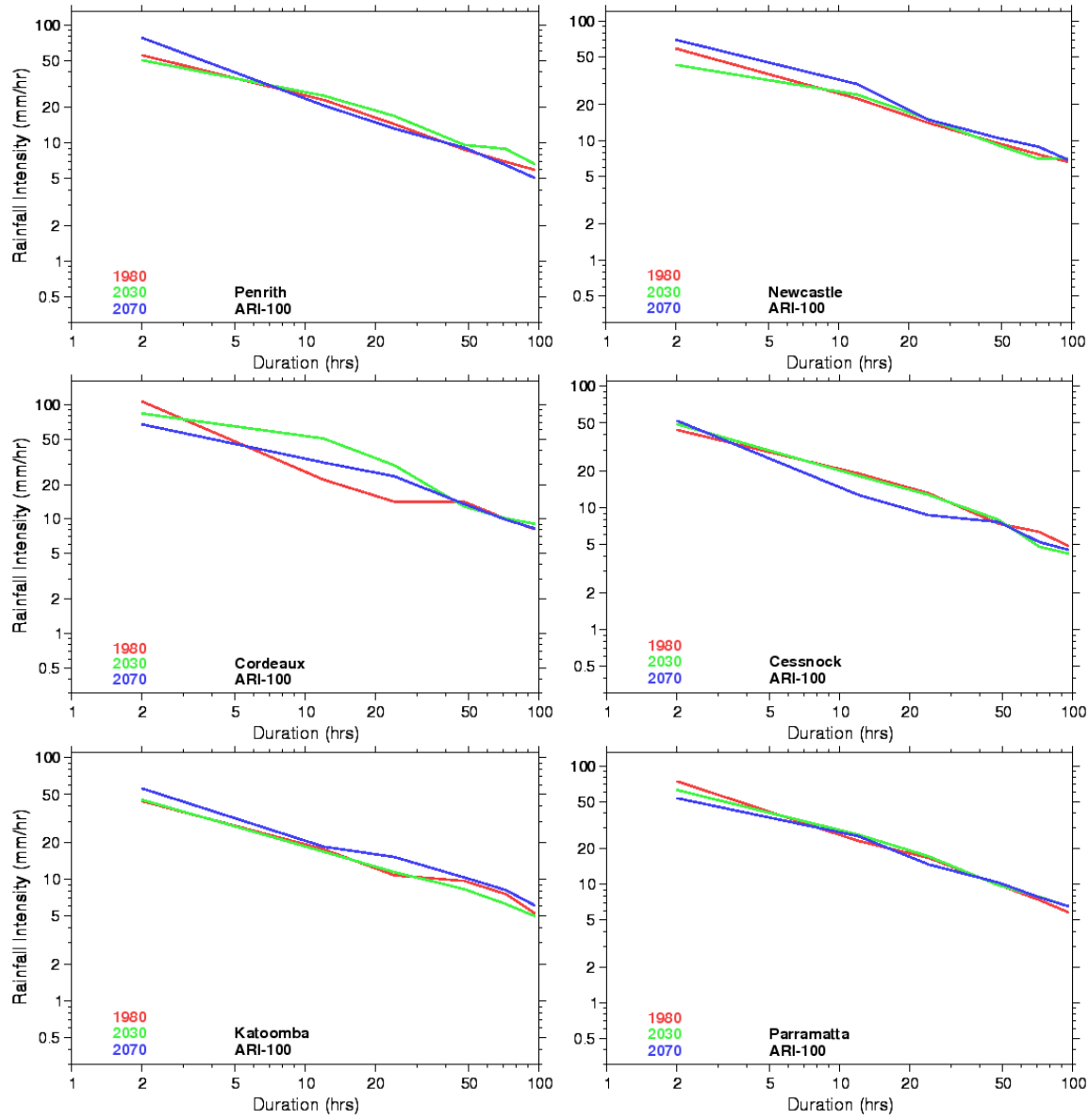

Figure 24: Intensity-frequency-duration charts corresponding to 100 year ARI events for Penrith, Newcastle, Cordeaux, Cessnock, Katoomba and Parramatta.

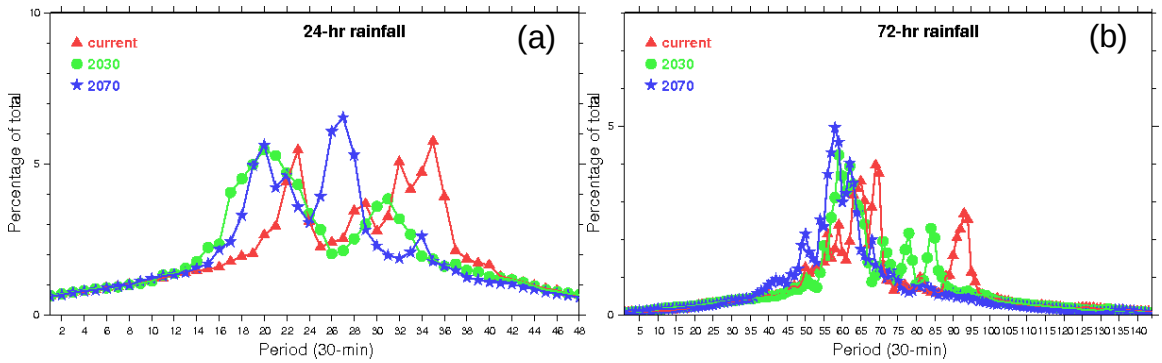

Figure 25: Temporal curves for the study region for (a) 24-hour and (b) 72-hour rainfall bursts.

5.4 Recommendations for use in hydrological applications

Examination of the various figures presented above reveal significant spatial variability in the results, both within a single model, and between the three models, thus highlighting the difficulty of defining a single value for projected changes in extreme rainfall intensity due to climate change for individual locations. This variability/uncertainty needs to be accounted for in hydrological applications and recommendations with examples are presented below. . In addition, the numerical constraints referred to in Section 5.1 mean that the spatial detail apparent in Figure 20 and Figure 21 cannot be considered real.

The following recommended method may be used for applications in either a specific location or for a larger region such as a catchment. For each location or larger region it is possible to create a Probability Density Function of the projected change that accounts for both the uncertainty between the models and for the spatial variability, for example due to terrain, within a model. A summary of such an analysis for the change in the 100-year event at selected sites is presented in Table 6.

The results in this table have been created by using the projected change from each model for each grid point within a radius of 20 km of the location (e.g. Parramatta). This provides a sample of results that captures the local uncertainty between the models and the spatial variability within the models. This sample has then been used to calculate the mean, minimum, and maximum of the sample and the 10^{th}, 25^{th}, 50^{th}, 75^{th} and 90^{th} percentile values from the sample. It is proposed that hydrological applications perform sensitivity studies by using these results to scale design rainfall from AR&R for input into applications such as hydrological models. The outputs from the hydrological models will be a small set of outputs that account for some of the uncertainty inherent in climate change science.

Thus, for applications where a greater level of risk is acceptable, hydrological modelling based on three experiments using design rainfall scaled by the 25^{th} percentile, median and 75^{th} percentile values may be used. For applications with a low risk profile these experiments could be supplemented by two additional experiments using design rainfall scaled by the 10^{th} and 90^{th} percentile values. The minimum and maximum values should not be used as these correspond to calculated changes at a single grid point in one model.

		2-hour events		24-hour events		72-hour events	
		2030	*2070*	*2030*	*2070*	*2030*	*2070*
Parramatta	min	-49	-48	-55	-48	-46	-49
	10th %'ile	-26	-35	-22	-36	-29	-30
	25th %'ile	-13	-23	-12	-17	-20	-16
	mean	1	10	7	-1	17	8
	median	1	3	1	-4	13	11
	75th %'ile	13	36	26	15	37	26
	90th %'ile	30	60	42	31	75	42
	max	48	154	71	76	156	66
Katoomba	min	-66	-21	-34	-40	-48	-43
	10th %'ile	-38	2	-26	-20	-36	-33
	25th %'ile	-25	20	-18	-3	-31	-19
	mean	0	36	3	27	-3	23
	median	0	36	-3	14	4	-2
	75th %'ile	20	49	18	51	14	75
	90th %'ile	36	65	39	94	27	100
	max	75	99	81	171	83	156
Cordeaux	min	-49	-60	-71	-60	-63	-69
	10th %'ile	-38	-30	-21	-37	-19	-42
	25th %'ile	-28	-6	-10	-9	0	-10
	mean	-6	12	23	21	16	14
	median	-10	7	14	24	15	22
	75th %'ile	11	26	35	44	33	42
	90th %'ile	27	61	73	68	47	57
	max	87	122	236	199	119	84
Cessnock	min	-55	-37	-62	-64	-59	-53
	10th %'ile	-38	-26	-47	-45	-43	-33
	25th %'ile	-29	-17	-40	-34	-35	-20
	mean	-12	5	-24	-20	-18	-4
	median	-18	-4	-29	-21	-24	-6
	75th %'ile	-2	10	-14	-8	-11	8
	90th %'ile	-25	53	10	2	17	29
	max	78	159	47	65	56	75

Table 6: Projected percentage changes relative to 1980 in the intensity of 100 year ARI extreme rainfall events for durations of 2. 24 and 72 hours for Parramatta, Katoomba, Cordeaux, and Cessnock. Projected decreases are in red.

6. DISCUSSION & FUTURE WORK

In this report we have identified the synoptic-scale weather systems that are conducive to extreme rainfall over the Central Coast of New South Wales. The results from that analysis have been used to determine the ability of the CC-UK2, CC-Mk2 and CC-M20 models to simulate these events and their likelihood of occurrence. We have found that CC-UK2 and CC-M20 are able to simulate the weather conditions, and their likelihood of occurrence, conducive to extreme rainfall for the Central Coast of NSW. The older CC-Mk2 model does not capture the climatology of MSLP patterns conducive to extreme rainfall over the study region. It is likely that this relatively poor performance is related to the Mark 2 global model from which it obtains its boundary forcing. Both CC-UK2 and CC-M20 simulated an increase in the occurrence of East Coast Lows affecting the Sydney region – an increase of 18% over 1980 climate numbers is projected.

The CCAM model has provided the initial and boundary forcing for three high-resolution (4 km grid spacing) downscaling studies over the region using the RAMS model. In general, these high-resolution simulations have been able to represent the spatial distribution of extreme rainfall realistically and the magnitude of the extremes is close to observed, although there is an apparent over-estimation of extremes in various mountainous regions.

Climate changes simulations based on climates representative of 2030 and 2070, show that there is considerable spatial variation in the regions of extreme rainfall increase and the magnitude of that increase. To overcome difficulties inherent in the analysis of spatially varying outputs, ensemble averages and "consensus" maps were calculated.

Widespread increases in extreme rainfall intensity are not projected to occur until the second half of the 21st Century and will predominantly be experienced by shorter duration events. By 2070 the 2-hour and 24-hour rainfall events are projected to experience widespread increases in intensity for most regions. The 2-hours events are projected to experience a larger increase in intensity than the 24-hour and 72-hour events. By comparing the results obtained by averaging over the top 10 and top 50 events it is apparent that the less frequent events are projected to experience greater percentage increases in intensity than the more frequent events. In some locations, for example west of Katoomba, the recurrence interval curves for the current climate and 2070 are likely to cross, especially for rainfall durations of 24-hours and longer. For these durations the low frequency events are projected to become more intense in the future and the higher frequency events less intense. Thus, when extreme rainfall events occur in the future they are likely to be characterised by more intense bursts of rainfall than currently occurs but, in many locations, with a total accumulation smaller than occurs in the current climate. A comparison of the projections for 2030 indicates that the impact of global warming on extreme rainfall may be non-linear, with widespread decreases in extreme rainfall intensity in the early 21st Century which gradually change with time to become increases in extreme rainfall intensity.

Outputs from the Extreme Value Analysis (EVA) have been used to create (1) return period curves, (2) intensity-frequency-duration curves for selected locations in the study region, and temporal curves for the entire region. Examination of the return period and intensity-frequency-duration curves, combined with the spatial patterns of change results, highlights the difficulty of defining location-specific values for projected changes in extreme rainfall intensity due to climate change. Recommendations to accounting for climate change in hydrological applications are described and brief examples given. The temporal curves also suggest that in the future the main rainfall burst in longer duration (i.e. 72-hour) events may occur earlier than at present.

The projections described in this report are based on an equal weighting of the outputs from each of the three models even though the older CC-Mk2 model does not capture the climatology the MSLP patterns conducive to extreme rainfall over the study region. Similar projections based on the outputs from only the R-CC-UK2 and R-CC-M20 model could be created. These projections would have the advantage that they use the RCMs that have been found to have the best representation of the climatology of the MSLP patterns conducive to extreme rainfall over the study region but they have the disadvantage that they are sampling fewer models and thus less of the uncertainty space.

The results form this study highlight the importance of considering the results from more than one model when developing projections of climate change. The CCAM output used to initialise RAMS in this study originates from simulations that have been undertaken between 2003 and 2007 using versions with varying parameterisation schemes, configuration and grid spacings. Ideally, any future downscaling work should use a standard configuration and version of the model so that this form of model uncertainty can be ruled out. A series of CCAM simulations using a standard version of the model nested in various international GCMs has become available since this study was completed and simulations such as these will be used for future extreme rainfall downscaling.

7. REFERENCES

Abbs, D.J., 1998: A numerical modeling study to investigate the assumptions used in the calculation of probable maximum precipitation. *Water Resources Research*, **35**, 785-796.

Abbs, D. J., and K.L. McInnes, 2004: The impact of climate change on extreme rainfall and coastal sea levels over south-east Queensland. Part 1, Analysis of extreme rainfall and wind events in a GCM: a project undertaken for the Gold Coast City Council, CSIRO Atmospheric Research. Aspendale, Vic., 48 p.

Abbs, D. J., 2006: The atmospheric model component of the Relocatable Ocean Atmosphere Model – report on tasks 3, 5 and 6. Report prepared for the Royal Australian Navy as part of the BLUElink project . Aspendale, Vic.: CSIRO Marine and Atmospheric Research. 61 p.

Anderson, T. W., and D.A. Darling, 1952: Asymptotic theory of certain "goodness-of-fit" criteria based on stochastic processes. *Annals of Mathematical Statistics.* **23**, 193–212.

BTE, 2001: *Economic costs of natural disasters in Australia*. Bureau of Transport Economics, Canberra.

Canadell, J., C. Le Quéré, M. Raupach, C. Field, E. Buitehuis, P. Ciais, T. Conway, N. Gillett, R. Houghton, and G. Marland, 2007: Contributions to accelerating atmospheric CO2 growth from economic activity, carbon intensity and efficiency of natural sinks. *Proceedings of the National Academy of Sciences*, **104,** 18866–18870

Grasso, L.D., 2000: commentary and analysis: The Difference Between Grid Spacing and Resolution and Their Application to Numerical Modeling. *Bull. Amer. Meteor. Soc.*, **81**, 579–580.

Hewitson, B., and R. Crane, 1992: Regional Climates in the GISS Global Circulation Model: Synoptic-Scale Circulation. *J. Climate*, **5**, 1002–1011.

Institution of Engineers, Australia (I. E. Aust.), 1987: Australian Rainfall and Runoff: A Guide to Flood Estimation. Book IV, I. E. Aust., Canberra.

IPCC, 2000: *Special Report on Emissions Scenarios.* A special report of Working Group III of the Intergovernmental Panel on Climate Change. Nakićenović, N and R. Swart (Eds.). Cambridge University Press, UK. 570pp

Jeffrey, S.J., Carter, J.O., Moodie, K.M and Beswick, A.R. 2001: Using spatial interpolation to construct a comprehensive archive of Australian climate data, Env Modelling and Software, Vol 16/4, pp 309-330.

Lavery, B., A. Kariko, N. Nicholls, 1992: A historical rainfall dataset for Australia. *Aust. Meteorol. Mag.*, **40**, 33-39.

McInnes, K.L., D.J. Abbs, G. D. Hubbert and S. E. Oliver, 2002: A Numerical Modelling Study of Coastal Flooding. *Meteorol. Atmos. Phys.*, **80**, 217-233.

Pielke, R. A., 1984: *Mesoscale Meteorological Modeling.* Academic Press, 612 pp.

Pilgrim, D.H., I. Cordery, and R. French, 1969: Temporal patterns of design rainfall for Sydney, Institution of Engineers, Australia, Civil Eng. Trans., **CE11**, 9-14.

Rahman, A., S. M. Islam, K. Rahman, S Khan and S Shrestha, 2005: A Windowsbased program to derive design rainfall temporal patterns for design flood estimation. In Zerger, A. and Argent, R.M. (eds) MODSIM 2005 International Congress on Modelling and Simulation. Modelling and Simulation Society of Australia and New Zealand, December 2005, pp. 170-176.

(see http://www.mssanz.org.au/modsim05/papers/rahman_a.pdf)

Rahmstorf, S., A. Cazenave, J. Church, J. Hansen, R. Keeling, D. Parker, and R. Somerville, 2007: Recent climate observations compared to projections. *Science*, 316(5825): 709.

Perkins, S.E., A.J. Pitman, N.J. Holbrook, and J. McAneney, 2007: Evaluation of the AR4 Climate Models' Simulated Daily Maximum Temperature, Minimum Temperature, and Precipitation over Australia Using Probability Density Functions. *J. Climate*, **20**, 4356–4376.

Sheehan, P. and F. Sun, 2007: Energy Use and CO2 Emissions in China: Interpreting changing trends and future directions, CSES Climate Change Working Paper No. 13. Centre for Strategic Economic Studies, Victoria University, Melbourne.

Suppiah, R., Hennessy, K. J., Whetton, P. H., Mcinnes, K. L., Macadam, I., Bathols, J. M., Ricketts, J. H., and Page, C. M. (2007). Australian climate change projections derived from simulations performed for the IPCC 4th Assessment Report . *Australian Meteorological Magazine,* 56 (3): 131-152.

Viney, N.R. and B.C. Bates, 2004: It never rains on Sunday: the prevalence and implications of untagged multi-day rainfall accumulations in the Australian high quality data set. *Int. J. Climatol.*, **24**, 1171-1192.

Yarnal, B. 1993: Synoptic Climatology in Environmental Analysis: A Primer, Belhaven Press, London.

APPENDIX A

The following table lists the rainfall stations used to identify extreme rainfall days used for the synoptic typing component of this study. The location of these stations, colour-coded by length of record is shown in Figure 26.

060009	COOLONGALOOK STATE FOREST	32.2000	152.3167	1938	1970	100
060045	GLOUCESTER (BERRICO)	32.0667	151.8333	1962	1978	100
060047	BUNGWAHL (BUTTABA)	32.3900	152.4000	1961	1994	100
060074	FAILFORD POST OFFICE	32.0833	152.4500	1965	1966	100
060088	PACIFIC PALMS (BOOMERANG BEACH)	32.3500	152.5333	1968	1983	100
060089	WARDS RIVER (MOANA)	32.2500	151.9833	1968	1979	100
060143	DYERS CROSSING (WANG WAUK ROAD)	32.1611	152.2522	1995	1996	95
061001	ALLANDALE (TINGARA)	32.7167	151.4167	1902	1971	100
061003	AVOCA BEACH	33.4667	151.4333	1934	1970	100
061004	MUSWELLBROOK (BENGALLA)	32.2500	150.8667	1923	1966	100
061005	BRANXTON POST OFFICE	32.6500	151.3500	1886	1969	100
061006	BRINDLEY PARK 2	32.1000	150.3000	1885	1960	100
061008	CAMPBELLS HILL	32.7000	151.5000	1912	1965	100
061009	CESSNOCK POST OFFICE	32.8272	151.3661	1903	1992	100
061015	DANGERFIELD	32.1500	151.0000	1933	1965	100
061018	MUSWELLBROOK (EDDERTON)	32.4000	150.8333	1911	1985	100
061019	FASSIFERN	33.0000	151.5500	1924	1961	100
061021	GOORANGOOLA	32.3000	151.2000	1885	1967	100
061023	GOSFORD (GERTRUDE PLACE)	33.4336	151.3381	1877	1993	100
061025	GRETA POST OFFICE	32.6833	151.3833	1902	1978	100
061028	RAVENSWORTH (HILLVIEW)	32.4333	151.0667	1911	1979	99
061029	KULNURA (WILLIAM ROAD)	33.2333	151.2000	1951	1981	100
061030	HOWES VALLEY (KINDARUN)	32.8667	150.8333	1914	1975	100
061032	LOCHINVAR	32.7000	151.4500	1896	1973	100
061034	EAST MAITLAND BOWLING CLUB	32.7483	151.5833	1902	1994	100
061036	MANGROVE MOUNTAIN POST OFFICE	33.3000	151.2000	1942	1979	100
061037	MARATHON (MERRIWA)	32.2000	150.4667	1942	1968	100
061043	MILLERS FOREST SCHOOL	32.7500	151.7000	1913	1976	100
061044	MITCHELLS FLAT	32.5667	151.2833	1937	1976	100
061045	MONKERAI UPPER (REDLEAF)	32.2833	151.8333	1914	1970	100
061047	MOUNT OLIVE (FAIRHOLME)	32.4167	151.2000	1947	1983	100
061052	MUSCLE CREEK (CLENDINNING)	32.2667	151.0667	1901	1976	100
061057	OLNEY STATE FOREST	33.1000	151.2500	1938	1967	100
061058	OWENS GAP (T.O.K.)	32.0500	150.7000	1902	1977	100
061060	PLASHETT	32.4833	150.8833	1903	1966	100
061061	POINT STEPHENS LIGHTHOUSE	32.7500	152.2000	1951	1973	100

061062	POKOLBIN 1 POST OFFICE	32.8000	151.3000	1900	1964	100
061064	RAYMOND TERRACE POST OFFICE	32.7617	151.7400	1882	1992	100
061066	ROUCHEL BROOK	32.1500	151.0833	1897	1974	100
061068	SALISBURY POST OFFICE	32.2167	151.5500	1938	1981	100
061069	SCONE (PHILIP STREET)	32.0458	150.8708	1873	1992	100
061070	SINGLETON POST OFFICE	32.5667	151.1667	1881	1969	100
061091	WOLLOMBI (GLEN AVON)	32.9833	151.1167	1951	1961	100
061098	BELLTREES HOMESTEAD	32.0000	151.1333	1887	1978	99
061121	LOSTOCK POST OFFICE	32.3167	151.4667	1952	1971	100
061122	DUNGOG (TILLEGRA)	32.3167	151.7167	1960	1986	100
061129	HALTON (KINROSS)	32.3167	151.5167	1960	1985	100
061132	WOLLOMBI (YANGO CREEK)	33.0000	151.1000	1959	1973	100
061133	BOLTON POINT (KANIMBLA)	33.0058	151.6133	1962	1990	100
061134	BALAIBLUAN	32.1667	150.5500	1961	1968	100
061137	BRUSH CREEK (BEBEAH)	33.1500	151.2667	1959	1970	100
061138	GUNGAL (BEBREW)	32.2333	150.4833	1960	1974	100
061139	MOUNT YENGO (MARENA STUD)	33.0000	151.0833	1959	1972	100
061141	QUORROBOLONG (EMMAVALE)	32.9500	151.4000	1959	1971	100
061145	CARRABOLLA	32.2000	151.4000	1960	1964	100
061147	CEDAR CREEK	32.7667	151.2833	1959	1970	100
061149	GLEN ALICE (EURELLA)	33.0167	150.2500	1914	1969	100
061150	BULGA (CHARLTON)	32.6333	151.0667	1959	1973	99
061154	EGLINFORD	32.9667	151.2667	1959	1970	100
061160	HILLDALE POST OFFICE	32.5000	151.6500	1960	1976	100
061161	HOLBROOK (WIDDEN VALLEY)	32.6500	150.3500	1960	1972	100
061167	BRANXTON (LAMBS VALLEY)	32.5500	151.4833	1960	1977	100
061169	GRESFORD (DURHAM PARK)	32.3667	151.6333	1960	1988	100
061171	JERRYS PLAINS (CARRINGTON)	32.5167	150.9667	1959	1987	100
061172	MEEREA	32.6333	151.0000	1959	1960	101
061173	MILBRODALE 2	32.6833	151.0000	1959	1967	100
061174	MILLFIELD COMPOSITE	32.9000	151.2667	1959	1983	100
061176	MOUNT OLIVE 2	32.4167	151.2000	1960	1969	100
061177	MOUNT VIEW TOWNSHIP	32.8500	151.2667	1959	1961	100
061179	MULLEE	32.2000	151.2000	1962	1967	100
061181	BROKE (OAKLEY)	32.7500	151.1667	1959	1974	100
061182	MILBRODALE (OAKLEIGH)	32.7000	150.9500	1959	1975	100
061183	POKOLBIN (MOUNT BRIGHT)	32.8333	151.2667	1961	1971	100
061184	MARSHDALE (RAGLAN)	32.4667	151.8667	1960	1976	100
061186	MERRIWA (ROSEBANK)	32.2000	150.2000	1960	1969	100
061187	ROUCHEL UPPER (MULUMLA)	32.1167	151.2333	1960	1977	100
061188	BROKE (SENTRY BOX)	32.7092	151.0622	1959	1996	100
061189	ECCLESTON (SHELLBROOK)	32.2000	151.5000	1960	1981	100
061193	WOLLOMBI (STOCKYARD CREEK)	32.9000	151.0833	1959	1969	99

061194	THE RANCH 2 (MARTINDALE)	32.6000	150.7167	1962	1969	100
061197	BROKE (VERE)	32.6833	151.1333	1959	1986	100
061198	WOLLOMBI (WALLABADAH)	33.0500	151.0167	1959	1968	100
061200	WARKWORTH HOMESTEAD	32.5667	151.0333	1959	1980	100
061203	KERRABEE (WIDDEN)	32.5167	150.3667	1960	1968	100
061207	MAITLAND POWER STATION	32.7000	151.5500	1961	1964	100
061208	RAVENSWORTH ELECTRICITY COMMIS	32.4333	151.0500	1961	1969	100
061210	HOWES SWAMP	33.1333	150.6833	1962	1963	100
061212	LIDDELL (POWER STATION)	32.3767	150.9600	1963	1996	96
061214	HIGHER MACDONALD	33.2167	150.9167	1963	1975	100
061218	SOMERSBY (SILVESTERS ROAD)	33.3500	151.2500	1962	1968	100
061219	DOORALONG	33.1833	151.3500	1963	1976	100
061221	MANGROVE UPPER	33.3000	151.1333	1962	1974	100
061222	ST ALBANS (MOGO CREEK)	33.1672	151.0639	1963	1998	99
061223	MARYVILLE	32.9131	151.7500	1964	1993	100
061232	SINGLETON PITT STREET	32.5667	151.1667	1964	1975	100
061233	DENMAN (HORSESHOE)	32.5000	150.8000	1964	1975	100
061234	WESTBROOK (BENALLA)	32.4333	151.3167	1964	1970	100
061237	POKOLBIN (KEIRA)	32.7833	151.3167	1961	1972	100
061240	WOLLOMBI (BLAIR)	32.9667	151.1333	1959	1981	99
061243	OAKLANDS (RAVENS WORTH)	32.4333	151.0167	1920	1965	100
061245	MILBRODALE A.R.G.	32.6833	151.0333	1965	1969	100
061248	KINCUMBER	33.4667	151.4000	1967	1975	100
061249	GRESFORD EAST (STRATHISLA HMSD)	32.4000	151.5500	1965	1972	100
061252	BULGA (REEDY CREEK)	32.6500	151.0000	1968	1974	100
061253	HOLGATE (WATTLE TREE ROAD)	33.4000	151.4167	1968	1971	96
061254	CHARLESTOWN	32.9667	151.7000	1968	1972	100
061255	WAMBERAL (DILLON ROAD)	33.4197	151.4472	1968	1988	100
061256	COAL POINT (ROBEY ROAD)	33.0500	151.6167	1968	1977	100
061257	MIRANNIE	32.3833	151.3833	1894	1980	100
061258	MARTINS CREEK (GOSTWYCK HOUSE)	32.5675	151.6069	1967	1971	100
061259	MAITLAND WEST AERO	32.7000	151.4667	1968	1974	100
061262	MUNMORAH POWER STATION	33.2167	151.5500	1963	1969	100
061263	WAPPINGUY (WYNDHAM)	32.1667	150.4000	1968	1969	100
061264	BAERAMI CREEK (BOREEWAN)	32.4500	150.4500	1968	1984	100
061269	DOYLES CREEK (DOYLES 2)	32.5333	150.8000	1967	1968	100
061271	BRANXTON STATION STREET	32.6667	151.3500	1969	1978	100
061272	GLENNIES CREEK (SYDENHAM)	32.4500	151.1333	1969	1974	100
061275	SINGLETON ARMY	32.6133	151.1717	1969	1990	100
061289	QUORROBOLONG POST OFFICE	32.9167	151.3667	1959	1981	99
061291	MERRIWA (MOUNTAIN STATION)	32.0000	150.3500	1969	1970	100
061293	BULGA POLICE STATION	32.6667	151.0167	1968	1975	100
061296	HOWES VALLEY (OWENSDALE)	32.9233	150.7267	1970	1995	100

061305	MUSWELLBROOK (MIRRABOOKA)	32.2106	150.7606	1971	1986	100
061307	ROTHBURY (BROOKLANDS)	32.7667	151.3167	1965	1971	100
061308	POKOLBIN (TYRRELLS VINEYARD)	32.7667	151.2667	1964	1973	100
061313	MILLFIELD (CEDAR CREEK)	32.8667	151.2000	1971	1982	100
061317	SANDY HOLLOW (MT DANGER VINEYAR	32.3333	150.5667	1972	1975	100
061321	GUNGAL (SPRINGFIELD)	32.2167	150.5500	1972	1972	101
061323	DORA CREEK (COORANBONG ROAD)	33.0800	151.4919	1972	1993	100
061326	CESSNOCK (O'CONNOR)	32.7833	151.3333	1965	1979	100
061328	GRESFORD EAST (DURHAM RD)	32.4333	151.5500	1973	1976	100
061331	ECCLESTON (MARILA PARK)	32.2167	151.5167	1973	1976	100
061335	STEWARTS BROOK COMPOSITE	32.0000	151.2833	1891	1983	99
061340	WARDS RIVER (MEROO)	32.2333	151.8500	1970	1977	100
061341	WOY WOY SOUTH (WOY WOY RD)	33.5000	151.3167	1977	1979	100
061361	DUNGOG (WALLARINGA)	32.4678	151.6833	1968	1998	100
061362	WARNERVALE (HAKONE ROAD)	33.2422	151.4714	1988	1993	99
061370	BARNSLEY (BENDIGO STREET)	32.9336	151.5792	1991	2001	100
061378	BATEAU BAY (ROTHERHAM ST)	33.3806	151.4544	1993	1997	100
061379	WILLIAMTOWN COMPARISON AWS	32.8081	151.8419	1995	1999	92
062001	BROGANS CREEK CEMENT QUARRY	33.0000	149.9667	1950	1978	100
062006	CHARBON STANDARD PORTLAND CEME	32.9000	149.9667	1929	1978	98
062012	CUDGEGONG (KIORA)	32.7333	149.7500	1898	1970	100
062016	KANDOS	32.8667	149.9667	1938	1967	100
062020	BYLONG (MONTORO)	32.5014	150.0333	1935	1991	100
062023	OLINDA (SPRINGDALE)	32.8500	150.1333	1898	1967	100
062030	WALLAROI	32.8000	149.0333	1925	1973	100
062033	HARGRAVES (WEEROONA)	32.8667	149.3667	1897	1971	100
062034	STUART TOWN	32.8000	149.0833	1889	1972	100
062041	DOONDI	32.0333	149.8167	1960	1970	100
062043	RYLSTONE (GULFS HEAD)	32.6500	150.0167	1960	1970	100
062045	ULAN (MITTAVILLE)	32.3167	149.8833	1960	1982	100
062047	PETERS CREEK	32.5833	149.9333	1960	1961	101
062048	BYLONG (POGGY)	32.2833	150.0833	1960	1977	100
062050	BORAMBIL (ROSEBUD)	32.1000	149.9833	1961	1979	100
062052	TWO MILE FLAT POST OFFICE	32.4167	149.3333	1959	1975	100
062053	ULAN POWER STATION	32.2667	149.7333	1960	1974	100
062054	WILTON DOWNS	32.1833	149.8667	1960	1969	100
062055	RYLSTONE (MARSDEN FOREST)	32.9500	150.0500	1948	1984	89
062069	MERRIWA (PEMBROKE)	32.0167	150.1500	1930	1980	100
062074	LINBURN (LANDFALL)	32.4167	149.7167	1967	1968	100
062077	CUDGEGONG (LINCOLN HILLS)	32.8667	149.7667	1968	1975	100
062078	UPPER BOTOBOLAR (TRIG HILL)	32.5667	149.8667	1968	1968	101
062083	HILL END (ALPHA)	32.9667	149.4333	1971	1976	100
062087	CULLENBONE (WANDU)	32.4833	149.5000	1971	1972	84

062088	UPPER BOTOBOLAR (CLIFTON)	32.5333	149.8333	1971	1972	92
062090	CLANDULLA (EDENVALE)	32.9500	149.9500	1973	1977	100
063001	ORANGE (ADAIR)	33.1944	149.0083	1908	2000	88
063002	BARRY	33.6500	149.2667	1916	1979	100
063004	BATHURST GAOL	33.4167	149.5500	1858	1983	100
063006	CADIA COMPOSITE	33.5000	149.0000	1926	1968	100
063008	BARRALLIER	34.3000	150.0667	1936	1971	100
063010	BLAYNEY POST OFFICE	33.5350	149.2600	1885	1992	100
063014	BURRAGA	33.9667	149.5333	1949	1968	100
063019	CARCOAR	33.6167	149.1333	1881	1969	99
063025	TARALGA (GRATHAWAI)	34.2833	149.7833	1896	1985	100
063031	GLEN DAVIS (THE GULLIES)	33.1167	150.2500	1940	1969	100
063034	HAMPTON (KIRRAWA STUD)	33.6500	150.0333	1945	1976	100
063037	OBERON (JENOLAN STATE FOREST)	33.7497	150.0381	1939	1998	100
063040	KINGS TABLELANDS	33.7667	150.3833	1903	1971	100
063042	KURRAJONG POST OFFICE	33.5556	150.6683	1932	1991	96
063045	LEURA POST OFFICE	33.7117	150.3417	1908	1996	100
063046	LIDSDALE STATE FOREST	33.4500	150.0500	1938	1978	100
063048	LITTLE HARTLEY (SHEEPCOMBE)	33.5667	150.2000	1899	1976	100
063050	LYNDHURST	33.7000	149.0000	1897	1961	100
063051	MARRANGAROO (GLENROY)	33.4500	150.1167	1946	1986	100
063056	MOUNT VICTORIA (MT VICTORIA (SE	33.5917	150.2544	1872	1990	100
063057	MOUNT WILSON (NOOROO)	33.5000	150.3667	1876	1978	100
063058	MULLION CREEK (MULLION RANGE FO	33.0934	149.1280	1938	1999	99
063063	OBERON (BUCKLEY CRESCENT)	33.7167	149.8667	1888	1989	100
063065	ORANGE POST OFFICE	33.2833	149.1000	1870	1968	100
063067	ORANGE 3	33.3333	149.1000	1892	1968	100
063068	PEELWOOD	34.1167	149.4333	1936	1970	100
063070	PORTERS RETREAT	34.0333	149.7833	1938	1966	100
063075	SODWALLS POST OFFICE	33.5167	150.0000	1952	1976	100
063082	THOMPSONS CREEK	33.9500	149.5500	1949	1960	100
063084	TUENA	34.0167	149.3167	1891	1966	100
063086	BLAYNEY (VITTORIA)	33.4500	149.3333	1902	1977	100
063090	WELLWOOD	33.3167	149.1500	1885	1975	100
063091	BURRAGA (EMDEN VALE)	34.0833	149.6167	1961	1971	100
063092	WENTWORTH FALLS POST OFFICE	33.7167	150.3833	1898	1973	100
063097	KIRKCONNELL (SUNNY CNR)	33.4000	149.8000	1910	1960	100
063099	BUCKEMALL CREEK	33.8167	149.9333	1954	1970	100
063101	DUCKMALOI RIVER	33.7500	149.8833	1954	1967	100
063102	EDITH	33.7833	149.9167	1951	1972	100
063103	EDITH (MELROSE PARK)	33.7833	149.9333	1954	1967	100
063105	GROSE VALE	33.5833	150.6500	1954	1971	100
063106	HAZELGROVE	33.6667	149.9000	1954	1973	100

063108	OBERON DAM	33.7167	149.8667	1956	1988	97
063109	PEEL POST OFFICE	33.3167	149.6333	1955	1973	100
063110	TYAR	33.0000	150.1500	1935	1964	100
063111	KIRKCONNELL PRISON CAMP	33.4167	149.8500	1954	1977	100
063121	QUOBLEIGH	34.1500	149.7500	1960	1967	100
063122	OBERON FORESTRY OFFICE	33.7000	149.8500	1956	1968	100
063123	FERNLEIGH	34.2500	149.9333	1961	1962	100
063129	VITTORIA (TARINGA)	33.4500	149.2833	1962	1977	100
063131	ANGUS PLACE (WOLGAN GAP)	33.3167	150.1167	1959	1982	100
063133	WALLERAWANG (THOMPSONS CREEK)	33.4000	150.0333	1959	1971	100
063134	KAROO (MEADOW FLAT)	33.4333	149.9333	1959	1966	100
063135	GARRYOWEN	33.5167	149.8167	1959	1966	100
063137	YETHOLME (WOMBOYNE PARK)	33.4700	149.7731	1959	1995	100
063138	TARANA (ROSELYN)	33.5167	149.9167	1959	1986	100
063140	HILLMEADS	33.5167	150.2500	1959	1969	100
063141	HARTLEY VALE (VELLACOTT PARK)	33.5242	150.2144	1959	1992	100
063143	CLOVER DOWNS	33.5833	149.9833	1959	1971	100
063144	SOUTH BOWENFELS	33.5167	150.1333	1959	1980	100
063145	WISEMANS CREEK (FAIRVIEW)	33.6333	149.7333	1959	1972	100
063147	CARLWOOD (KANBARA)	33.6167	149.8500	1959	1979	100
063148	BELOWRA	33.7167	150.0000	1959	1964	100
063149	ARLAMONT	33.7000	149.9333	1959	1969	100
063150	HAZELGROVE (THE MEADOWS)	33.6333	149.9333	1959	1974	100
063151	LITTLE HARTLEY (KANIMBLA)	33.6272	150.1900	1959	1990	100
063152	KANIMBLA VALLEY (GWENLEA)	33.6689	150.2100	1959	1991	83
063153	INVERNESS	33.5833	149.7667	1959	1966	100
063156	JOCELYN (SWEET BRIAR)	33.6500	149.7833	1959	1976	100
063157	LOCHLENE	33.8167	149.8333	1959	1964	100
063158	OBERON (MULWAREE)	33.7833	149.8167	1959	1976	100
063159	KENTUCKY	33.7667	149.7500	1959	1969	100
063160	GINGKIN (TUGLOW VIEW)	33.9667	149.9167	1959	1974	100
063161	MEGALONG (HILLVIEW)	33.7167	150.2333	1959	1967	100
063162	MEGALONG (GREEN GULLY)	33.7667	150.2167	1959	1970	100
063163	RICHLANDS TELEGRAPH OFFICE	34.3333	149.8167	1959	1976	100
063166	TRUNKEY CREEK (ARKELL)	33.7167	149.3833	1962	1973	100
063168	CAPERTEE (LOCHABER)	33.1500	149.9833	1962	1981	100
063170	GARLAND (WOODVIEW)	33.7167	149.0167	1962	1969	100
063171	BLACKHEATH (CLIFFVIEW)	33.6667	150.2667	1962	1967	100
063173	ROTHESAY (WENTWORTH FALLS)	33.7167	150.3833	1962	1970	100
063174	MEGALONG (SUNNY RIDGE)	33.7667	150.2167	1962	1974	100
063176	WALLERAWANG POWER STATION	33.4000	150.0667	1902	1973	100
063177	GLEN DAVIS POST OFFICE	33.1167	150.2833	1962	1986	81
063178	CROWN VIEW	33.2000	150.0167	1962	1968	100

063179	CAPERTEE (THE MEADOWS)	33.1800	150.1506	1962	2001	97
063180	GLEN ALICE (WATERVALE)	33.0650	150.0951	1931	2000	100
063181	COLO UPPER 1	33.4333	150.7333	1928	1971	100
063182	BILPIN (MOUNTAIN LAGOON)	33.4500	150.6333	1962	1973	100
063184	BLAXLAND RIDGE	33.5000	150.7500	1962	1979	100
063216	CARCOAR (ICELY STREET)	33.6167	149.1333	1969	1973	100
063226	BOWENFELS (COOERWULL)	33.4833	150.1500	1878	1973	100
063230	BLAXLAND WESTERN HIGHWAY	33.7500	150.6000	1968	1980	100
063232	RYDAL (BONHOLME)	33.5833	150.0333	1968	1976	100
063235	GLEN ALICE (WONGARA)	33.0167	150.1500	1968	1972	100
063237	ORANGE TV CHANNEL CNB8	33.3000	149.1167	1968	1968	101
063240	NEWBRIDGE POST OFFICE	33.5833	149.3667	1968	1987	100
063241	CAPERTEE (BERNINA)	33.1300	149.9789	1968	1997	99
063243	JERRONG (BELVEDERE)	34.1667	149.8500	1962	1979	100
063244	ORANGE (WOLAROI)	33.3000	149.1167	1969	1975	100
063247	GLENARA	33.6000	150.6500	1899	1969	100
063248	GROSE WOLD ROAD	33.6017	150.6783	1969	1994	100
063253	ORANGE (ROSETEAGUE)	33.3167	149.0500	1955	1983	100
063256	BULLABURRA (FAIRVIEW)	33.7333	150.4167	1970	1978	100
063259	CARCOAR (ERROWANBANG)	33.5500	149.0500	1900	1972	100
063261	HILLEND (BRUINBUN)	33.1383	149.4567	1973	1983	100
063263	MILLTHORPE (TOP VIEW)	33.0367	149.6000	1973	1980	100
063264	KATOOMBA CITY COUNCIL	33.7167	150.3167	1967	1973	100
063266	COLO UPPER WARD BROS	33.3833	150.7000	1972	1973	100
063274	FULLERTON (PINE GROVE)	34.2361	149.5500	1978	1986	80
063281	BLACKHEATH M.C.A.	33.6333	150.2833	1981	1983	100
064011	DUNEDOO (MARTINDALE 2)	32.0000	149.4000	1959	1988	100
064019	BOSTON (GOLLAN)	32.2833	149.0833	1962	1973	99
064051	COBBORA (KANDIMULLA)	32.0272	149.2281	1989	1997	100
065003	BODANGORA POST OFFICE	32.4500	149.0000	1899	1968	100
066001	AUDLEY NATIONAL PARK BOTTOM ST	34.0667	151.0500	1899	1979	100
066002	BALGOWLAH (ETHEL STREET)	33.7997	151.2508	1940	1989	100
066003	BANKSTOWN (CONDELL PARK)	33.9167	151.0167	1906	1979	100
066005	BONDI BOWLING CLUB	33.8833	151.2667	1939	1982	100
066007	BOTANY NO.1 DAM	33.9333	151.2167	1870	1978	100
066008	BROOKLYN	33.5500	151.2333	1913	1970	100
066010	CHATSWOOD COUNCIL DEPOT	33.8014	151.1917	1897	1993	98
066012	CHATSWOOD WATER SUPPLY	33.8000	151.2000	1894	1970	100
066015	CROWN ST. RESERVOIR	33.8833	151.2000	1882	1960	100
066018	EARLWOOD BOWLING CLUB	33.9333	151.1167	1914	1975	100
066019	EASTWOOD COCOS AVENUE	33.7833	151.0833	1927	1961	100
066021	ALEXANDRIA (ERSKINEVILLE)	33.9167	151.2000	1948	1973	100
066027	HORNSBY MWSDB	33.7000	151.1000	1946	1973	100

066028	HORNSBY (PRETORIA PARADE)	33.7083	151.0839	1923	1995	87
066032	LINDFIELD WEST	33.7822	151.1486	1950	1992	100
066035	MANLY TOWN HALL	33.8000	151.3000	1914	1963	100
066041	MOSMAN WATER SUPPLY	33.8333	151.2500	1904	1967	100
066046	PARRAMATTA	33.8167	151.0000	1832	1960	97
066047	PENNANT HILLS	33.7333	151.0667	1900	1969	100
066049	PENSHURST	33.9667	151.0833	1904	1970	100
066055	LIDCOMBE (CARNARVON GOLF CLUB)	33.8667	151.0333	1906	1970	100
066056	ROSEVILLE BOWLING CLUB	33.7833	151.1833	1914	1979	100
066057	RYDE PUMPING STATION	33.8167	151.1000	1894	1978	100
066060	SUTHERLAND MWSDB	34.0333	151.0667	1907	1972	100
066061	SYDNEY NTH BOWLING CLUB	33.8333	151.2000	1950	1974	100
066063	WAHROONGA RESERVOIR	33.7206	151.1128	1906	1991	100
066064	CONCORD WALKER HOSPITAL	33.8333	151.1000	1894	1972	100
066066	WAVERLEY SHIRE COUNCIL	33.9000	151.2500	1932	1964	100
066067	WOLLSTONECRAFT	33.8333	151.2000	1915	1975	100
066068	VAUCLUSE	33.8667	151.2833	1934	1975	100
066069	HURSTVILLE GROVE (WAITARA PARAD	33.9833	151.1000	1952	1981	100
066074	ROCKDALE BOWLING CLUB	33.9500	151.1333	1949	1974	100
066075	WAVERTON BOWLING CLUB	33.8411	151.1967	1955	2001	98
066076	WILEY PARK (ROSELANDS)	33.9367	151.0700	1949	1987	100
066077	TERREY HILLS	33.6833	151.2333	1963	1966	100
066081	NORTH RYDE STROUD STREET	33.8000	151.1333	1960	1979	100
066082	CONCORD WEST PLASTER MILLS	33.8333	151.0833	1961	1982	100
066083	PALM BEACH COASTERS RETREAT	33.6000	151.3000	1960	1983	80
066084	PENNANT HILLS WEST (SAWENI)	33.7500	151.0500	1961	1962	100
066085	GRANVILLE RSL BOWLING CLUB	33.8361	151.0128	1958	2000	97
066088	MANLY NORTH	33.7833	151.2833	1959	1975	100
066089	MANLY NORTH BOWLING CLUB	33.7939	151.2692	1961	1987	100
066092	DURAL	33.6833	151.0333	1963	1972	100
066115	MARSFIELD	33.7833	151.1167	1964	1965	100
066116	BUNDEENA COMPOSITE	34.0833	151.1500	1964	1978	100
066117	TURRAMURRA NORTH	33.7167	151.1667	1964	1967	100
066118	FRENCHS FOREST FITSPATRICK AVE	33.7500	151.2333	1964	1982	100
066121	CHESTER HILL	33.8833	151.0000	1964	1976	100
066122	MAROUBRA RSL BOWLING CLUB	33.9500	151.2500	1964	1974	100
066123	INGLESIDE	33.6833	151.2667	1964	1977	100
066126	COLLAROY (LONG REEF GOLF CLUB)	33.7333	151.3167	1965	1979	100
066127	BEACON HILL RAAF	33.7500	151.2500	1968	1973	100
066129	BEECROFT	33.7500	151.0667	1905	1962	100
066130	NORTHBRIDGE (SAILORS BAY)	33.8167	151.2167	1924	1980	100
066133	WATTAMOLLA R.N.P.	34.1333	151.1167	1967	1968	101
066135	SILVERWATER (RANAD NEWINGTON)	33.8333	151.0667	1967	1973	100

066136	CARINGBAH (LILLI PILLI)	34.0667	151.1167	1968	1973	100
066139	PADDINGTON	33.8833	151.2167	1968	1976	100
066140	COTTAGE POINT (NOTTINGS)	33.6167	151.2000	1969	1969	100
066143	KURING-GAI CHASE (WEST HEAD)	33.5800	151.2983	1969	1991	90
066144	PEAKHURST FOREST ROAD	33.9667	151.0667	1964	1969	100
066145	SEAFORTH CASTLE CIRCUIT	33.7894	151.2392	1968	1993	100
066146	BROKEN BAY NATL FITNESS CAMP	33.5667	151.2667	1969	1975	100
066154	HOLDSWORTHY AIR CAVALRY	33.9500	150.9500	1970	1974	100
066155	BROOKLYN (WOBBY BEACH)	33.5500	151.2500	1970	1975	100
066156	MARSFIELD (MACQUARIE UNIVERSITY	33.7744	151.1156	1970	1997	100
066159	HORNSBY (MOUNT WILGA)	33.6939	151.0925	1969	1987	100
066166	CREMORNE GRASMERE ROAD	33.8283	151.2217	1963	1989	100
066169	VILLAWOOD ARCHIVES	33.8333	151.0000	1975	1977	100
066171	MOOREBARK N.B.GOLF CLUB	33.9500	150.9500	1964	1980	100
066174	DUNDAS	33.8167	151.0333	1962	1967	100
066187	TAMARAMA (CARLISLE ST)	33.8997	151.2681	1991	1999	88
067004	EMU PLAINS	33.7500	150.6667	1880	1973	100
067005	FAIRFIELD POST OFFICE	33.8833	150.9500	1930	1960	100
067006	FAIRFIELD MWSDB	33.9000	150.9500	1947	1970	100
067008	GUILDFORD	33.8667	150.9833	1958	1977	100
067009	GLENFIELD (MACQUARIE)	33.9667	150.9000	1886	1983	100
067013	LIVERPOOL	33.9167	150.9333	1926	1966	100
067016	MINCHINBURY	33.8000	150.8333	1901	1970	100
067018	PENRITH LADBURY AVENUE	33.7542	150.6783	1890	1994	99
067024	ST MARYS BOWLING CLUB	33.7667	150.7667	1897	1984	100
067025	ST MARYS MWSDB	33.7333	150.7667	1947	1973	100
067030	WILBERFORCE (GLEN ROCK)	33.5500	150.8000	1938	1966	100
067032	WESTMEAD AUSTRAL AVENUE	33.8144	150.9833	1944	1992	100
067033	RICHMOND RAAF	33.6022	150.7794	1928	1994	100
067035	LIVERPOOL(WHITLAM CENTRE)	33.9272	150.9128	1962	2001	100
067036	AUSTRAL EIGHTH AVE	33.9333	150.8167	1964	1989	100
067039	AJANA	33.6500	150.7667	1963	1964	100
067044	LOWER PORTLAND (ORANGE GROVE)	33.4481	150.8806	1963	1988	100
067045	SILVERDALE	33.9167	150.6000	1963	1965	100
067059	BLACKTOWN	33.7694	150.8856	1963	1993	100
067060	LONG POINT	34.0167	150.9000	1964	1968	100
067063	COBBITTY (CUTHILL)	33.9833	150.6667	1965	1973	100
067064	CECIL PARK ANDERSONS RES.FARM	33.8667	150.8333	1964	1970	100
067067	EMU PLAINS	33.7600	150.6567	1911	1996	100
067068	BADGERYS CREEK MCMASTERS F.STN	33.8683	150.7278	1936	1996	99
067069	GREENVALLEY (MILLER)	33.9167	150.8667	1967	1971	100
067071	THORNLEIGH BRIDGEVIEW CRESCENT	33.7167	151.0833	1968	1972	100
067072	FAIRFIELD HEIGHTS POST OFFICE	33.8667	150.9333	1968	1975	100

067073	MARALYA BOUNDARY ROAD	33.6200	150.8967	1963	1995	100
067083	MOUNT DRUITT FRANCIS STREET	33.7667	150.8000	1970	1976	100
067087	GLENORIE (GATELEIGH PARK)	33.6167	151.0167	1972	1973	100
067091	CABRAMATTA	33.9000	150.9167	1945	1967	100
067092	QUAKERS HILL DOUGLAS RD.	33.7333	150.8833	1963	1971	100
067097	PRESTONS BERNERA ROAD	33.9333	150.8667	1983	1985	100
067101	BOX HILL JUNCTION ROAD	33.6649	150.8780	1985	1995	92
067103	CATTAI MITCHELL PARK ROAD	33.5583	150.9161	1988	1996	96
067106	BERKSHIRE PARK FIRST RD	33.6708	150.7972	1992	1995	100
067107	VARROVILLE (ST JAMES ROAD)	33.9928	150.8178	1992	1998	100
067118	OAKHURST (LAWTON PLACE)	33.7431	150.8356	1997	1999	100
067120	HOXTON PARK (RANIERI PLACE)	33.9319	150.8553	1998	2001	100
068001	APPIN CHURCH ST	34.2069	150.7931	1917	1999	82
068002	AVON DAM MWSDB	34.3500	150.6333	1919	1967	100
068005	BOWRAL POST OFFICE	34.5000	150.4000	1885	1965	100
068006	BELANGLO STATE FOREST	34.5367	150.2528	1940	1990	100
068011	CAMDEN BOWLING CLUB	34.0500	150.7167	1883	1977	100
068012	CAMDEN MWSDB	34.0500	150.7000	1946	1970	100
068013	MENANGLE JMAI	34.1258	150.7375	1861	1998	100
068014	CAMPBELLTOWN 1	34.0667	150.8000	1845	1961	100
068015	CAMPBELLTOWN 2 MWSDB	34.0667	150.8167	1946	1970	100
068017	CATARACT RIVER	34.2333	150.7500	1883	1966	100
068018	CORDEAUX NO.1 DAM	34.3333	150.7333	1909	1967	100
068019	CORDEAUX NO.2 DAM	34.4333	150.7833	1915	1967	100
068020	CORDEAUX QUARTERS	34.3333	150.7500	1932	1967	100
068023	DAPTO WEST (STANE DYKES)	34.4708	150.7736	1898	1987	100
068025	EXETER	34.6000	150.3000	1908	1975	100
068031	BURRUER (ILLAROO)	34.8667	150.4500	1902	1963	100
068032	JAMBEROO (LORNA)	34.6500	150.7833	1885	1963	100
068037	KENNY HILL	34.0500	150.7667	1925	1970	100
068039	MADDENS CREEK	34.2500	150.9333	1907	1970	100
068040	MITTAGONG (MAGUIRES CROSSING)	34.4833	150.5333	1928	1970	100
068043	MINTO SURREY STREET	34.0283	150.8433	1889	1990	100
068046	MOUNT PLEASANT	34.4000	150.9000	1907	1964	100
068047	NEPEAN DAM	34.3333	150.6000	1926	1970	100
068051	PENROSE (PANORAMA)	34.6667	150.2333	1900	1975	100
068054	ROBERTSON POST OFFICE	34.5833	150.6167	1890	1989	100
068056	SHERBROOKE	34.3000	150.9000	1892	1970	100
068057	SUBLIME POINT (TOOMA)	34.3167	150.9000	1940	1967	100
068058	SUTTON FOREST (URALBA)	34.5667	150.3500	1901	1966	100
068059	THE OAKS JOHN STREET	34.0833	150.5833	1912	1975	100
068060	UNANDERRA	34.4667	150.8333	1903	1969	100
068061	VIADUCT CREEK	34.5167	150.7000	1933	1968	100

068063	WATERFALL (GARRAWARRA H)	34.1667	150.9667	1907	1970	100
068065	WEDDERBURN	34.1667	150.8167	1930	1971	100
068066	WILTON	34.2000	150.6000	1869	1967	100
068067	WINGELLO STATE FOREST	34.7167	150.2000	1940	1972	100
068068	WOLLONDILLY (BULLIO)	34.3472	150.1500	1941	1988	100
068071	YERRINBOOL	34.3667	150.5500	1916	1970	100
068073	KANGALOOM E (GLEN MAVIS)	34.5167	150.5333	1953	1979	100
068074	WOLLONGONG (SMITHS HILL)	34.4333	150.9000	1938	1972	100
068075	SUTTON FOREST (CHERRY TREE HILL	34.5500	150.2667	1956	1980	100
068076	NOWRA RAN AIR STATION	34.9449	150.5450	1942	2000	98
068078	HYMAS BEACH CYRUS STREET	35.1000	150.7000	1960	1974	100
068079	JERVIS BAY NATURE RESERVE	35.1319	150.7056	1958	1993	98
068081	CAMPBELLTOWN SWIMMING CENTRE	34.0833	150.8167	1959	1984	100
068084	TERARA	34.8667	150.6333	1961	1965	100
068086	MOUNT KEIRA SCOUT CAMP	34.4031	150.8433	1944	1992	100
068087	SPRING HILL (WARANA)	34.4333	150.5000	1959	1967	97
068090	BANGADILLY	34.4833	150.1167	1959	1966	100
068091	BERRIMA WEST POST OFFICE	34.4833	150.2667	1959	1969	100
068092	BERRIMA (HILLVIEW)	34.4833	150.3667	1959	1967	100
068094	BRIDGEWATER	34.6000	150.2167	1959	1967	100
068095	CANYONLEIGH (MEGALONG)	34.5500	150.1500	1959	1972	100
068096	CANYONLEIGH (GLENCOE)	34.6000	150.1167	1945	1980	100
068097	SPRING VALLEY (WINGELLO)	34.6500	150.1333	1959	1963	100
068099	BOYTON LEA	34.4333	150.3333	1960	1968	100
068103	MOUNT KEIRA SUMMIT	34.4000	150.8500	1962	1966	100
068106	CLIFTON (COALCLIFF)	34.2453	150.9697	1943	1998	100
068107	COLEDALE RAILWAY STATION	34.2833	150.9500	1943	1984	100
068109	TALLONG (CAOURA)	34.7833	150.1667	1919	1975	100
068111	BUDGONG	34.7667	150.4833	1962	1971	100
068112	GARIE BEACH	34.1667	151.0667	1962	1985	98
068113	DUNMORE (KURRAWONG)	34.6000	150.8500	1962	1974	100
068114	BUNDANOON (MERYLA)	34.6667	150.3667	1962	1971	100
068115	OCEAN VIEW (ROBERTSON)	34.5667	150.6167	1962	1969	100
068116	PHEASANTS GROUND	34.6000	150.6500	1962	1969	100
068118	CAMBEWARRA (TAPI TALLIE)	34.8333	150.5333	1962	1978	100
068119	TOWRADGI	34.3833	150.9000	1962	1975	100
068120	WILTON POST OFFICE	34.2500	150.7000	1962	1980	100
068121	YALLAH	34.5333	150.7833	1962	1973	100
068124	UPPER KANGAROO RIVER	34.6750	150.5917	1962	1992	100
068126	NIDGEE STUD	34.4500	150.8167	1962	1972	100
068127	DOUGLAS PARK POST OFFICE	34.1833	150.7167	1962	1977	100
068128	ALPINE	34.4000	150.5167	1962	1970	100
068129	ALBION PARK (PARKVALE)	34.6000	150.7500	1962	1967	91

068130	YALLAH (IANWYN)	34.5333	150.7167	1962	1981	100
068132	STANWELL PARK (HILLCREST)	34.2333	150.9833	1963	1974	100
068133	TAHMOOR POST OFFICE	34.2167	150.6000	1962	1974	100
068146	KEMBLA HEIGHTS MWSDB	34.4167	150.8167	1956	1973	100
068158	PICTON RUMPKER STREET	34.1833	150.6000	1964	1987	100
068161	WATTAMOLLA	34.7333	150.6167	1966	1975	100
068163	LEICESTER PARK	34.4167	150.4000	1957	1970	100
068164	OAKDALE (SILVER HILL)	34.1000	150.5167	1956	1967	100
068168	KNIGHTS HILL (CHANNEL 5A)	34.6244	150.6939	1964	1990	99
068170	MOUNT NEBO COLLIERY	34.4333	150.8000	1966	1979	100
068171	WOLLONGONG OBRIENS ROAD	34.4333	150.8500	1966	1971	100
068172	MOUNT KEMBLA 2	34.4333	150.8167	1966	1967	100
068173	KEMBLA HEIGHTS CORDEAUX ROAD	34.4333	150.8000	1967	1968	101
068174	WOODHILL BROGERS CREEK ROAD	34.7183	150.6850	1967	1994	100
068176	TAHMOOR (RANFURLY)	34.2500	150.6333	1968	1972	100
068177	MADDENS PLAINS (BOOMERANG GOLF	34.2517	150.9444	1907	1990	100
068178	BARREN GROUNDS NATURE RES.	34.6833	150.7167	1973	1976	100
068179	KANGALOON POST OFFICE	34.5500	150.5333	1968	1976	100
068182	NERRIGA (GLENGARRY)	35.1333	150.1333	1969	1973	100
068183	NERRIGA (TOUGA)	34.9500	150.0833	1961	1977	100
068184	BOWRAL CENTENNIAL ROAD	34.4667	150.3833	1967	1977	100
068185	WILDES MEADOW (LONGVIEW)	34.6167	150.5333	1953	1988	99
068191	BARRALLIER (BELL BIRD)	34.3000	150.0667	1971	1973	100
068193	BARGO POST OFFICE	34.2833	150.5833	1902	1970	100
068203	SASSAFRAS (ETTREMA)	35.0850	150.2300	1962	1992	100
068207	COBBITY (ROSENEATH)	34.0167	150.6833	1888	1974	100
068208	WERONBI POST OFFICE	33.9833	150.5833	1954	1975	100
068220	MINTO (ALDERNEY STREET)	34.0411	150.8458	1984	1996	91
068225	CAMDEN (CAMTRAC)	34.0400	150.6983	1986	2000	98
068227	AMBARVALE CLENNAM AVE	34.0867	150.7917	1988	2001	98
069000	ARALUEN POST OFFICE	35.6500	149.8167	1891	1970	100
069001	BATEMANS BAY POST OFFICE	35.7086	150.1769	1895	1996	100
069031	ULLADULLA	35.3667	150.4833	1937	1974	100
069038	MORUYA BOWLING CLUB	35.9167	150.0667	1886	1966	100
069043	MORUYA (DEUA RIVER FARM)	35.8333	149.9833	1971	1976	100
069046	MONGARLOWE	35.4333	149.9333	1960	1966	100
069092	NELLIGEN CLYDE ROAD	35.6500	150.1167	1967	1971	100
069098	TOMAKIN (BEVIAN PARK)	35.8167	150.2167	1968	1973	100
069102	NORTH ARALUEN	35.6333	149.8000	1969	1980	100
069105	ARALUEN (MERRICUMBENE)	35.7333	149.8667	1970	1979	100
069106	WOODBURN STATE FOREST	35.4000	150.4333	1925	1980	100
069113	BROOMAN (GEJU)	35.4667	150.2500	1974	1974	100
069115	GUNDILLION (WYANBENE)	35.7833	149.6667	1974	1977	100

069126	KIOLOA (LONDON FOUNDATION)	35.5467	150.3767	1980	1986	83
070001	MARULAN (ARTHURSLEIGH)	34.5667	150.0500	1913	1976	100
070003	BANNISTER STATION	34.6000	149.5000	1943	1977	100
070006	BOX GULLY	34.6500	150.2500	1945	1967	100
070007	BREADALBANE (SWEETWOOD LEA)	34.7667	149.4667	1902	1974	100
070015	CANBERRA FORESTRY	35.3000	149.1000	1927	1981	99
070029	DICKSON	35.2500	149.1000	1942	1962	100
070030	BUNGENDORE (DOUGLAS)	35.1833	149.4000	1885	1973	100
070033	FOREST LODGE	34.6000	149.7000	1926	1960	100
070037	GOULBURN	34.7500	149.8667	1857	1967	100
070039	TOWRANG GREENWICH PARK	34.6000	149.9333	1945	1982	99
070041	GOULBURN (GUNDARY PLAINS)	34.8500	149.7500	1946	1967	100
070042	GUNDAROO (BAIRNSDALE)	35.0333	149.2667	1877	1966	100
070046	HANWORTH TELEGRAPH OFFICE	34.4000	150.0667	1945	1971	100
070051	KAIN (CLAIRMONT)	35.7333	149.5667	1952	1969	100
070056	KOWEN FOREST	35.2978	149.2817	1927	1993	98
070065	MICHELAGO RAILWAY	35.7167	149.1667	1941	1962	100
070066	QUEANBEYAN (MOUNT CAMPBELL)	35.4500	149.2000	1891	1973	100
070079	TARAGO (KILDARE)	35.1167	149.6000	1884	1982	100
070081	TARLO (BLYTHBURN)	34.6000	149.8000	1945	1978	100
070086	TARAGO (WILLEROO)	35.0333	149.5167	1911	1971	100
070101	QUEANBEYAN (CARWOOLA)	35.4167	149.3833	1891	1973	100
070110	CHAIN-O-PONDS	34.6167	149.1333	1958	1968	94
070118	KYEEMA	35.1167	149.9333	1942	1971	100
070121	BRAIDWOOD (BANOON)	35.2833	149.7000	1961	1972	100
070122	WINDELLAMA (ROSEVIEW)	35.0167	149.8500	1961	1970	100
070125	TARALGA (GREENMANTLE)	34.4167	149.9667	1959	1982	100
070127	STRATHAVEN	34.4833	150.0000	1959	1967	100
070128	WILLOWGUM HILL	34.4833	149.6667	1959	1966	100
070129	REDMOUNT	34.4667	149.5833	1959	1963	100
070130	CROOKWELL (SPRINGWOOD)	34.5333	149.4667	1959	1974	100
070132	MIDDLE ARM (HOLMWOOD)	34.5167	149.6833	1959	1967	100
070133	KERRAWARY	34.5000	150.0333	1959	1965	100
070134	THE FOREST (BIDGEE)	34.6167	149.7333	1959	1976	100
070138	STRATHMERE	34.8333	149.6167	1959	1971	100
070139	NORWOOD (GOULBURN)	34.7000	149.7167	1959	1969	100
070140	ALLAMBIE	34.6833	149.7833	1959	1966	100
070141	WINDFARTHING	34.7667	149.8833	1959	1973	100
070142	TOWRANG (RIVERVIEW)	34.6667	149.8833	1959	1968	100
070145	STRATHAIRD (CLOVERDALE)	34.4100	149.7528	1960	1993	100
070146	WOODHOUSELEE (WYNN VIEW)	34.6017	149.6250	1960	1995	90
070148	KERRAWARRA	34.5333	150.0167	1960	1964	100
070149	KINGSDALE	34.7000	149.7000	1960	1963	100

070151	GOONUREA	34.4833	149.5167	1961	1973	100
070152	GOULBURN H.M.TRAINING CENTRE	34.7500	149.7333	1962	1969	100
070170	MEDWAY (MARULAN 575)	34.7167	150.0167	1961	1967	100
070210	GOULBURN AERO CLUB	34.8167	149.7333	1967	1971	100
070215	PARKERS GAP (KINDERVALE)	35.6333	149.5167	1968	1977	100
070218	BEVANDALE (WYANGALA)	34.5000	149.0000	1971	1975	100
070230	WINDELLAMA (BUBURBA)	35.0167	149.8667	1970	1976	100
070234	BUNGENDORE OLD KOWEN	35.2667	149.3333	1970	1976	100
070235	GUNDAROO (TILLYGREIG)	35.0667	149.2667	1970	1971	101
070243	CHIFLEY	35.3500	149.0833	1971	1976	100
070244	TORRENS	35.3833	149.0833	1971	1977	100
070245	FARRER LONGERENONG STREET	35.3833	149.1000	1971	1995	95
070248	CURTIN	35.3333	149.0833	1971	1990	100
070253	O'CONNOR (BELCONNEN WAY)	35.2614	149.1083	1971	1995	93
070254	FYSHWICK CITY PARKS	35.3267	149.1500	1971	1997	97
070257	CAMPBELL	35.2833	149.1500	1971	1991	100
070259	FISHER	35.3667	149.0500	1971	1990	99
070262	WESTON CAMPUS C.I.T.	35.3306	149.0600	1971	2001	97
070271	GOULBURN FILTRATION PLANT	34.7500	149.7000	1972	1977	100
070274	RIVETT	35.3500	149.0333	1973	1978	100
070275	MACQUARIE BENNELONG CRESCENT	35.2500	149.0667	1973	1991	100
070276	NERRIGA (OALLEN)	35.1678	149.9583	1972	1992	100
070282	CANBERRA CITY	35.2667	149.1167	1974	1988	100
070284	KIALLA (GLEN ABER)	34.5333	149.4500	1974	1981	100
070285	GOULBURN ST JOHNS	34.7667	149.7000	1975	1978	100
070293	PINE ISLAND	35.4250	149.0600	1978	1987	100
070305	WANNIASSA	35.4025	149.0772	1980	1994	98
070307	BRUCE CIT CAMPUS	35.2506	149.0917	1981	2001	100
070311	HOLDER CITY PARK	35.3319	149.0506	1983	1988	99
070314	WANNIASSA HILLS HOLDEN CRESC	35.3928	149.0819	1983	1991	97
070315	GUNGAHLIN	35.2197	149.1283	1984	1990	87
070318	RICHARDSON	35.4325	149.1200	1985	1990	100
070319	GOWRIE	35.4000	149.1167	1985	1988	100
070332	THEODORE (CONLON ST)	35.4500	149.1167	1989	2001	95
070338	CANBERRA AERO COMPARISON	35.3083	149.1936	1995	1997	99

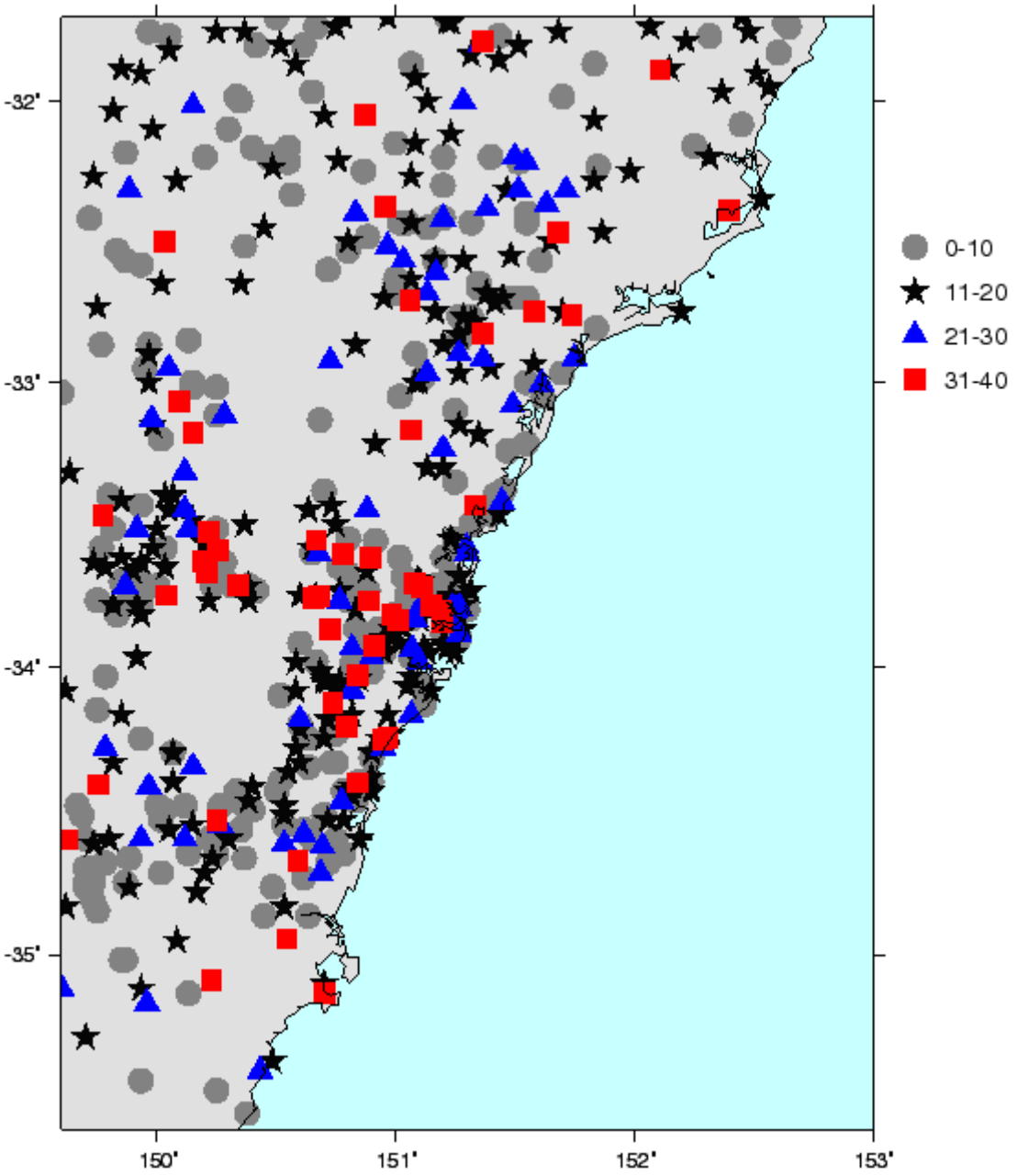

Figure 26: Locations of rainfall stations used to identify extreme rainfall days. Stations are colour-coded by post-1960 length of record.

APPENDIX B

The pressure patterns associated with extreme rainfall are analysed to determine the synoptic-scale weather patterns that are conducive to the extreme weather conditions in the study region. The technique used is known as synoptic typing and follows the method of Yarnal (1993). This is a correlation-based, gridded map-typing technique in which days are grouped based on the Pearson product-moment correlations (r_{xy}) to establish the degree of similarity between map pairs. Similar fields are identified on the basis of similar spatial structures (i.e. highs and lows in similar positions) with little emphasis on the magnitude of the patterns.

To establish a synoptic climatology compatible with the output from the climate models, this technique was first applied to NCEP 12 UTC MSLP fields corresponding to the period approximately 12 hours before the recorded rainfall events. Thus, for the example used previously, the selection criteria identified 6 August 1986 as the date of maximum rainfall and thus the MSLP field for 12 UTC 5 August 1986 was selected for synoptic typing. The MSLP fields were extracted for the 81 points (9×9) corresponding to 145E to 165E and 45S to 25S: the region outlined by the dashed rectangle in Figure 5. The following steps were then applied to this dataset.

In this procedure, each daily MSLP grid is first normalised:

$$Z_i = \frac{x_i - \overline{X}}{s} \qquad \textbf{(2.1)}$$

where Z_i is the normalised value of grid-point i, x_i is the observed value at grid-point i, $\overline{X}$ is the mean of the N-point grid and s is the standard deviation of the grid. The effect of this normalisation is to eliminate the seasonal impact on pressure pattern intensity, thus permitting direct inter-seasonal map comparisons.

Once normalised, each daily map pattern in the extreme rainfall subset is compared with all other maps in the subset using Pearson product-moment correlations (r_{xy}).

$$r_{xy} = \frac{\sum_{i=1}^{N}\left[\left(x_i - \overline{X}\right)\left(y_i - \overline{Y}\right)\right]}{\sqrt{\sum_{i=1}^{N}\left(x_i - \overline{X}\right)^2 \sum_{i=1}^{N}\left(y_i - \overline{Y}\right)^2}} \qquad \textbf{(2.2)}$$

In this formula, x_i and y_i represent the variable at each of the N grid points of the two maps being compared. $\overline{X}$ and $\overline{Y}$ represent the means of the N-point grids. Pairs of MSLP maps are considered similar if $r_{xy} \geq 0.7$. Correlations for each row and column of the 9×9 grid were also calculated to ensure pattern similarity in all areas of the grid. Yarnal (1993) discusses the numerous sources of subjectivity in choosing a correlation threshold. The value of 0.7 was chosen after experimentation showed that it provided an acceptable balance between the number of patterns produced and the number of days that were not classified.

Once all days have been compared with all other days in the dataset, the day with the largest numbers of r_{xy} values meeting the threshold criteria is designated “key day” 1 and is considered representative of the first map type. This “key day’ as well as all the days with which it is considered to be similar on the basis of the correlations are then removed from the analysis. All days deemed to be similar to each of those days are also removed. The analysis is then repeated

with the reduced dataset to find “key day 2”, and so on, until all days are classified into m groups of 3 days or more. The remainder are considered unclassified. Once the “key days” are established, a second pass over the entire data set is made. This is necessary because it is possible for any grid to be significantly correlated with more than one grid. In this step, each map pattern is assigned to the map pattern represented by the “key day” for which it produces the highest correlation. A second pass was also made over the unclassified days so that days that had a relatively high correlation value could be classified into the most appropriate synoptic type. A correlation threshold of 0.5 was chosen for this step.

APPENDIX C

A small number of extreme rainfall events affecting the study region since the mid-1970s were identified and modelled using the model configuration described in Section 5.1. A detailed analysis of these events is not attempted; the results are provided as guidance to the skill of the model in simulating extreme rainfall that has occurred in historic events.

For these simulations initial and boundary conditions were provided by the NCEP reanalyses which have a grid spacing of 2.5°×2.5°. Unlike the models that are used for numerical weather prediction, the initial conditions used here have not been enhanced by the assimilation of surface and upper level atmospheric information. This approach is analogous to the downscaling method used in this study as obviously observations for the future are not available for assimilation into the climate change simulations. The coarse grid spacing of the initial and boundary conditions has implications for the results of the simulations as a small error (e.g. 1 grid spacing) in the location of the extreme rainfall producing weather system means that the location of modelled rainfall will likely be in error. This is a possible reason for the poorer simulation of rainfall in Cases 3, 5 and 6.

The impact of improved initial conditions is illustrated by a simulation of the Pasha Bulker storm of June 2007. In this case the initial conditions were provided by Bureau of Meteorology MALAPS model. MALAPS analyses have a grid spacing of 0.1°×0.1° grid. The model assimilates satellite radiances and winds, providing an improved representation of the marine environment. In this case the grid spacing used for the simulation was 1 km in comparison to 4 km used for Cases 1 to 6. The impact of higher resolution allowed the development of individual convective cells along the leading edge of the east coast low. The modelled characteristics of these convective cells was similar to that observed by radar.

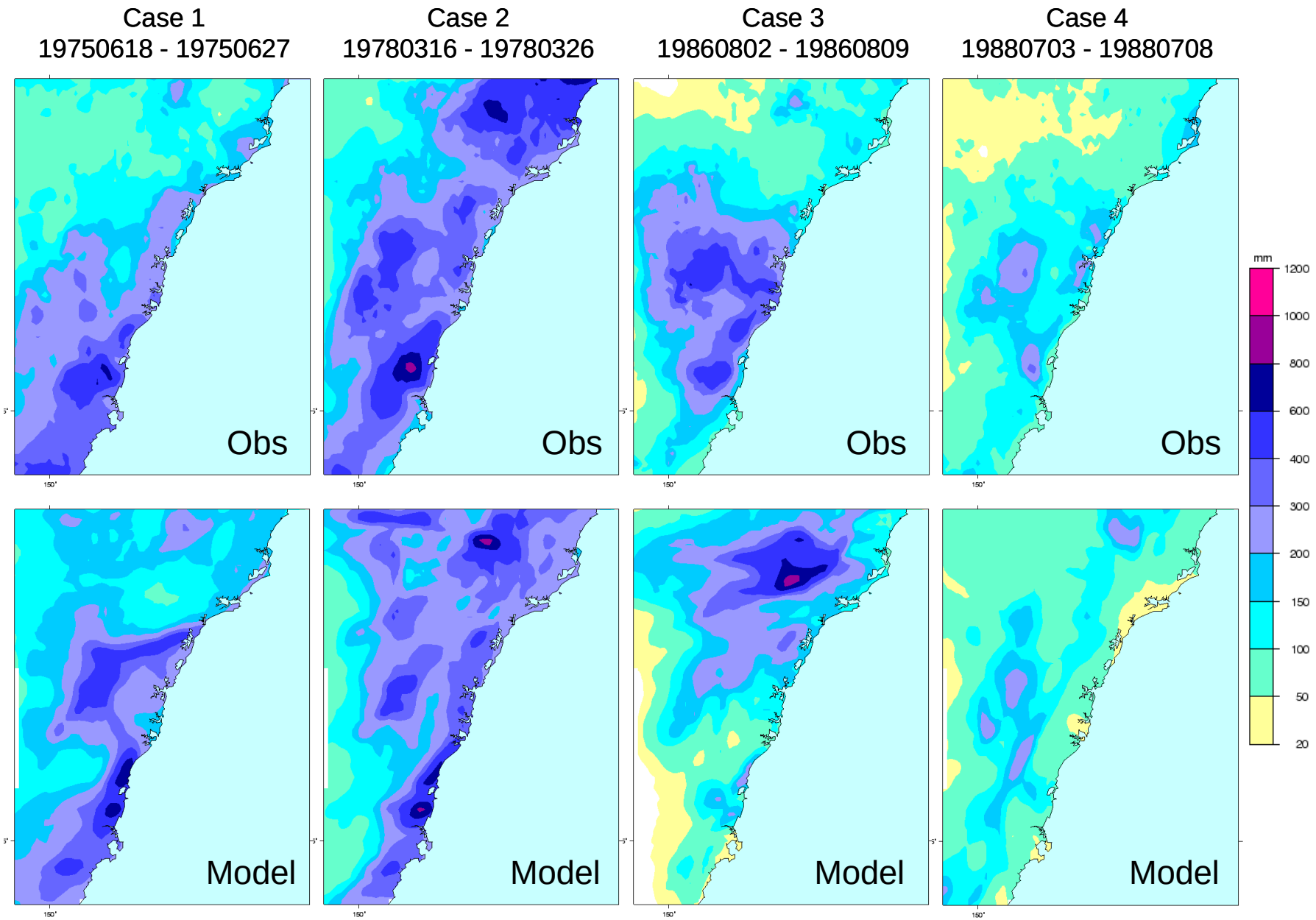
Case 1
19750618 - 19750627
Case 2
19780316 - 19780326
Case 3
19860802 - 19860809
Case 4
19880703 - 19880708
Obs
Obs
Obs
Obs
Model
Model
Model
Model
mm
1200
1000
800
600
400
300
200
150
100
50
20

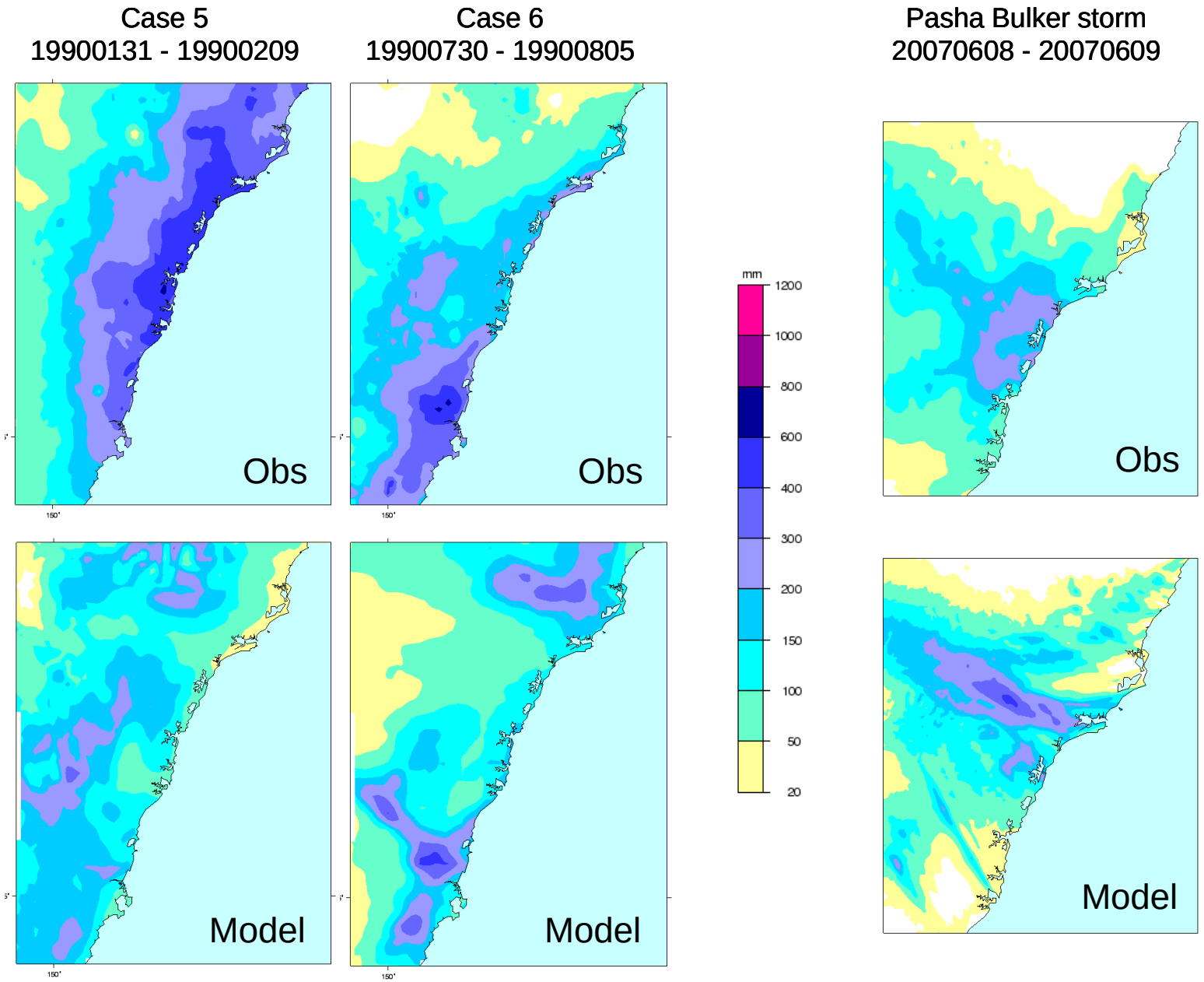

Figure 27: (top) Observed accumulated rainfall and (bottom) modelled accumulated rainfall for the 7 cases studies identified.

APPENDIX D

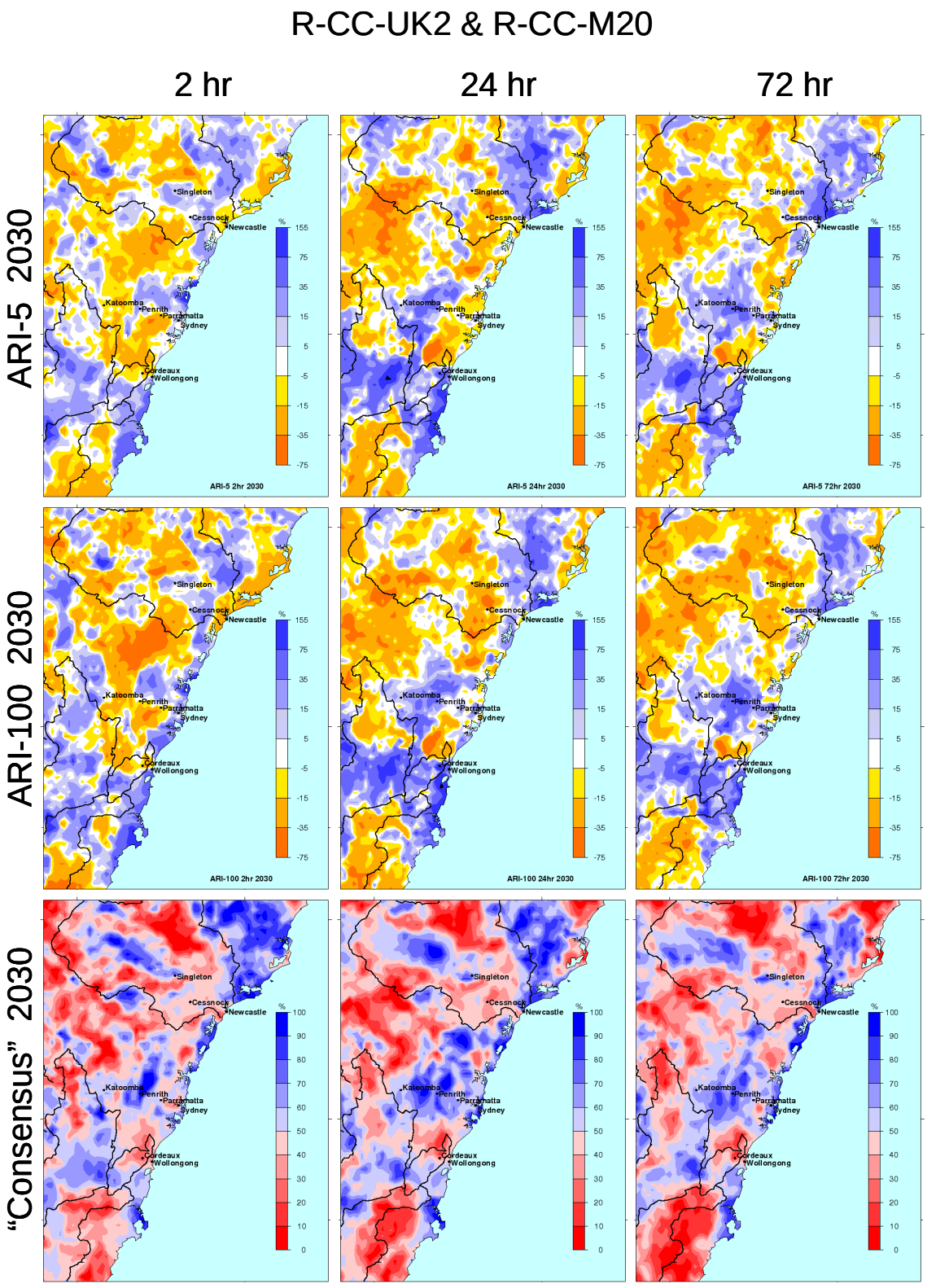

Figure 28: As for Figure 20 but for a composite of R-CC-UK2 and R-CC-M20.

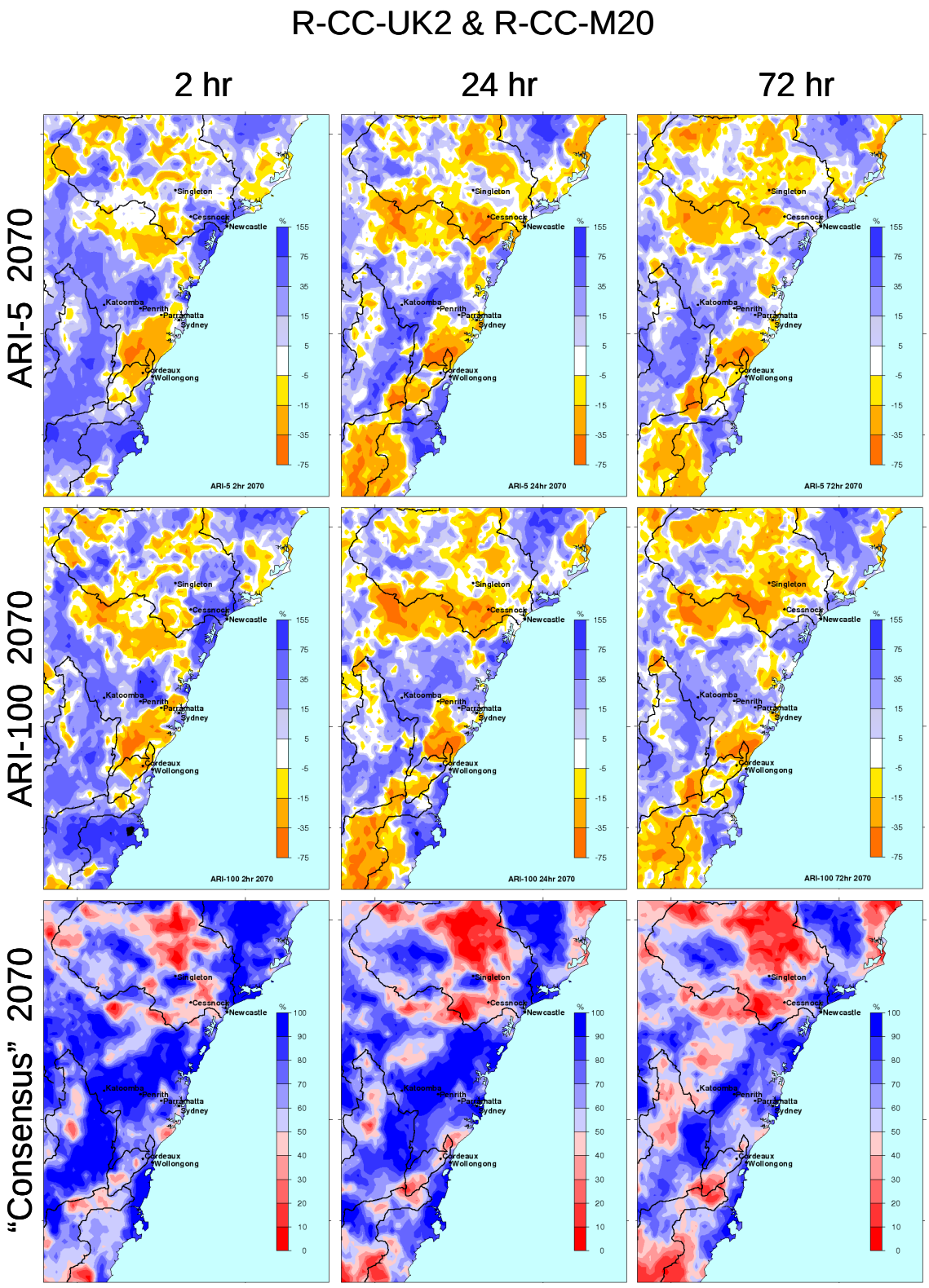

Figure 29: As for Figure 21 but for a composite of R-CC-UK2 and R-CC-M20

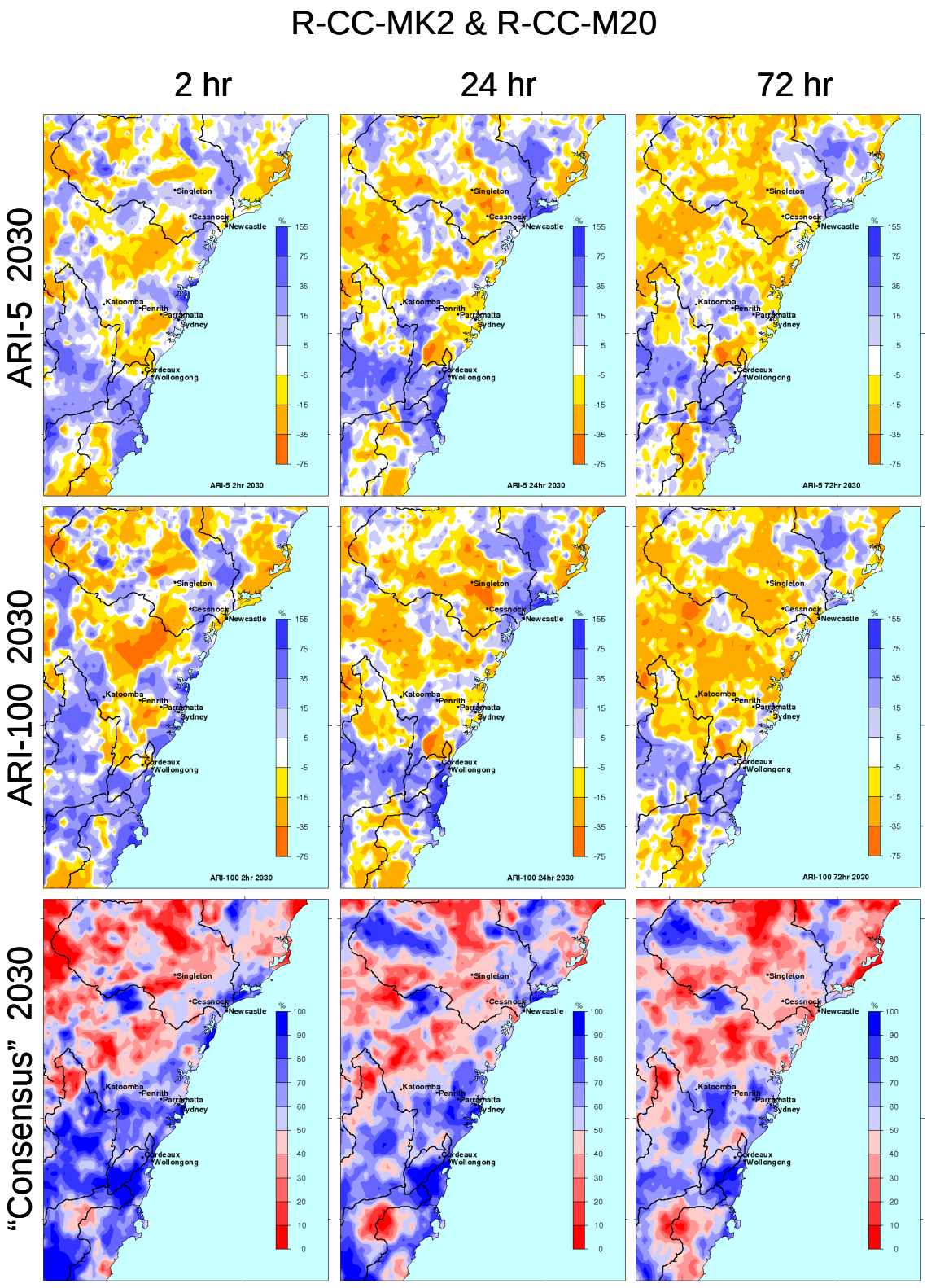

Figure 30: As for Figure 20 but for a composite of R-CC-MK2 and R-CC-M20.

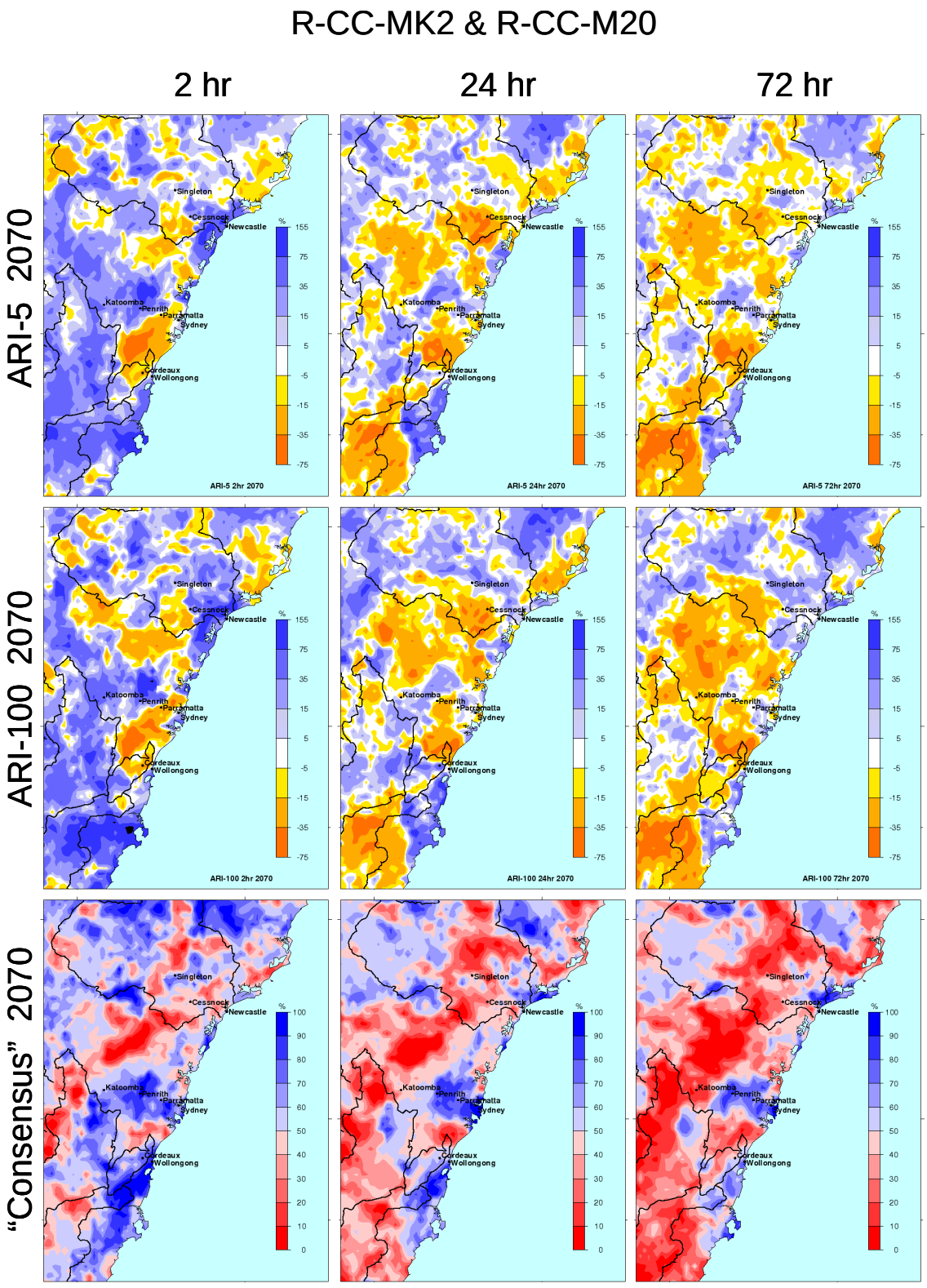

Figure 31: As for Figure 21 but for a composite of R-CC-MK2 and R-CC-M20

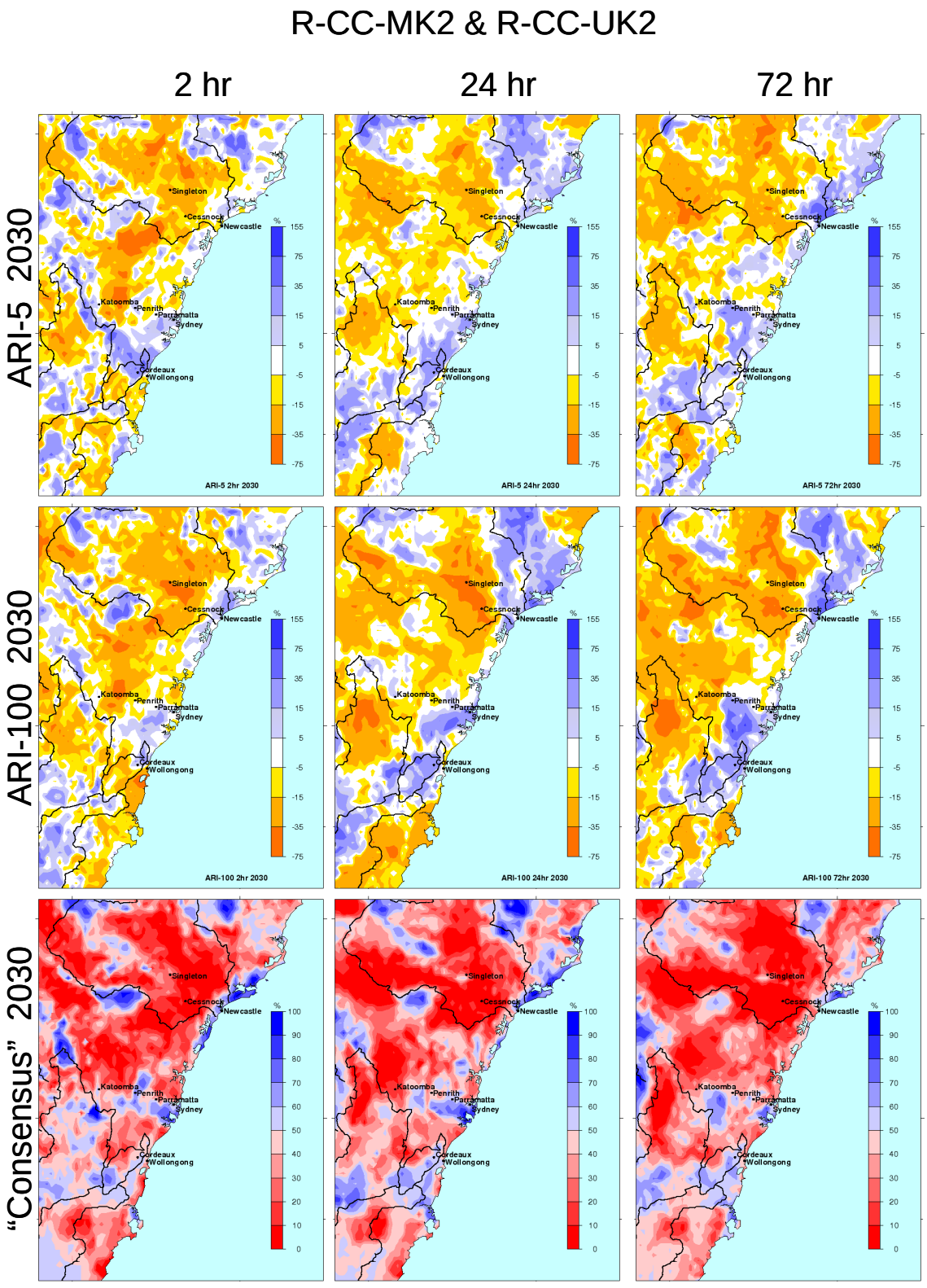

Figure 32: As for Figure 20 but for a composite of R-CC-MK2 and R-CC-UK2.

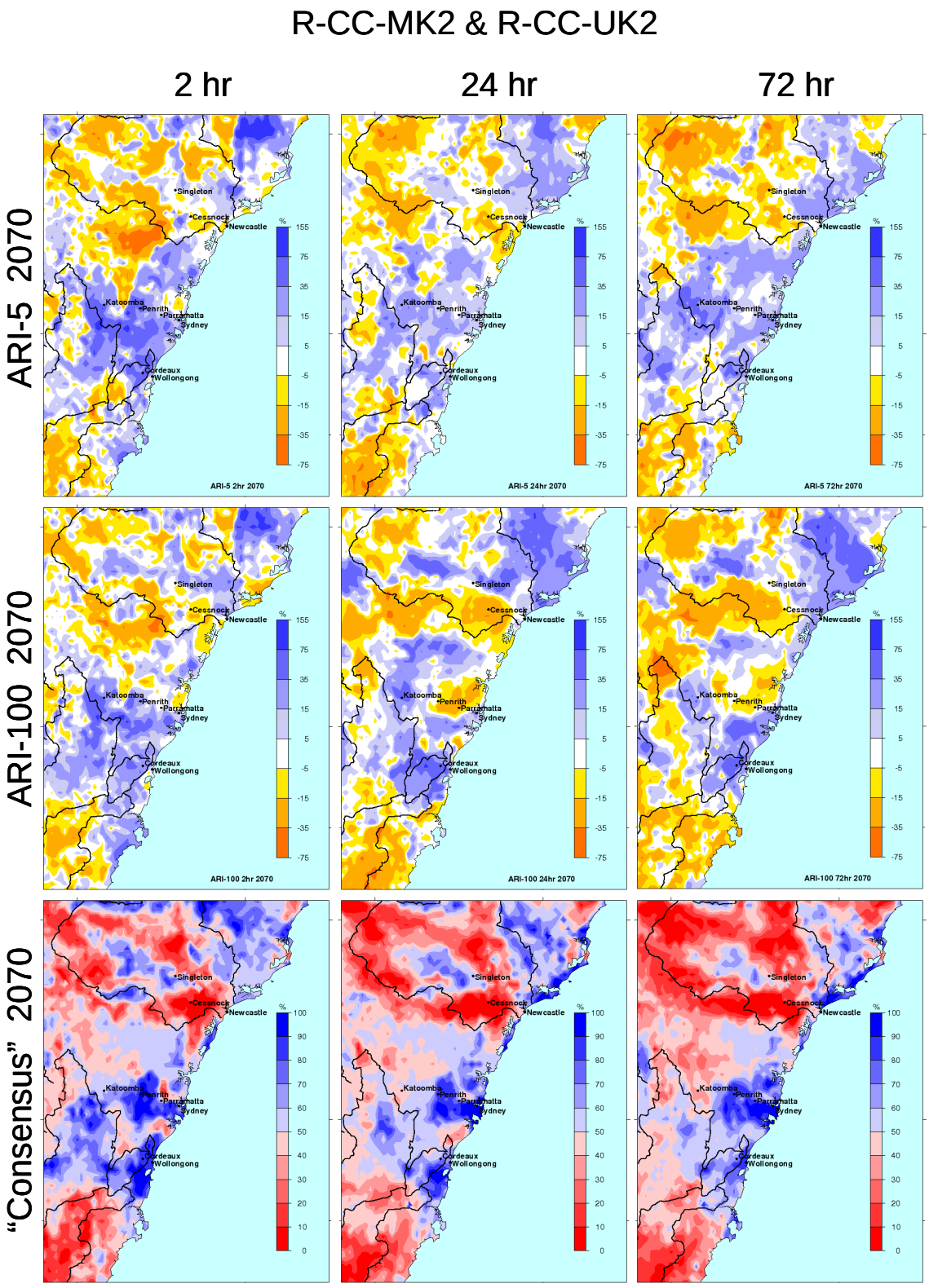

Figure 33: As for Figure 21 but for a composite of R-CC-MK2 and R-CC-UK2

APPENDIX E

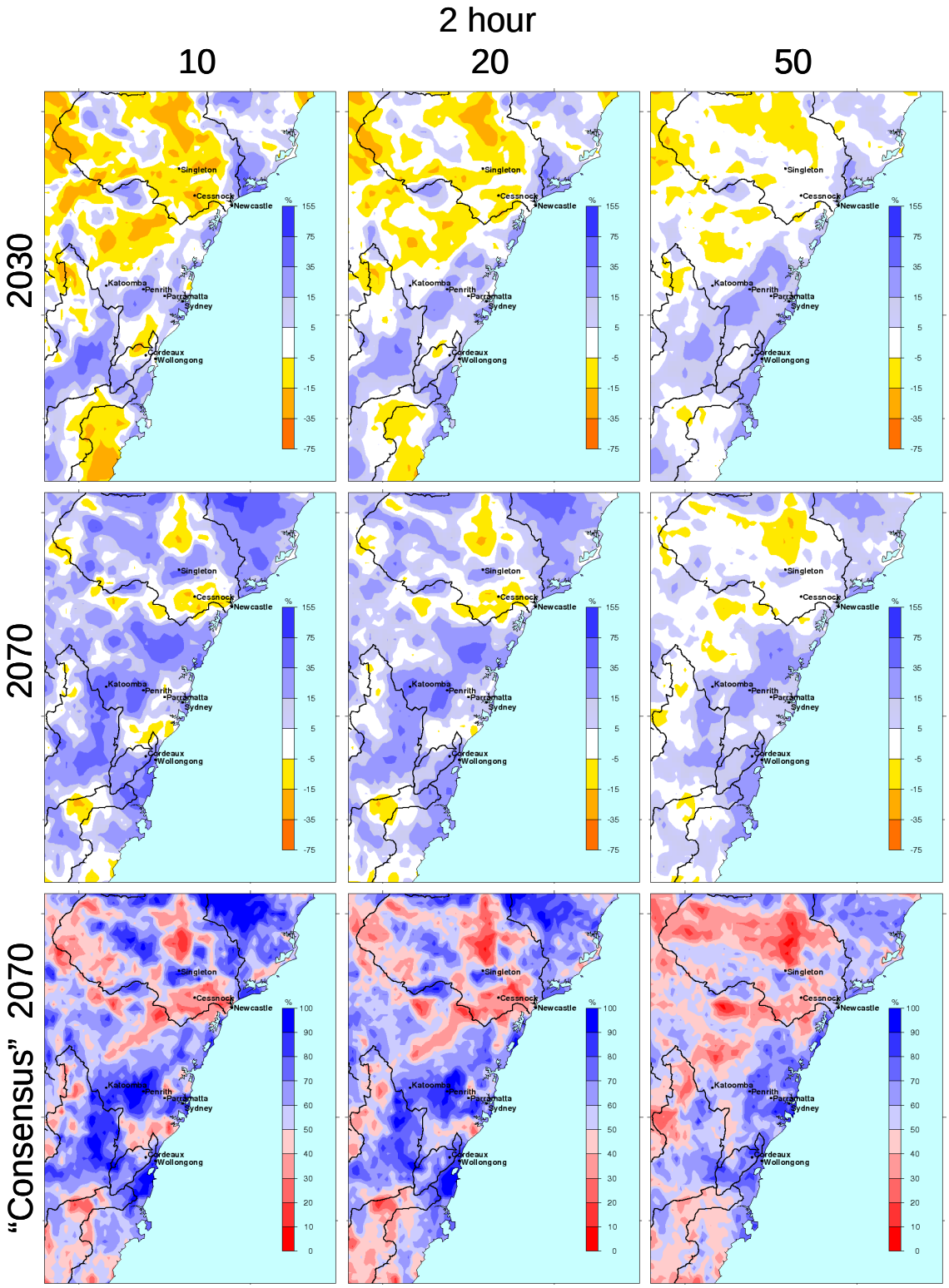

Figure 34: As for Figure 22 but for 2-hour extreme rainfall events.

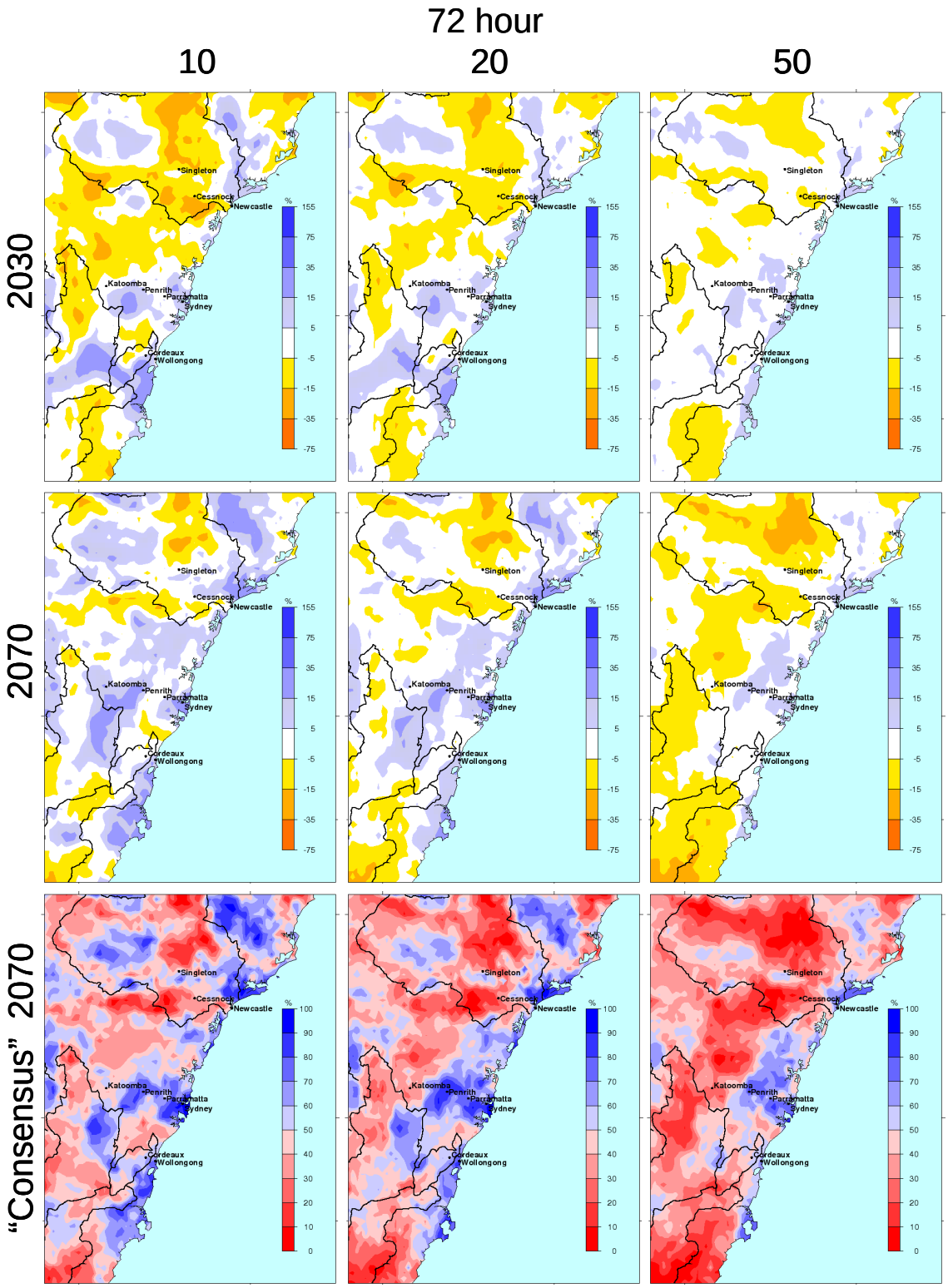

Figure 35: As for Figure 22 but for 72-hour extreme rainfall events.

Contact Us
Phone: 1300 363 400
+61 3 9545 2176
Email: enquiries@csiro.au
Web: www.csiro.au

Your CSIRO

Australia is founding its future on science and innovation. Its national science agency, CSIRO, is a powerhouse of ideas, technologies and skills for building prosperity, growth, health and sustainability. It serves governments, industries, business and communities across the nation.